SÃO PAULO STATE UNIVERSITY – UNESP

JABOTICABAL CAMPUS

OBTAINING CARBON FEEDBACKS IN THE BIG DATA ERA: A PERSPECTIVE TO CENTRAL-NORTH OF BRAZIL

Gustavo André de Araújo Santos

Agronomist

2020

SÃO PAULO STATE UNIVERSITY – UNESP

JABOTICABAL CAMPUS

OBTAINING CARBON FEEDBACKS IN THE BIG DATA ERA: A PERSPECTIVE TO CENTRAL-NORTH OF BRAZIL

Gustavo André de Araújo Santos

Advisor: Prof. Dr. Newton La Scala Jr

Co-Advisor: Prof. Dr. Carlos Antonio da Silva Junior

The thesis presented to the College of Agricultural and Veterinarian Sciences – UNESP, Jaboticabal Campus, as partial fulfillment of the Doctor degree in Agronomy (Soil Science).

2020

Santos, Gustavo André de Araújo
S237o OBTAINING CARBON FEEDBACKS IN THE BIG DATA ERA: A PERSPECTIVE TO CENTRAL-NORTH OF BRAZIL / Gustavo André de Araújo Santos. – – Jaboticabal, 2020
132 p. : tabs., fotos, mapas

Tese (doutorado) - Universidade Estadual Paulista (Unesp), Faculdade de Ciências Agrárias e Veterinárias, Jaboticabal
Orientador: Newton La Scala Jr
Coorientador: Carlos Antonio da Silva Junior

1. Carbon Cycle. 2. Climate Change. 3. MODIS. 4. OCO-2. 5. SIF. I. Título.

Sistema de geração automática de fichas catalográficas da Unesp. Biblioteca da Faculdade de Ciências Agrárias e Veterinárias, Jaboticabal. Dados fornecidos pelo autor(a).

UNIVERSIDADE ESTADUAL PAULISTA

Câmpus de Jaboticabal

CERTIFICADO DE APROVAÇÃO

TÍTULO DA TESE: OBTAINING CARBON FEEDBACKS IN THE BIG DATA ERA: A PERSPECTIVE TO CENTRAL-NORTH OF BRAZIL

AUTOR: GUSTAVO ANDRÉ DE ARAÚJO SANTOS
ORIENTADOR: NEWTON LA SCALA JUNIOR
COORIENTADOR: CARLOS ANTONIO DA SILVA JUNIOR

Aprovado como parte das exigências para obtenção do Título de Doutor em AGRONOMIA (CIÊNCIA DO SOLO), pela Comissão Examinadora:

Prof. Dr. NEWTON LA SCALA JUNIOR (Participaçao Virtual)
Departamento de Engenharia e Ciências Exatas (DECEx) / FCAV / UNESP - Jaboticabal

Prof. Dr. ROGÉRIO TEIXEIRA DE FARIA (Participaçao Virtual)
Departamento de Engenharia e Ciências Exatas (DECEx) / FCAV / UNESP - Jaboticabal

Prof. Dr. CARLOS EDUARDO PELLEGRINO CERRI (Participaçao Virtual)
Departamento de Ciência do Solo / ESALQ - USP - Piracicaba/SP

Prof. Dr. RAFAEL COLL DELGADO (Participaçao Virtual)
Departamento de Ciência do Solo-UFRRJ / Seropédica/RJ

Prof. Dr. DANIEL DE BORTOLI TEIXEIRA (Participaçao Virtual)
UNIMAR / Marília/SP

Jaboticabal, 18 de dezembro de 2020

AUTHOR'S CURRICULUM DATA

GUSTAVO ANDRÉ DE ARAÚJO SANTOS – Son of Magno Mansueto dos Santos Araújo and Maria Leônora de Araújo, he was born in Imperatriz - MA, on February 17, 1991. He attended minor elementary school at the Escola Municipal Samaritana and the middle school at the Amaral Raposo State College, in that same school he finished high school in 2008. In August 2010, he joined the Agronomy course at the Center for Agrarian and Environmental Sciences of the Federal University of Maranhão (UFMA-CCAA) campus of Chapadinha. He was a scientific student fellow in three projects. In September 2012, he began his international academic mobility through the Ciências sem fronteiras program at the Instituto Superior de Agronomia in Lisbon - Portugal, with a return in August 2013. In January 2016, he underwent banking for monograph defense, approved as a bachelor's degree in Agronomy. In March 2016, he started the Master's degree in Agronomy (Soil Science), at the Faculty of Agrarian and Veterinary Sciences (FCAV-UNESP), Campus of Jaboticabal-SP. On July 17, 2017, he submitted to the Master's defense, approved as a Master in Agronomy (Soil Science). In August 2017, he started his Ph.D. course in Agronomy (Soil Science) also from FCAV-UNESP. In 2018 he attended the summer school in Data Science at the International Centre for Theoretical Physics (ICTP) in Trieste, Italy, with UNESCO support. In December 18, 2020, he submitted the doctoral thesis to an examination panel, and received his Ph.D. degree in Agronomy (Soil Science) at UNESP/FCAV.

"Educação não transforma o mundo. Educação muda as pessoas. Pessoas transformam o mundo."

Paulo Freire

"You cannot hope to build a better world without improving the individuals. To that end, each of us must work for his own improvement and, at the same time, share a general responsibility for all humanity, our particular duty being to aid those to whom we think we can be most useful."

Marie Curie

I DEDICATE

To the greatest **loves of my life**, which are the force that moves my dreams, **Maria Leônora** and **Magno Mansueto**, my parents.

I OFFER

To Brazilian people, who with great effort contributed through their taxes in the financing of my studies, it would not have been possible to get here without them.

ACKNOWLEDGMENTS

To my parents, Maria Leonôra and Magno Mansueto, to had lived this dream with me, for always believing in me, sometimes, much more than myself, for still supporting me, for love, understanding, trust, and especially for the teachings you have given me for life, you are the most influential teachers I have in life. My sister Debora Magda also, for love and friendship.

To my family, my aunts Vânia Maciel, Aline Araújo, Eline Araújo and Poliana Araújo for the love and affection every time I came back to Imperatriz, my beloved grandmother Alice, a sweet person, an example of a woman and grandmother, my maternal grandmother Débora Dantas (*in memoriam*) that although I did not know her, she was essential for me, to be here today, to Luis Bandeira (*in memoriam*) and Manoel André (*in memoriam*) my grandfathers, to my sweet uncle Raimundo Santos for the affection, and finally, to my dear cousins and cousins Débora Luiza, Pâmela Maciel, Nicole, Thiago, Daniela, Karol, Salmo and Matheus.

To my dear advisor and mentor, Dr. Newton La Scala Júnior, for his patience, guidance, trust, support, friendship, for the coffees in the cafeteria and for the following sentence at the beginning of my doctorate "Gustavo, who does a doctorate is not to be limited". Thanks so much for contributing to my professional, personal, and intellectual training. I will be eternally grateful to you for my training as a scientist.

To my co-advisor, Dr. Carlos Antonio da Silva Junior, to have received me so fraternally in his laboratory at UNEMAT-SINOP and always being willing to ask all my doubts, his contribution was indispensable. Thank you very much.

To the members who participated in my qualification exam: Dra. Teresa Cristina Tarlé Pissarra and Dr. Alan Rodrigo Panosso.

To the examination panel members of the thesis defense: Dr. Carlos Eduardo Pellegrino Cerri, Dr. Daniel De Bortoli Teixeira, Dr. Rafel Coll Delgado and Dr. Rogério Teixeira Faria.

To the great friends, I made during graduate school at UNESP-FCAV and at the Department of Exact Sciences, Thiago Águas, Taynara Valeriano, Robson Medeiros, Kamila Meneses, Katharine Batista, Aline Moreno, Valter Santos, Kárita Almeida, Washigton Pereira, Nayanne Lima, Paulo Alexandre, Maria Elisa, Deise Nogueira, Stefany Souza, Jonas Júnior, José Reinaldo, Romário Pimenta, Gabriela Almeida, Welliny Rocha, Naum Collins, Jeferson Martins, Tatiana Santos, Beth Kazama and to all the others who helped me during this period.

To my friends, brothers and sisters that life has given me Alex Bruno, Adalziza Neta, Grazieli Brito, Ludhanna Veras, Camila Vieira, Francisca Farias, Rebekah Maria, Sebastião Yattan, Larissa Portela, Joab Pedrosa, Mayanna Karla, Rosieli Silva, Marcilene Ribeiro, Alice Vöttel, Vanessa Rufino, Zaldy D. Catedrilla, Maria Leticia Pacheco, Fernanda Francetto, Débora Boaventura, Emanuele Silva, Juliana Soares and Ana Isa.

To the research F_{CO2} group members: Adriano Maltezo, Luciano Maria, Wanderson Lucena and Daniel Costa. A special hug to Bruna Oliveira and Fernando Morais, who have been with me since the beginning and today are great friends.

The Mara Regina Moitinho and Daniel De Bortoli Teixeira for all the teachings and contributions in my academic background. I admire you very much.

To my students of scientific initiation, Felipe Facco, Luis Miguel, and Gabriel Scarabel, I could learn a lot from you. Thank you!

To my colleagues at the GAAF (UNEMAT-SINOP), especially my friend Fernando Rossi.

To my friends from NEURON Data Science and Artificial intelligence: Felipe Polo, Leonardo, Samuel, Jhonatan Batista, Edvaldo, Vanessa, Ana Clara, Cauê and Professor Marcelo Botelho.

To the professors of the Department of Exact Sciences (For me it will be eternally the department of exact sciences), Danísio Prado Munari, Amanda Liz Pacífico Manfrim,

Alan Rodrigo Panossos, Dilermando Perecin, Glauco de Souza Rolim, Euclides Braga Malheiros, Jose Carlos Barbosa , Nelson José Peruzzi and to all employees of the department: Maria José Servidone Trizólio (Zezé), Shirley Aparecida Martineli de Sousa, Adriana Elisabete Takakura (Dri), Vanessa Sayury Souza and Carlos Alberto Santa Capita (Carlão), thanks for the pleasant coexistence during my journey.

Thanks also at Universidade Estadual Paulista, Câmpus de Jaboticabal and Programa de pós-graduação em Agronomia (Ciência do Solo) for the opportunity to be able to study his doctorate in one of the best programs in the country.

This study was financed in part by the Coordenação de Aperfeiçoamento de Pessoal de Nível Superior (CAPES, Brazil) under the funding code 001.

The databases SCOPUS, ScienceDirect, WEB OF SCIENCE, SCIELO, and the Periódico Capes facilitated the search for my literature review and understanding of my results. To the Facebook group (Capes Fellows) for relaxed moments with the most fun "memes" involving the academic world.

The UNESCO and the Abdus Salam International Centre for Theoretical Physics (ICTP) for the opportunity to be in 2018 in the summer school of data science in Trieste, Italy. And to my dear friends on this journey, Atul Saini and Ashok Rai.

To Paloma, a friend I discovered at the end of my PhD. Thanks for the fun times and for giving lightness to my days.

And to all who contributed directly and indirectly to the conduct of my study.

And finally, why not me? Yes, to me, especially for never giving up my dreams and believing that the impossible is also possible.

SUMMARY

Page
ABSTRACT....xiv
LIST OF ABBREVIATIONS AND ACRONYMS xv
LIST OF FIGURES....xvii
CHAPTER 1 – General considerations 20
1 INTRODUCTION....20
1.2 THESIS GOAL....22
1.2.1 Specific goals and general hypothesis 23
1.3 LITERATURE REVIEW....23
1.3.1 Carbon cycle 23
1.3.2 Carbon-climate-feedbacks....26
1.3.3 Climate change: A perspective in Brazil 27
1.3.4 Greenhouse gas measurements from space....29
1.3.5 Big data era: The role of remote sensing on the carbon feedbacks 33
REFERENCES....38
CHAPTER 2 – The role of the vegetation and the weather on the temporal variability of XCO2 and SIF: A perspective to biomes and planted forest in Brazil 46
ABSTRACT....46
2.1 Introduction 47
2.2 Material and Methods....49
2.2.1 Study Area....49
2.2.2 Big data remotely sensed acquisition and processing....50
2.2.3 Platforms for data extraction....51
2.2.3.1 Orbiting Carbon Observatory-2 (OCO-2)....53
2.2.3.2 Data extraction on the AppEEARS platform....54
2.2.3.3 Weather data from NASA POWER 54
2.2.3 Statistical analysis 55
2.3 Results 55
2.4 Discussion 67
2.4.1 Temporal variability for XCO2 67

2.4.2 Temporal variability of SIF....68
2.5 Conclusions....70
References....71
CHAPTER 3 – Space-time variability of XCO2 and SIF from OCO-2: A case study in the Mato Grosso State, Brazil....80
ABSTRACT....80
3.1 Introduction....81
3.2 Material and Methods....82
3.2.1 Study area....82
3.2.2 Data acquisition....83
3.2.2.1 Orbiting carbon observatory-2 (OCO-2)....84
3.2.3 Statistical analysis and temporal variation of data....85
3.2.4 Spatial variability (ordinary kriging)....86
3.3 Results....87
3.3.1 Temporal variation....87
3.3.2 Spatial variability....88
3.4 Discussion....91
3.5 Conclusions....93
References....94
CHAPTER 4 – Hot spots and anomalies of CO2 over eastern Amazonia, Brazil....100
ABSTRACT....100
4.1 Introduction....101
4.2 Material and Methods....103
4.2.1 Study area....103
4.2.2 Remotely sensed and meteorological data....104
4.2.2.1 Orbiting Carbon Observatory-2 (OCO-2)....105
4.2.2.2 Meteorological data....106
4.2.2.3 MODIS data....106
4.2.3 Statistical analysis....107
4.2.3.1 Descriptive data statistics to hot moments....107
4.2.3.2 Hot Spot analysis (Getis-Ord Gi*)....108

4.2.3.3 XCO2 anomaly model 109
4.3 Results 109
4.3.2 Hot and cold moments 109
4.3.3 Spatial hot and cold spots to XCO2 and SIF 771 113
4.3.4 XCO2 anomalies 115
4.4 Discussion 116
4.5 Conclusions 119
References 120
CHAPTER 5 – Final remarks 128
APPENDICES 130

OBTAINING CARBON FEEDBACKS IN THE BIG DATA ERA: A PERSPECTIVE TO CENTRAL-NORTH OF BRAZIL

ABSTRACT – With the emergence of the era of earth observation in high resolution, remote sensing data's exponential growth has occurred in recent years. Thus, it is possible to carry out studies to monitor the carbon cycle on a global and regional scale, thus generating carbon feedback that can contribute to climate governance and decision-making to mitigate the effects that cause climate change. Therefore, this study was designed with the purpose of printing feedbacks related to the carbon cycle using Big Data in earth observation using remote sensing and climatic variables obtained by simulation models for the Central-North of Brazil, an important region due to the presence of important biomes such as the Amazonia, Cerrado, Pantanal and Atlantic Forest, besides being one of the most representative regions in the advancement of Brazilian agribusiness. Three studies were carried separately for the following sub-regions: Mato Grosso, Mato Grosso do Sul, and Eastern Amazonia. For each region were discussed different problems. A time series was analyzed from January 2015 to December 2018. The variables X_{CO2}, Solar-induced fluorescence at 757nm, and 771nm were extracted from Orbiting Carbon Observatory-2 -OCO-2. The NDVI (MOD13A1), EVI (MOD13A1), and evapotranspiration (MOD16A2), data from Moderate Resolution Imaging Spectroradiometer - MODIS and climate variables (precipitation, wind speed, air temperature and relative humidity) as of Prediction of Worldwide Energy Resources - NASA POWER. The data were submitted to descriptive statistics, regression, correlation, temporal analysis and spatial interpolation with the kriging method and hotspots. It was observed that both in biomes and forest areas in Mato Grosso do Sul, the temporal variation of atmospheric CO_2 concentration is mainly governed by photosynthesis ($SIFR^2adj.$ = 0.07-0.55; $p<0.05$, $NDVIR^2adj.$ = 0.18-0.63; $p<0.05$, and $EVIR^2adj.$ = 0.20-0.49; $p<0.05$) and that photosynthesis is positively related to evapotranspiration ($R^2adj.$ = 0.20-0.44; $p<0.001$) and air temperature ($R^2adj.$ = 0.26-0.44; $p<0.001$). In Mato Grosso and Eastern Amazonia, SIF was also an important variable in explaining the temporal variability of X_{CO2} (r= -0.84; $p<0.01$). However, in these regions, this relationship is also observed spatially. In general, the time variations of X_{CO2} in the north-central region of Brazil varies between the dry and rainy periods, this was clear in all studies. As for the spatial variation of X_{CO2}, it varies according to the type of land use and the time of year. Given the results presented in this work, it is clear that the use of big data from remote sensing observations are valuable tools in understanding the carbon cycle since the relationships observed in the intersection of these data generate results that are clearly explained by the physical and biological processes around the soil-plant-atmosphere system.

Keywords: Carbon cycle, Climate Change, MODIS, NASA POWER, OCO-2, SIF

LIST OF ABBREVIATIONS AND ACRONYMS

AIRS-NASA - Atmospheric Infrared Sounder from the National Aeronautics and Space Administration

CH_4 – Methane

CO_2 - Carbon dioxide

COP21 - 21st Climate Conference

DSD - Degree of spatial dependence

ESA - European Space Agency

EVI - Improved Vegetation Index

fAPAR - Fraction of photosynthetically active radiation absorbed by vegetation

GEOS-4 - Global Model and Assimilation Office

GHG - greenhouse gas

GOSAT - Greenhouse Gases Observing Satellite

IBGE - Brazilian Institute of Geography and Statistics

INMET - National Institute of Meteorology

IoT - Internet of Things

IPCC - Intergovernmental Panel on Climate Change

JAXA - Japan Aerospace Exploration Agency

LAI - Leaf area index

LAPIG - Image Processing and Geoprocessing Laboratory

MODIS - Moderate Resolution Imaging Spectroradiometer

N_2O - Nitrous oxide

NASA/POWER - National Aeronautics and Space Administration / Prediction of Worldwide Energy Resources

NDVI - Normalized difference vegetation index

NOAA - National Oceanic and Atmospheric Administration

OCO-2 - Orbiting Carbon Observatory-2

OCO-3 - Carbon Observatory – 3

SCIAMACHY-ESA - Scanning Imaging Absorption Spectrometer for Atmospheric CHartographY from European Space Agency

SIDRA - Automatic Recovery System

SIF - Sun-induced chlorophyll fluorescence

SMAP - Soil Moisture Active Passive

TES - Tropospheric Emission Spectrometer

W m^{-2} sr^{-1} μm^{-1} – Watt per steradian per square metre per micrometres

X_{CO2} - Column-averaged dry-air mole fraction

LIST OF FIGURES

Page

Figure 1 (Chapter 1). Major carbon reservoirs in the Earth system and their present capacities in units of kg m^{-2}…… 23

Figure 2 (Chapter 1). A sub-cycle within the land carbon cycle…… 24

Figure 3 (Chapter 1). Time series of articles indexed in journals in the base "SCOPUS" with the term "climate change" (Search bean on 10/20/2020)…… 26

Figure 4 (Chapter 1). Milestones in remote sensing of the terrestrial C cycle……... 29

Figure 5 (Chapter 1). Documents indexed in journals in the base of SCOPUS with the term "GOSAT" by year (A), country (B) and subject area (C)…… 31

Figure 6 (Chapter 1). Documents indexed in journals in the base of SCOPUS with the term "OCO-2" by year (A), country (B) and subject area (C)…… 32

Figure 7 (Chapter 1). Arrays of chlorophyll molecules bound to protein absorb and process solar photons in plant leaves. A variable fraction (φf, typically ∼1%) of these leaks back out as fluorescent photons. The absorbed photon can be lost as radiationless decay (Kd), re-emitted as a fluorescent photon (Kf), quenched by NPQs (Kn), or used for photochemistry (Kp)……... 35

Figure 8 (Chapter 1). Spectral detection of sun-induced chlorophyll fluorescence……... 36

Figure 1 (Chapter 2). Location of the state of Mato Grosso do Sul with their respective biomes and the points with the presence of Eucalyptus…….. 49

Figure 2 (Chapter 2). Flowchart of acquisition, processing and data analysis……. 49

Figure 3 (Chapter 2). boxplot graph with mean and temporal distribution of X_{CO2} (A and B), SIF 757 (C and D), and SIF 771 (E and F) for biomes and eucalyptus fields of Mato Grosso do Sul, Brazil……. 55
Figure 4 (Chapter 2). Heatmap with correlation matrix for (A) Cerrado, (B) Atlantic Forest, (C) Pantanal, and (D) Eucalyptus fields in the state of Mato Grosso do Sul…… 59
Figure 5 (Chapter 2). Linear regression between X_{CO2} and SIF771 (A), EVI (B) and NDVI (C)…….. 62
Figure 6 (Chapter 2). Linear regression of SIF771 with total evapotranspiration (A), EVI (B), NDVI (C) and Air temperature (D)……. 66
Figure 1 (Chapter 3). Characterization biomes in Mato Grosso state, Midwest of Brazil…… 83

Figure 2 (Chapter 3). Temporal variation of accumulated precipitation (bars) and average air temperature (lines) for the state of Mato Grosso, Brazil-based on data extracted from the NASA/POWER platform…… 83
Figure 3 (Chapter 3). Flowchart of the data acquisition and processing… 84
Figure 4 (Chapter 3). Temporal variation for X_{CO2} ppm and SIF to wet (a) and dry (b) period of Mato Grosso State, Brazil. …… 87
Figure 5 (Chapter 3). Pearson correlation to X_{CO2} with SIF considering the averages of the dry and rainy periods of each year studied (N=8)…….. 88
Figure 6 (Chapter 3). Spatial distribution of X_{CO2} (a) and SIF (b) in the state of Mato Grosso, Brazil considering the seasons…… 91
Figure 1 (Chapter 4). Location of the Eastern Amazonia region in Maranhão State, Brazil. …….. 104
Figure 2 (Chapter 4). Flowchart of the data acquisition and processing… 105
Figure 3 (Chapter 4). Temporal series of $X_{CO2adjusted}$ to daily observations (A), annual average (B) and monthly averages (C) between 2015 and 2018 for Amazon biome in the Maranhão State of Brazil……. 110
Figure 4 (Chapter 4). Heatmap of Pearson correlation matrix for X_{CO2} with SIF 757, SIF 771, precipitation, wind speed at 2 meters, wind speed at 10

meters, relative humidity at 2 meters, wind direction at 2 meters and NDVI for Amazon biome in the Maranhão, State of Brazil…… 111

Figure 5 (Chapter 4). Linear regression analysis of X_{CO2} (ppm) with SIF 757 (W m^{-2} sr^{-1} μm^{-1}), SIF 771 (W m^{-2} sr^{-1} μm^{-1}) and precipitation (mm) for Amazon biome in the Maranhão State of Brazil…….. 112

Figure 6 (Chapter 4). Spatial hot and cold spots to X_{CO2} and SIF 771 for Amazon biome in the Maranhão State of Brazil……. 113

Figure 7 (Chapter 4). Timeline variation of hot and cold spots of A) X_{CO2} and B) SIF 771 for Amazon biome in the Maranhão State of Brazil……. 115

Figure 8 (Chapter 4). Spatial distribution of X_{CO2} anomalies (a), anomalies data distribution (b) and latitude distribution (c)…… 116

APPENDIX B (APPENDICES). Land use cover to Amazonia rainforest of Maranhão, Brazil…… 133

CHAPTER 1 – General considerations

1 INTRODUCTION

Between 1880 and 2012, the average temperature of the planet increased around 0.85 ºC. The increase in temperature observed in recent decades is mainly due to increased greenhouse gas (GHG) emissions (Diffenbaugh et al., 2015; Medhaug et al., 2017). The carbon dioxide CO_2 concentrations have increased by about 40% since the beginning of the industrial era. This exponential increase in CO_2 emissions is due to the burning of fossil fuels, deforestation and land-use change (Quéré et al., 2015; Schimel et al., 2015). Given this perspective, numerous studies try to prospect the responses of different regions of the planet under scenarios related to the climate system (Parazoo et al., 2016; Silva Junior et al., 2020)

The soil-plant-atmosphere system is closely related to these scenarios since the biogeochemical cycles of the leading gases responsible for the greenhouse effect pass through the soil, plants and atmosphere, with particular attention to carbon and nitrogen (Finzi et al., 2011). In addition to these, water is also a part of its cycle with in the soil, therefore being a closed, complete and complex system (Seneviratne et al., 2010). Thus, researchers have joined forces to try to understand how climate change can interfere with the ecosystem, seeking alternatives that mitigate the effects of climate change, especially in agriculture (La Scala et al., 2000; Santos et al., 2019; Silva et al., 2019; Xavier et al., 2020).

It is important to emphasize that carbon plays a crucial role in the supply of energy with in the soil-plant-atmosphere system through its cycle (Chapin, Matson, 2011). In this cycle, a series of feedback mechanisms are responsible for the carbon response to the increase in the planet's temperature (NRC, 2003). There is evidence that carbon feedbacks are sensitive to temperature, hydrological cycle and land-use change (Goodwin et al., 2019; Williams et al., 2019). However, these sensitivities are still uncertain due to the uncertainties related to other factors that also influence the carbon cycle, such as nutrient availability like nitrogen (Goodwin, 2019). Besides, the availability of data for significant studies again emerges as a limiting factor.

On the other hand, as the development of technologies aimed at earth observation, especially remote sensing through satellites, a quantity of massive data related to the carbon cycle has been made available in recent decades (Chi et al., 2016; Xu and Xiaoping, 2020), being possible to apply in various fields of science (Silva Junior et al., 2020; Rossi and Santos, 2020; Taylor et al., 2021). The explosion in data generation in the most diverse areas of knowledge has been called the big data era (Chen et al., 2014). This expression is related to the volume, speed, and variety of information produced by different sources in a short time (Lioutas, 2020). A large amount of data generated today is only possible on account to the emergence of technologies such as mobile devices, social networks, satellites, portable sensors, weather stations and model applications for estimated data (Kamilaris et al., 2017; Majumdar et al., 2017)

The advance in data generation has contributed to innovative discoveries in various areas of knowledge in climate science, e.g., the variety and quantity of data have states available in a way never seen before (Shannon, 2019). Furthermore, climate science promises to be one of the largest data sources for data-driven research (Faghmous & Kumar, 2014). According to these authors, it is estimated that in 2010 the available climate data had already reached the volume of 10 Petabyytes (1PB= 1.000TB). This number tends to increase exponentially to about 350 Petabytes by 2030. For example, The National Aeronautics and Space Administration (NASA) is considered one of the most important institutions in data generation, being able to generate 12.1TB of data daily through its active missions around Earth and space. Besides, with advances in orbital sensors' development, NASA expects that some of the space agency's missions can generate up to 24 TB a day (Shannon, 2019).

From this perspective, in 2014, NASA launched the Orbiting Carbon Observatory-2 (OCO-2) (Annmarie Eldering et al., 2017). With the launch of the OCO-2 spacecraft, NASA presented the world with an important tool regarding understanding fundamental processes that act on the absorption and emission of CO_2. However, OCO-2 was not the first satellite launched to measure atmospheric CO_2. Before that, we had other soucers as the Scanning Imaging Absorption Spectrometer for Atmospheric CHartographY from European Space Agency (SCIAMACHY-ESA) were launched, both able to do this monitoring, but these missions were closed in 2012

(Pan et al., 2021). NASA launched AURA in July 2004 with the Tropospheric Emission Spectrometer (TES) with a better spatial resolution than AIRS and SCIAMACHY. The Greenhouse Gases Observing Satellite (GOSAT) was launched in January 2009 by Japanese national Aerospace (JAXA) to detect CO_2 and CH_4 (Yokota et al., 2009; Frankenberg et al., 2011). However, The OCO-2 was the first to provide the high accuracy, resolution and coverage needed to observe regional carbon sources and sinks. This is due to the OCO-2 ability to make about 16 million measurements each cycle with orbit trails separated by less than 1.5 degrees longitude at the equator (Eldering et al., 2017; Schwandner et al., 2017).

Two of the most important variables measured by OCO-2 are the carbon dioxide (CO_2) column-averaged dry-air mole fraction (X_{CO2}) and Solar Induced Fluorescence (SIF). X_{CO2} is the average CO_2 concentration in a column that goes from the earth's surface to the top of the atmosphere (Crisp et al., 2012). SIF is considered the most modern in vegetation analysis via remote sensing because SIF is directly related to photosynthesis's internal mechanisms (Xiao et al., 2019). In this sense, the SIF stands out because it can indicate the photosynthetically active vegetation, unlike other more traditional vegetation indicators such as NDVI, which detect only green leaves' presence (Mohammed et al., 2019).

The understanding of carbon dynamics via remote sensing using various sensors and OCO-2 data has been wide of the world (Gao et al., 2020; He et al., 2020). Zhaleh Siabia et al. (2019) observed in Iran that both soil cover and vegetation cover play essential roles in the spatial distribution of CO_2 and the discovery of carbon dioxide sources and sinks. In India, Chhabra and Gohel, (2019) also observed the importance of vegetation and different soil cover types in controlling atmospheric CO_2 concentrations.

1.2 THESIS GOAL

Although Brazil, is a key part of the global carbon cycling, the use of OCO-2 data in conjunction with other data sources is little explored. Therefore, this study was designed with the purpose of printing feedbacks related to the carbon cycle using Big Data from earth observation using remote sensing and climatic variables obtained by

simulation models for the Central-North of Brazil, an important region due to the presence of important biomes such as the Amazonia, Cerrado, Pantanal and Atlantic Forest, besides being one of the most representative regions in the advancement of Brazilian agribusiness.

1.2.1 Specific goals and general hypothesis

The general hypothesis of this study is based on the association of temporal and spatial variability of column-averaged of carbon dioxide in the atmosphere (X_{CO2}) and Solar Induced Fluorescence (SIF) the different types of land use and cover (Brazilian biomes) and the intrinsic climatic conditions of each. Therefore, the specific goals were: (1) Characterize the temporal variability of the carbon dioxide (CO_2) column-averaged dry-air mole fraction (X_{CO2}) and Solar Induced Fluorescence (SIF) and its main control factors in biomes and planted forests with eucalyptus in the state of Mato Grosso do Sul, Brazil with the use of remote sensing data (Chapter 2); (2) Detect the seasonal spatial variability of X_{CO2} and SIF for the state of Mato Grosso, Brazil, through Ordinary Kriging using OCO-2 data to find potential carbon sources and sinks; and (3) Characterize the hot spots, hot moments, anomalies of column-averaged of carbon dioxide in the atmosphere (X_{CO2}, ppm) and their interactions with climate and vegetation indices in the eastern Amazonia using the Orbiting Carbon Observatory-2 (OCO-2) data from Nasa.

1.3 LITERATURE REVIEW

1.3.1 Carbon cycle

Carbon corresponds to ~50% of living beings' dry weight, therefore being one of the most critical elements for terrestrial life due to its essentiality (Ussiri and Lal, 2017). Carbon is responsible for the flow of energy in various systems, such as ecosystems, humans and even industrial systems (Andrén and Kätterer, 2009). This

is only possible thanks to plants' ability to transform solar energy into chemical energy (Ryu et al., 2019).

An important fact is that carbon is an extremely dynamic element due to the series of processes (biological, chemical and physical) behind its absorption (Chapin, Matson, 2011). In this sense, carbon can be stored in the biosphere, its main reservoirs being the atmosphere, oceans, soils, vegetation and lithosphere(Lal, 2004; Hutyra, 2014). It is important to note that each reservoir's capacity and the residence time vary between them (Wallace and Hobbs, 2006) (Figure 1).

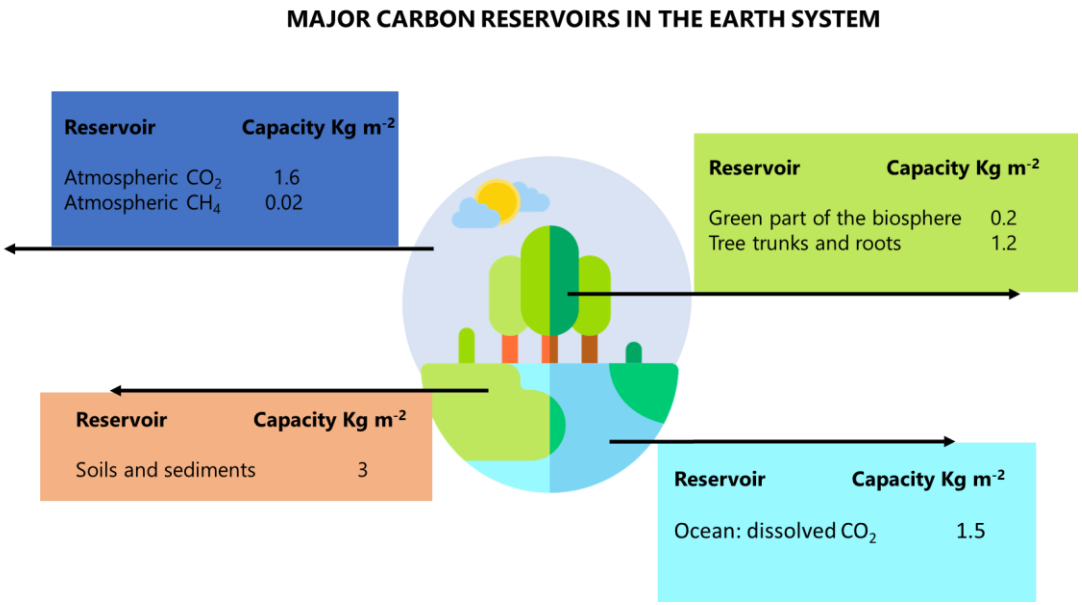

Figure 4. Major carbon reservoirs in the Earth system and their present capacities in units of kg m^{-2}.

Assuming the Earth as a system, the above components play the role of carbon reservoirs because they are responsible for storing significant amounts of carbon. In these reservoirs, any carbon movement between them is called carbon flux (Madani et al., 2017; Piao et al., 2020; Qiu et al., 2020). Thus, in integrated systems, the flows join the reservoirs creating carbon cycles and feedbacks.

When the carbon present in the atmosphere is used by photosynthesis, this already characterizes a carbon cycle (Figure 2). In this cycle, plants transform solar energy into chemical energy into organic carbon molecules that provide biochemical

mechanisms underlying the evolution and use of environmental energy, the essential attribute of life (Chapin and Matson, 2011; Ussiri and Lal, 2017). On a global scale, this process is responsible for transferring significant amounts of carbon between the atmosphere and plants (Frankenberg et al., 2016; Ryu et al., 2019). Over the years, plants complete their life cycle, and in the process of decomposition, carbon can return to the atmosphere.

The energy that is fixed through photosynthesis is responsible for the growth of plants that will later be consumed by animals and microorganisms (Andrén and Kätterer, 2009). For this reason, carbon constitutes half of the organic matter present on Earth (Ussiri and Lal, 2017). However, photosynthesis may be limited by control factors, factors that can also be called photosynthetic reagents and are they: light energy, CO_2, temperature, and nitrogen availability. Each of these plays an essential role to photosynthesis to occur. In the case of nitrogen, it is responsible for producing photosynthetic enzymes (Chapin and Matson, 2011).

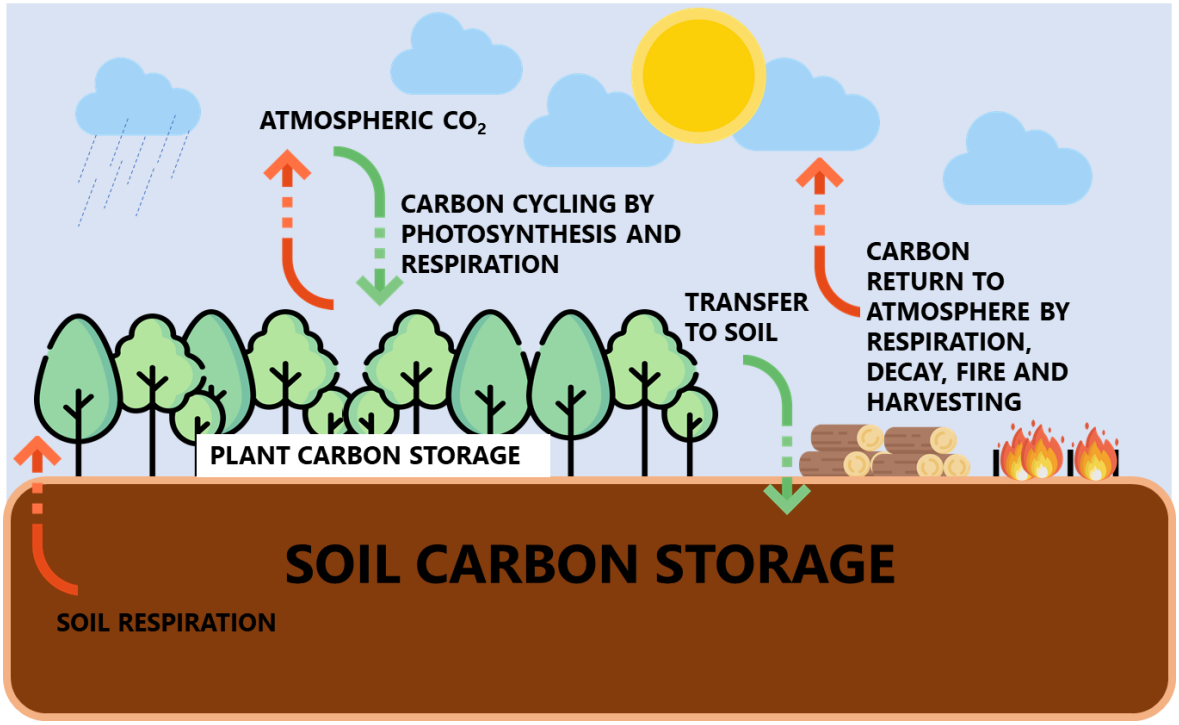

Figure 5. A sub-cycle within the land carbon cycle.

Respiration is another important process within the carbon cycle (Hutyra, 2014; Santos et al., 2019). In plants and other organisms, breathing is the chain responsible for returning carbon to the atmosphere (Gonsamo and Chen, 2017). However, this

occurs when plant cells use the sugars (carbohydrates) resulting from the photosynthetic process to obtain energy in the plants. It is estimated that at least half of the carbon absorbed by plants returns to the atmosphere. Concerning soil respiration, this occurs through the decomposition of organic matter present in the soil by microorganisms. Several studies point to soil moisture and temperature as important control factors (Santos et al., 2019; Silva et al., 2019; Xavier et al., 2020).

Thus, it is observed the prominent role carbon has in ecosystems (biosphere), climate and society. Thus, it is of fundamental importance that there is an understanding of the main factors responsible for regulating the carbon cycle and the exchanges between the biosphere and atmosphere.

1.3.2 Carbon-climate-feedbacks

Feedback is considered when a system's outputs are conducted back as links of a cause-and-effect chain (Goodwin et al., 2019). Thus, a system capable of self-recycling. In the climate change field of knowledge, feedback is essential for understanding global warming (Sellers et al., 2018; Williams et al., 2019). This understanding lies in the reasons for the increase or decrease caused by the feedback processes of each climate force (Fu et al., 2020).

Knowing that feedback consists of a process in which changing the amount of an element in a chain or cycle will change the amount of a second element, and this change, in turn, changes the first. This feedback can be positive or negative; when positive, there is an amplification in the change in the first quantity, so that negative feedback acts on reduction (Quan et al., 2019).

Following the National Research Council-NRC (2003), feedback in the climate system can amplify or dampen the system response as there is a change in climate forces. Thus, they systematize the term feedback as the climatic system's interactions between the variables that characterize the earth's surface, the ocean, and the atmosphere. These authors also reinforce the need for more research efforts to understand better and model climate feedback processes and improve the interpretation of these feedback in climate change. For this to be possible, these efforts

should not only be strengthened in the monitoring of traditional climatic variables (precipitation and temperature) but also invariable ours that govern the feedback processes, such as precipitation, wind, temperature, humidity, radiation balance at the top of the atmosphere and on the surface, distribution of clouds, soil moisture, terrestrial vegetation, atmospheric CO_2 and others.

1.3.3 Climate change: A perspective in Brazil

Between the 1960s and 1990s, scientists began to understand what was going on with the climate, as the planet was warming. Since then, discussions on climate change have gained evidence. With the creation of the Intergovernmental Panel on Climate Change (IPCC), climate reports have been released to help understand what is happening with the climate through estimates and scientific findings. After the first IPCC report in 1990, research in this area began to gain momentum worldwide (Figure 3).

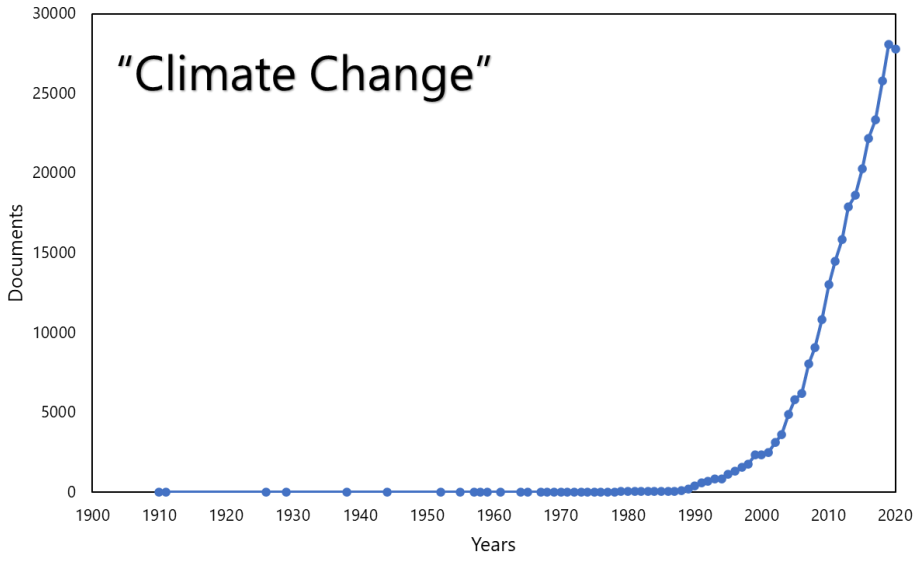

Figure 6. Time series of articles indexed in journals in the base "SCOPUS" with the term "climate change" (Search bean on 10/20/2020).

The increasing progress in the development of research focused on this area, made possible to identify that the emission of greenhouse gases could be the main responsible for the increase in the temperature of the planet due to the relationship

with the growth in the burning of fossil fuels, deforestation of forests and land-use change (Bergamaschi et al., 2018; Silva Junior et al., 2020; Rossi and Santos, 2020).

In a moment, the greenhouse effect is an important natural process for the planet since it is responsible for keeping the planet's temperature stable. Without its existence, the planet would be fully covered by ice (Schneider, 1988; Rodhe, 1990; Schuur et al., 2015; Xu and Cui, 2021). The greenhouse effect is the combination of three gases, the so-called greenhouse gases (GHG), which are carbon dioxide (CO_2), methane (CH_4) and nitrous oxide (N_2O), in addition to water vapor and fluorocarbons (Oertel et al., 2016). These gases have different heating power and concentrations in the atmosphere. The CH_4 and N_2O have a higher heating power than CO_2; however, 60% of the greenhouse gases emitted into the atmosphere corresponding to CO_2, making it the main gas responsible for the potential increase of the greenhouse effect (IPCC, 2014).

Within this context, the scientific community treats the addition of gases in the atmosphere as an "additional greenhouse effect", which would potentiate the natural greenhouse effect (Wang et al., 1976). Due to the complexity of this phenomenon, researchers from all over the world try to understand how the gas exchange between earth and atmosphere works, and what are the leading causes of the increased concentration of these gases and possible sources of GHG sinks in the most diverse regions of the world (Schwandner et al., 2017; Humphrey et al., 2018; Park et al., 2020; Babbar et al., 2021)

Each region has different anthropogenic activities, almost always related to the local economy, such as agriculture, industry, extractivism, and oil exploration. This is believed to generate different regionalized impacts (Seneviratne et al., 2016). In Brazil, agriculture deserves to be highlighted as one of the main economic activities since it holds 23% to 24% of the national GDP, and in times of crisis, it was the sector that grew the most in 2017, something around 14.5% (MAPA, 2017).

According to the IPCC, agriculture is responsible for issuing 20% of the total GHG emissions in the world. In Brazil, for example, anthropogenic activities are linked to agriculture. Cerri et al. (2007) frame Brazilian agriculture in a scenario where GHG emissions correspond to 70% of the country's total. Brazilian agriculture is an important phenomenon to be understood within climate change since, in addition to agricultural

production, it involves problems related to biological and climatic diversity because Brazil is a country of continental dimensions.

Although agriculture is an anthropogenic activity that plays an essential role in GHG emissions, it will also be one of the most affected climate change activities. For example, the increase in the temperature of the planet may change the spatial and temporal distribution of rainfall, being able to increase the risks of summers in the growing period of most crops (Ramanathan et al., 2001; Assad et al., 2008; Farhan et al., 2020). In contrast, excess rain is also a reality, which can culminate in soil degradation by erosion (Nearing et al., 2005; Serpa et al., 2015; Ciampalini et al., 2020).

In Brazil, production demand has driven the opening of new agricultural frontiers, which has resulted in deforestation and land-use changes. According to the Brazilian Climate Change Panel, between 1990 and 2005, total emissions from agriculture increased by 37%, equivalent to 114 megatons of CO_2.

Projections indicate that the increase in temperature in 3 ºC will make soybean production impossible in 50% of the territory of the state of São Paulo, and with an increase of 5.8 ºC it is estimated a reduction of 70% of the planted area for the crop throughout the country, since the corn crop would suffer less with these impacts, due to its physiological characteristic, of C4 plants, which allows greater resistance to high temperatures. However, an average increase of 5.8 ºC in global temperature would cause a decline of 5.1 million km² of the production area to 4.4 million km² (Assad et al., 2008).

1.3.4 Greenhouse gas measurements from space

Understanding the global carbon cycle is essential in developing carbon feedback projections. In this sense, remote sensing has played a key role in the last five decades (Figure 4), thanks to developing techniques capable of quantifying carbon flows and stock (Xiao et al., 2019). Due to the emergence of satellite observations of the earth's surface, research has been developed in the search for understanding of spatial patterns and temporal variability of carbon dynamics in ecosystems (Liu et al., 2014; Merrick et al., 2019; Qiu et al., 2020). CO_2 flows have been widely quantified

using normalized difference vegetation index (NDVI) (Rahman et al., 2001) or improved vegetation index (EVI) (Silva Junior et al., 2019), while carbon stocks are measured through Gross Primary Production (GPP) (Zarco-Tejada et al., 2013; Rossi and Santos, 2020).

Recently, scientists have joined forces to launch instruments capable of providing measurements of greenhouse gas concentration globally via remote sensing (Schwandner et al., 2017; Crisp and Eldering, 2018). With this, carbon flow models can be improved and contribute to the search for responses related to carbon sources and sinks in the atmosphere's biosphere and interaction.

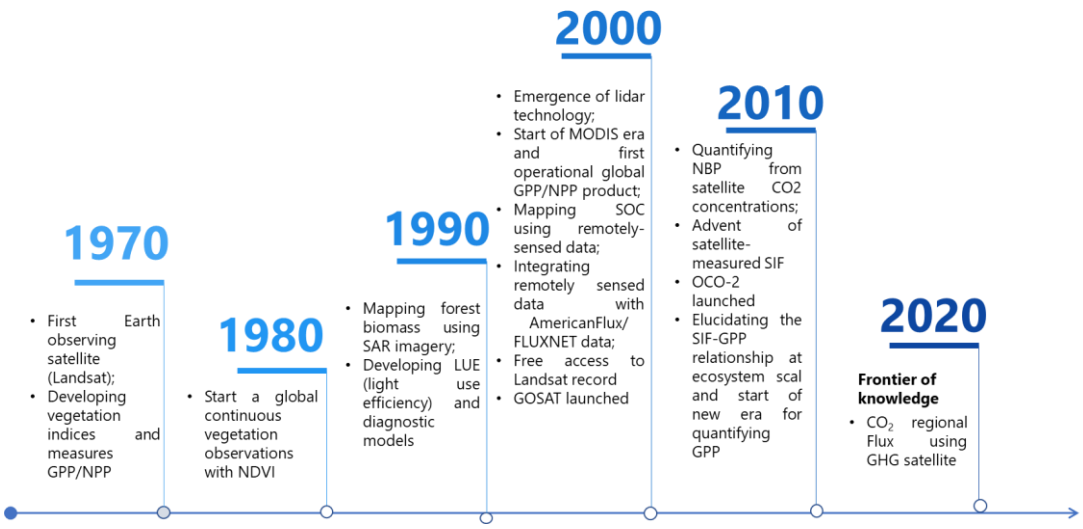

Figure 4. Milestones in remote sensing of the terrestrial C cycle (Adapted by Xiao et al., 2019).

One way to measure CO_2 from space is through the sunlight reflected from the earth's surface, so it is possible to quantify CO_2 molecules along the path of light between earth and atmosphere (Crisp et al., 2012). This measured CO_2 is termed as the average molar fraction of dry air from the carbon dioxide column or X_{CO2}. Japan's Greenhouse Gases Observing Satellite (GOSAT) and the NASA Orbiting Carbon Observatory-2 (OCO-2) use this method (Yokota et al., 2009; Annmarie Eldering et al., 2017).

Despite the recent launch of OCO-2 in 2014, satellites capable of measuring CO_2 in the atmosphere have been around for about two decades. In 2002, the

Atmospheric Infrared Sounder from the National Aeronautics and Space Administration (AIRS-NASA) Scanning Imaging Absorption spectroMeter for Atmospheric CHartographY from European Space Agency (SCIAMACHY-ESA) were launched, both able of doing this monitoring, but these missions were closed in 2012 (Pan et al., 2021). NASA launched AURA in July 2004 with the Tropospheric Emission Spectrometer (TES) with a better spatial resolution than AIRS and SCIAMACHY. The Greenhouse Gases Observing Satellite (GOSAT) was launched in January 2009 by Japanese national Aerospace (JAXA) to detect CO_2 and CH_4 (Yokota et al., 2009; Frankenberg et al., 2011). The GOSAT can observe CO_2 at a spatial resolution of 10X10 km with a three-day return interval. NASA launched the OCO-2 in July 2014 with a spatial resolution of 1.29 x 2.25 km and a 16-day temporal (Crisp et al., 2017; Schwandner et al., 2017). In December 2016, China launched the carbon satellite (TANSAT) with a spatial and temporal resolution much like that of the OCO-2 (Liu et al., 2018; Yang et al., 2018). In October 2018, JAXA launched GOSAT-2, delivering a much more robust performance than GOSAT (Yoshida et al., 2019). In 2019, NASA launched the OCO-3 that brought denser observations at sampling sites (Eldering et al., 2019; Taylor et al., 2021).

Regarding the research developed with GOSAT data (Figure 5), from 2009 to 2021, 707 documents have already been published according to the search made in the SCOPUS database on October 22, 2020. The country that presented the highest number of published documents was Japan (executing country of the project) (Figure 5B), followed by the United States, China, and Germany. Unfortunately, Brazil does not appear among the ten countries precisely because it has only four documents published. In the field of research (Figure 5C), planetary sciences lead the ranking, environmental and agricultural sciences are in seventh and 8th, representing 6.8 and 4.3% of all published documents.

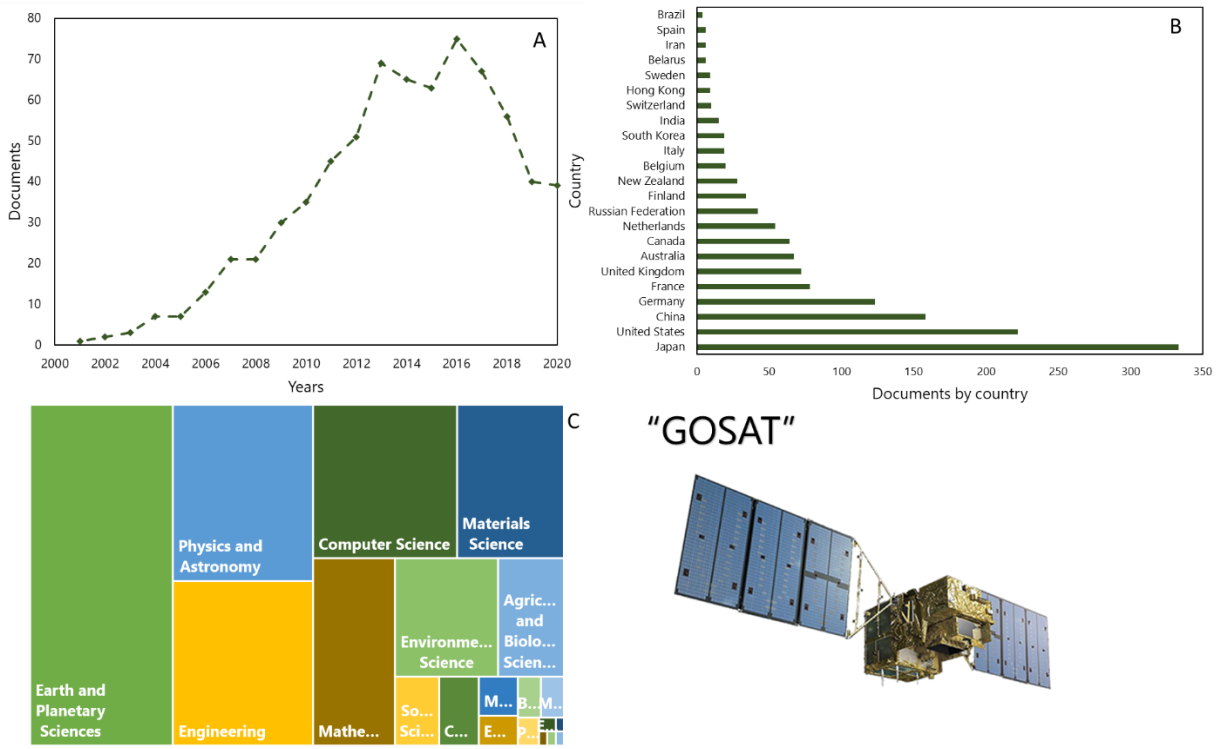

Figure 5. Documents indexed in journals in the base of SCOPUS with the term "GOSAT" by year (A), country (B) and subject area (C) (Search bean on 11/10/2020).

For OCO-2, the number of published documents is even lower, only 353 documents (Figure 6A), with the USA the leader (Figure 6B), followed by China, Germany, and Australia. Brazil once again does not appear in this search. As in GOSAT, planetary sciences lead among research fields that use OCO-2 (Figure 6C), environmental and agrarian sciences are in 6th and 7th, representing 7.3 and 6.7% in total, respectively. In general, OCO-2 data have been more applied in environmental and agricultural sciences compared to GOSAT.

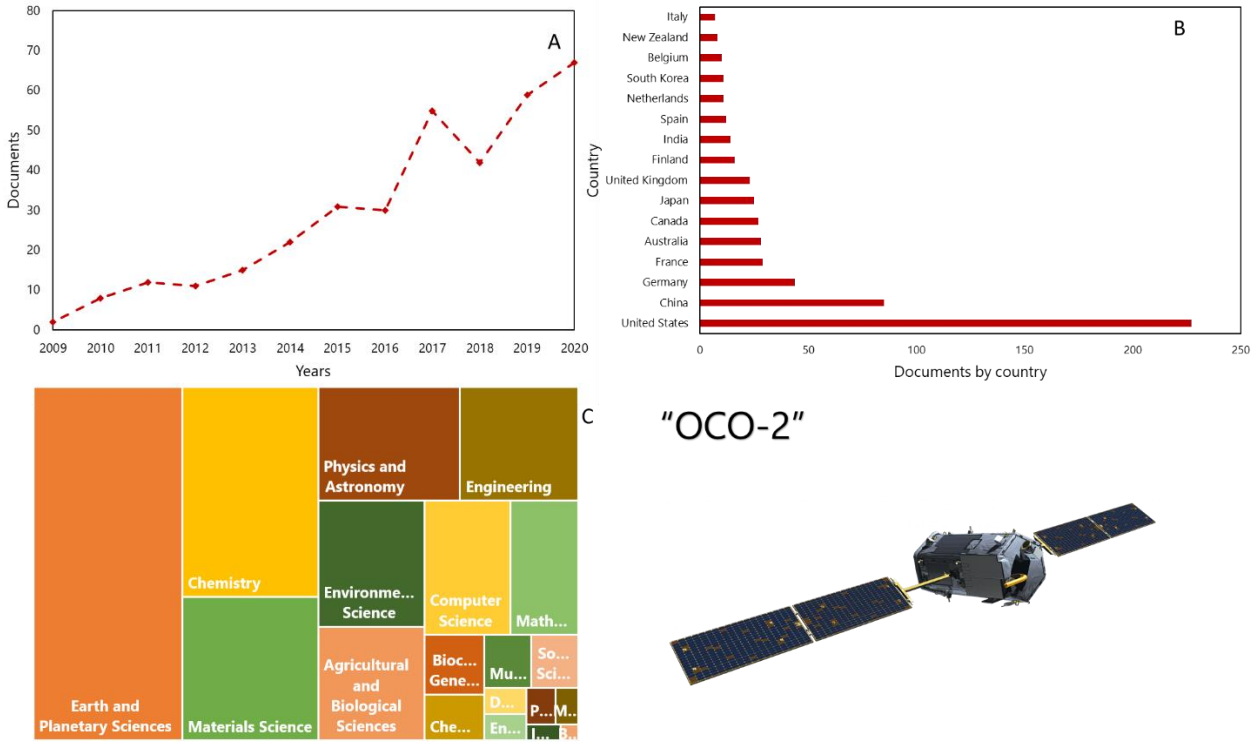

Figure 6. Documents indexed in journals in the base of SCOPUS with the term "OCO-2" by year (A), country (B) and subject area (C) (Search bean on 10/20/2020).

Understand the carbon cycle in ecosystems is essential to make better predictions regarding climate change in the future. In this respect, satellite data emerges as an alternative and should be used more widely in the most diverse areas of knowledge, especially in the environment and agriculture areas.

1.3.5 Big data era: The role of remote sensing on the carbon feedbacks

By the advancement of technology, access to computers, the internet, and sensors available for access to the population, we have achieved an explosion in data generation, never seen before. Especially in the last 20 years, there has been a huge increase in data in the most diverse knowledge areas.

In the last decade, the industrial sector has been interested in the high potential of big data use, and many government agencies have begun announcing big plans to accelerate big data applications, such as the White House in the United States, which

has invested more than $1 billion in the "Big Data Across the Federal Government" program (WH, 2012). Besides, the scientific journals Nature and Science have launched special editions to discuss big data challenges and impacts (NATURE, 2008; Science, 2011). The era of big data has already arrived for all and is the new frontier of innovation, productivity, and competitiveness (Majumdar et al., 2017; Sekhar et al., 2018; Lioutas, 2020)

With satellite monitoring, weather stations, the growing increase in the publication of scientific articles, the emergence of several platforms with open access databases and the Internet of Things (IoT) within the area of knowledge involving agriculture and the environment, the era of big data is already a reality. It estimated that investment in big data analysis applied to agriculture could generate profitability on top of the harvest around 20 billion dollars annually (Bunge, 2014)

The definition of big data is still an abstract concept, but it can already be characterized by five dimensions, which include volume, speed, variety, veracity, and valorization, the well-known 5V's (Chen et al., 2014). However, an essential part in the use of big data is related to the value of the knowledge generated, which will help in decision making, increasing mainly profitability, whether financial, environmental, or even in reducing the time to perform some activities, but all this is only possible if the sources of the databases are reliable since with reliable data must have answers with credibility.

Most databases built to study climate and greenhouse gas emissions comprise a time series, especially those using satellite data (Liu, 2015; Ma et al., 2015; Huang et al., 2018; Xu et al., 2020). The use of satellite databases is essential for studies involving climate change and has already resulted in important scientific journals (Silva Junior et al., 2020; C. Silva Junior et al., 2020; Huang et al., 2020; Peter and Messina, 2020)

As already mentioned in previous topics, remote sensing has emerged as an important tool to understand the carbon cycle. Today, it is possible to map CO_2 flows, detect changing land use, and obtain carbon feedback through satellites. Table 1 shows a list of variables that can be obtained free of charge, which helps understand the carbon cycle.

Table 1. Variables and sources for obtaining open access data related to the carbon cycle.

Group	Variable	Source	Coverage
VEGETATION	NDVI-EVI	MODIS	Global
	LAI		Global
	GPP		Global
	NPP		Global
	SIF	OCO-2/GOSAT	Global
	Evapotranspiration	MODIS/ SMAP	
GHG	X_{CO2}	OCO-2/GOSAT	Global
	X_{CH4}		Global
SOIL	Soil Moisture	SMAP/ESA	Global
	Soil classes	SoilGrids	Global
	Soil texture		Global
	Soil Ph		Global
	Soil Organic		Global
	Soil Nitrogen		Global
LAND USE	Land Use Change	MapBiomas	Brazil
	Land Use	LAPIG	Brazil
	Crop Production	SIDRAS -IBGE	Brazil
	Soybean lands	SOJAMAPS	Brazil
	Land Use Change	INPE	Brazil
WEATHER	Climate variables	NASA POWER INMET	Global/Brazil

The dynamics of vegetation has been observed for decades through the calculation of spectral issues. The most famous indexes are the Normalized Difference Vegetation Index (NDVI) (Rouse et al., 1973) and the Improved Vegetation Index (EVI) (Huete et al., 1997). NDVI is calculated NDVI = (NIR + RED) / (NIR - RED) where RED and NIR are the spectral reflectance in the visible red and near-infrared region of the

photosynthetically active radiation spectrum, respectively (François et al., 2019). Other data provided by MODIS, such as Area Foliar Lai Index, GPP, and NPP, are widely used in the carbon cycle studies. Both the leaf area index (LAI) and the fraction of photosynthetically active radiation absorbed by vegetation (fAPAR) can represent the biophysically complimentary forms in the description of vegetation that covers the earth's surface (Fan et al., 2019). The LAI consists of the one-sided green leaf area per unit of soil area in the broadleaf canopy. MODIS also provides gross primary production (GPP). In general, it represents carbon inputs into the ecosystem through photosynthesis. Its application has been carried out in several studies to understand the carbon cycle in adverse situations.

A significant advance in remote sensing was the recovery of sun-induced chlorophyll fluorescence (SIF) (François et al., 2019; Xiao et al., 2019). Biologically, within the leaves of plants, sunlight is absorbed by chloroplasts. After this process, the absorbed energy can be used to conduct reactions that have as product glucose. When the plant cannot use all the energy absorbed in glucose production, excess energy needs to be released. This is usually done by heat dissipation or through the fluorescence of sunlight (Frankenberg et al., 2014; Mohammed et al., 2019) (Figure 7).

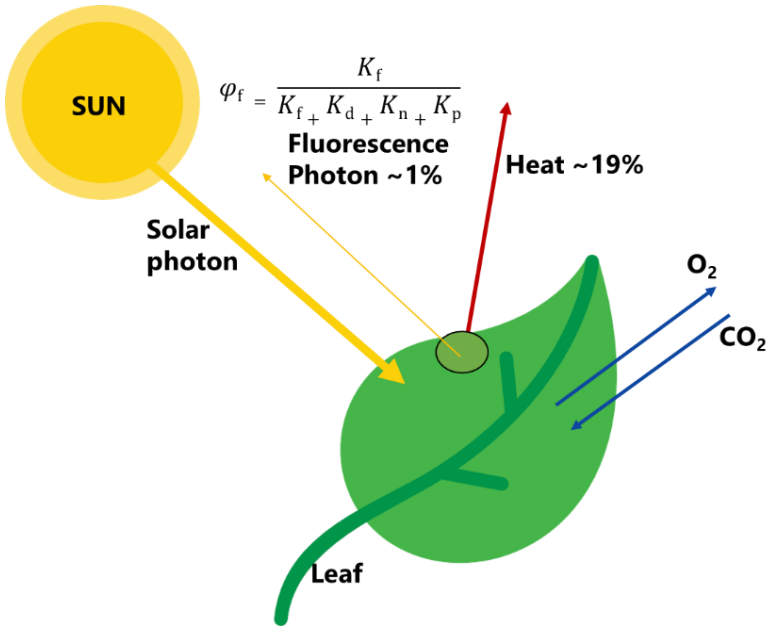

Figure 7. Arrays of chlorophyll molecules bound to protein absorb and process solar photons in plant leaves. A variable fraction (φf, typically ~1%) of these leaks back out as fluorescent photons. The absorbed photon can be lost as

radiationless decay (Kd), re-emitted as a fluorescent photon (Kf), quenched by NPQs (Kn), or used for photochemistry (Kp) (Frankenberg et al., 2013).

Unlike other spectral indices, SIF is related to the internal processes of photosynthesis. Thus, it can indicate photosynthetically active vegetation, while NDVI and EVI only detect the presence of green leaves. Fluorescence emitted under the influence of sunlight has its peaks of 730-740nm (near-infrared) and another peak of 685-690nm (red spectral) (Mohammed et al., 2019). However, despite the peaks, SIF can be detected between the 650-800nm bands. It is important to note that both photosystem I and photosystem II are detected in this spectrum range (Figure 8).

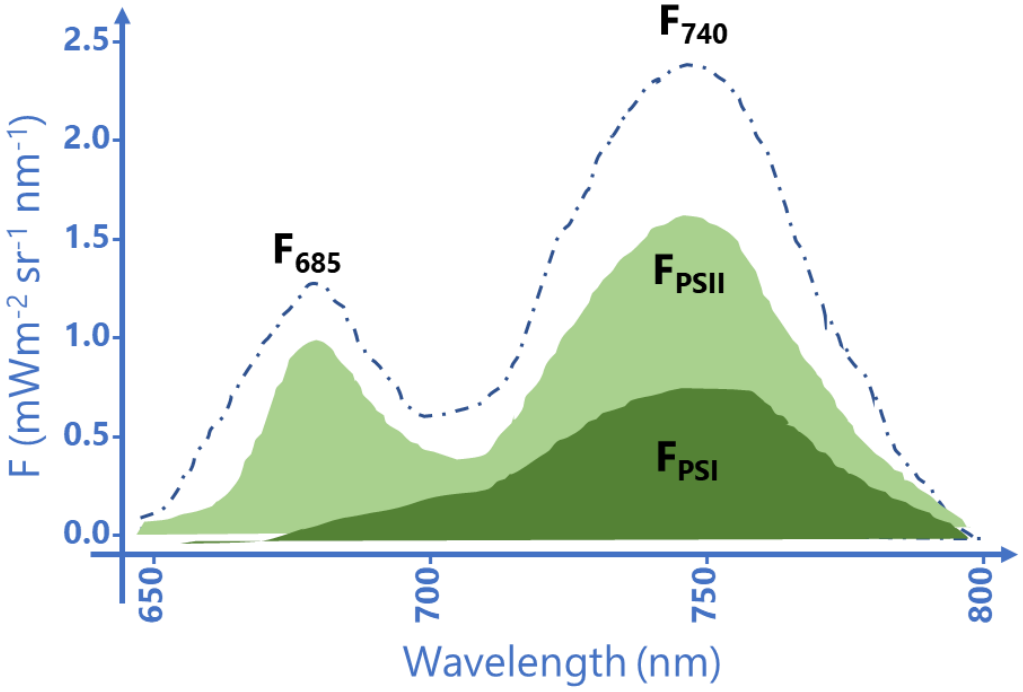

Figure 8. Spectral detection of sun-induced chlorophyll fluorescence (Mohammed et al., 2019).

After this, the potential and variability of the remote-sensing big data application in environmental studies are clear. The scientific community should explore this potential, mainly in developing countries where the recourses to make experimental science are reduced. The feedback founded from this data could help make political governance in climate change mitigation beyond developing the regional carbon models.

REFERENCES

ARAÚJO SANTOS, G. A. DE; MOITINHO, M. R.; OLIVEIRA SILVA, B. DE; XAVIER, C. V.; TEIXEIRA, D. D. B.; CORÁ, J. E.; JÚNIOR, N. L. S. Effects of long-term no-tillage systems with different succession cropping strategies on the variation of soil CO2 emission. **Science of the Total Environment**, v. 686, p. 413–424, 2019.

BABBAR, D.; AREENDRAN, G.; SAHANA, M.; SARMA, K.; RAJ, K.; SIVADAS, A. Assessment and prediction of carbon sequestration using Markov chain and InVEST model in Sariska Tiger Reserve, India. **Journal of Cleaner Production**, v. 278, p. 123333, 2021.

BERGAMASCHI, P. *et al.* **Atmospheric monitoring and inverse modelling for verification of greenhouse gas inventories**.

BUNGE, B. J. **Big Data Comes to the Farm , Sowing Mistrust: Seed Makers Barrel Into Technology Business**. Disponível em: <https://www.wsj.com/articles/SB10001424052702304450904579369283869192124>.

CERRI, C. E. P.; SPAROVEK, G.; BERNOUX, M.; EASTERLING, W. E.; MELILLO, J. M.; CERRI, C. C. Tropical agriculture and global warming: Impacts and mitigation options. **Scientia Agricola**, v. 64, n. 1, p. 83–99, 2007.

CHEN, M.; MAO, S.; LIU, Y. Big Data : A Survey. n. January, p. 171–209, 2014.

CHEN XU , XIAOPING DU, Z. Y. AND X. F. ScienceEarth : A Big Data Platform for Remote Sensing Data Processing. **Remote Sensing**, v. 607, n. 12, p. 2–20, 2020.

CHHABRA, A.; GOHEL, A. Dynamics of atmospheric carbon dioxide over different land cover types in India. **Environmental Monitoring and Assessment**, v. 191, n. July 2014, 2019.

CHI, M.; PLAZA, A.; BENEDIKTSSON, J. A.; SUN, Z.; SHEN, J.; ZHU, Y. Big Data for Remote Sensing: Challenges and Opportunities. **Proceedings of the IEEE**, v. 104, n. 11, p. 2207–2219, 2016.

CIAMPALINI, R.; CONSTANTINE, J. A.; WALKER-SPRINGETT, K. J.; HALES, T. C.; ORMEROD, S. J.; HALL, I. R. Science of the Total Environment Modelling soil erosion responses to climate change in three catchments of Great Britain. **Science of the Total Environment**, v. 749, p. 141657, 2020.

COMMITTEE, N. R. C. AND C. R. **Understanding Climate Change Feedbacks**. [s.l: s.n.].

CRISP, D. *et al.* The ACOS CO 2 retrieval algorithm - Part II: Global X CO2 data characterization. **Atmospheric Measurement Techniques**, v. 5, n. 4, p. 687–707, 2012.

CRISP, D. *et al.* The on-orbit performance of the Orbiting Carbon Observatory-2 (OCO-2) instrument and its radiometrically calibrated products. **Atmospheric Measurement Techniques**, v. 10, n. 1, p. 59–81, 2017.

CRISP, D.; ELDERING, A. Precision , Accuracy , Resolution , and Coverage : A few insights from GOSAT and OCO-2. 2018.

CRISP, D.; JOHNSON, C. The orbiting carbon observatory mission. **Acta Astronautica**, v. 56, n. 1–2, p. 193–197, 2005.
DIFFENBAUGH, N. S.; SWAIN, D. L.; TOUMA, D. Anthropogenic warming has increased drought risk in California. v. 112, n. 13, p. 3931–3936, 2015.

EDUARDO ASSAD, HILTON PINTO, JURANDIR ZULLO JR, FÁBIO MARIN, G. P. **Mudanças climáticas e a produção de grãos no Brasil : avaliação dos possíveis impactos**, 2008.

ELDERING, ANNMARIE *et al.* The Orbiting Carbon Observatory-2: First 18 months of science data products. **Atmospheric Measurement Techniques**, v. 10, n. 2, p. 549–563, 2017.

ELDERING, A. *et al.* The Orbiting Carbon Observatory-2 early science investigations of regional carbon dioxide fluxes. **Science**, v. 358, n. 6360, 2017.

ELDERING, A.; TAYLOR, T. E.; DELL, C. W. O.; PAVLICK, R. The OCO-3 mission : measurement objectives and expected performance based on 1 year of simulated data. p. 2341–2370, 2019.

F. STUART CHAPIN, PAMELA A. MATSON, P. M. V. **Principles of terrestrial ecosystem ecology**. Second edi ed. [s.l: s.n.]. v. 40

FAN, L. *et al.* Satellite-observed pantropical carbon dynamics. **Nature Plants**, v. 5, n. 9, p. 944–951, 2019.

FARHAN, M.; MOAZZAM, U.; LEE, B. G.; RAHMAN, G.; WAQAS, T. Spatial Rainfall Variability and an Increasing Threat of Drought , According to Climate Change in Uttaradit Province , Thailand. **Atmospheric and Climate Sciences**, v. 10, n. June, p. 357–370, 2020.

FINZI, A. C.; AUSTIN, A. T.; CLELAND, E. E.; FREY, S. D.; HOULTON, B. Z.; WALLENSTEIN, M. D. Responses and feedbacks of coupled biogeochemical cycles to climate change : examples from terrestrial ecosystems In a nutshell : 2011.

FRANÇOIS, J.; ANTHONY, E. A.; NUNO, B.; FISCHER, R. Understanding the Land Carbon Cycle with Space Data : Current Status and Prospects. **Surveys in Geophysics**, v. 40, n. 4, p. 735–755, 2019.

FRANKENBERG, C.; BERRY, J.; GUANTER, L. Remote sensing of terrestrial chlorophyll fluorescence from space. **SPIE Newsroom**, p. 2–5, 2013.

FRANKENBERG, C.; DREWRY, D.; GEIER, S.; VERMA, M.; LAWSON, P.; STUTZ, J.; GROSSMANN, K. Remote sensing of solar induced Chlorophyll Fluorescence from satellites, airplanes and ground-based stations. **International Geoscience and Remote Sensing Symposium (IGARSS)**, v. 2016- Novem, p. 1707–1710, 2016.

FRANKENBERG, C.; FISHER, J. B.; WORDEN, J.; BADGLEY, G.; SAATCHI, S. S.; LEE, J. E.; TOON, G. C.; BUTZ, A.; JUNG, M.; KUZE, A.; YOKOTA, T. New global observations

of the terrestrial carbon cycle from GOSAT: Patterns of plant fluorescence with gross primary productivity. **Geophysical Research Letters**, v. 38, n. 17, p. 1–6, 2011.

FRANKENBERG, C.; O'DELL, C.; BERRY, J.; GUANTER, L.; JOINER, J.; KÖHLER, P.; POLLOCK, R.; TAYLOR, T. E. Prospects for chlorophyll fluorescence remote sensing from the Orbiting Carbon Observatory-2. **Remote Sensing of Environment**, v. 147, p. 1–12, 2014.

FU, B. *et al.* Short-lived climate forcers have long-term climate impacts via the carbon–climate feedback. **Nature Climate Change**, v. 10, n. 9, p. 851–855, 2020.

GAO, Y.; WANG, S.; GUAN, K.; WOLANIN, A.; YOU, L.; JU, W.; ZHANG, Y. The ability of sun-induced chlorophyll fluorescence from OCO-2 and MODIS-EVI to monitor spatial variations of soybean and maize yields in the midwestern USA. **Remote Sensing**, v. 12, n. 7, 2020.

GONSAMO, A.; CHEN, J. M. Vegetation primary productivity. **Comprehensive Remote Sensing**, v. 1–9, n. April, p. 163–189, 2017.

GOODWIN, P. Quantifying the Terrestrial Carbon Feedback to Anthropogenic Carbon Emission. **Earth's Future**, v. 7, n. 12, p. 1417–1433, 2019.

GOODWIN, P.; WILLIAMS, R. G.; ROUSSENOV, V. M.; KATAVOUTA, A. Climate Sensitivity From Both Physical and Carbon Cycle Feedbacks. **Geophysical Research Letters**, v. 46, n. 13, p. 7554–7564, 2019.

HE, Z.; LEI, L.; ZENG, Z. C.; SHENG, M.; WELP, L. R. Evidence of carbon uptake associated with vegetation greening trends in Eastern China. **Remote Sensing**, v. 12, n. 4, 2020.

HUANG, N. *et al.* Spatial and temporal variations in global soil respiration and their relationships with climate and land cover. n. October, p. 1–12, 2020.

HUANG, Y.; ZHONG-XIN, C.; TAO, Y. U.; XIANG-ZHI, H.; XING-FA, G. U. Agricultural remote sensing big data: Management and applications. **Journal of Integrative Agriculture**, v. 17, n. 9, p. 1915–1931, 2018.

HUMPHREY, V.; ZSCHEISCHLER, J.; CIAIS, P.; GUDMUNDSSON, L.; SITCH, S.; SENEVIRATNE, S. I. Sensitivity of atmospheric CO2 growth rate to observed changes in terrestrial water storage. **Nature**, v. 560, n. 7720, p. 628–631, 2018.

HUTYRA, L. Terrestrial Ecosystems & the Carbon Cycle. **Global Change Biol.**, v. 1, n. December 1994, p. 77–91, 2014.

JR, N. L. S.; JR, J. M.; PEREIRA, G. T.; CORA, J. E. Short-term temporal changes in the spatial variability model of CO 2 emissions from a Brazilian bare soil. v. 32, p. 0–3, 2000.

KAMILARIS, A.; KARTAKOULLIS, A.; PRENAFETA-BOLDÚ, F. X. A review on the practice of big data analysis in agriculture. **Computers and Electronics in Agriculture**, v. 143, n. October, p. 23–37, 2017.

LAL, R. Soil carbon sequestration to mitigate climate change. **Geoderma**, v. 123, n. 1–2, p. 1–22, 2004.

LIOUTAS, E. D. Geoforum Big data in agriculture : Does the new oil lead to sustainability ? v. 109, n. September 2019, p. 1–3, 2020.

LIU, J., Bowman, K.W., Lee, M., Henze, D.K., Bousserez, N., Brix, H., James Collatz, G., Menemenlis, D., Ott, L., Pawson, S. and Jones, D., Carbon monitoring system flux estimation and attribution: Impact of ACOS-GOSAT XCO2 sampling on the inference of terrestrial biospheric sources and sinks. **Tellus, Series B: Chemical and Physical Meteorology**, v. 66, n. 1, 2014.

LIU, P. A survey of remote-sensing big data. v. 3, n. June, p. 1–6, 2015.

LIU, Y.; WANG, J.; YAO, L.; CHEN, X.; CAI, Z.; YANG, D.; YIN, Z.; GU, S.; TIAN, L.; LU, N.; LYU, D. The TanSat mission : preliminary global observations. **Science Bulletin**, v. 63, n. 18, p. 1200–1207, 2018.

MA, Y.; WU, H.; WANG, L.; HUANG, B.; RANJAN, R.; ZOMAYA, A. Remote sensing big data computing : Challenges and opportunities. **Future Generation Computer Systems**, v. 51, p. 47–60, 2015.

MADANI, N.; KIMBALL, J. S.; JONES, L. A.; PARAZOO, N. C.; GUAN, K. Global analysis of bioclimatic controls on ecosystem productivity using satellite observations of solar-induced chlorophyll fluorescence. **Remote Sensing**, v. 9, n. 6, 2017.

MAJUMDAR, J.; NARASEEYAPPA, S.; ANKALAKI, S. Analysis of agriculture data using data mining techniques : application of big data. **Journal of Big Data**, 2017.

MEDHAUG, I.; STOLPE, M. B.; FISCHER, E. M.; KNUTTI, R. Reconciling controversies about the "global warming hiatus". **Nature**, v. 545, n. 7652, p. 41–47, 2017.

MERRICK, T.; PAU, S.; JORGE, M. L. S. P.; SILVA, T. S. F.; BENNARTZ, R. Spatiotemporal patterns and phenology of tropical vegetation solar-induced chlorophyll fluorescence across brazilian biomes using satellite observations. **Remote Sensing**, v. 11, n. 15, 2019.

MOHAMMED, G. H. *et al.* Remote sensing of solar-induced chlorophyll fluorescence (SIF) in vegetation: 50 years of progress. **Remote Sensing of Environment**, v. 231, n. February, p. 111177, 2019.

NATURE. **Big data: Science in a petabyte era**. Disponível em: <https://www.nature.com/nature/volumes/455/issues/7209>. Acesso em: 23 out. 2020.

NEARING, M. A.; JETTEN, V.; BAFFAUT, C.; CERDAN, O.; COUTURIER, A. Modeling response of soil erosion and runoff to changes in precipitation and cover. v. 61, p. 131–154, 2005.

ANDRÉN; T. KÄTTERER. **Ecosystem Ecology**. [s.l: s.n.]. v. Ecosystem

OERTEL, C.; MATSCHULLAT, J.; ZURBA, K.; ZIMMERMANN, F.; ERASMI, S. Greenhouse gas emissions from soils — A review. 2016.

PAN, G.; XU, Y.; MA, J. The potential of CO 2 satellite monitoring for climate governance : A review. **Journal of Environmental Management**, v. 277, n. September 2020, p. 111423, 2021.

PARAZOO, N. C.; COMMANE, R.; WOFSY, S. C.; KOVEN, C. D.; SWEENEY, C.; LAWRENCE, D. M.; LINDAAS, J.; CHANG, R. Y.; MILLER, C. E. Detecting regional patterns of changing CO 2 flux in Alaska. n. 12, 2016.

PARK, H.; TAKEUCHI, W.; ICHII, K. Satellite-based estimation of carbon dioxide budget in tropical peatland ecosystems. **Remote Sensing**, v. 12, n. 2, p. 1–21, 2020.
PETER, B. G.; MESSINA, J. P. Crop climate suitability mapping on the cloud : a geovisualization application for sustainable agriculture. **Scientific Reports**, p. 1–17, 2020.

PIAO, S.; WANG, X.; WANG, K.; LI, X.; BASTOS, A.; CANADELL, J. G.; CIAIS, P.; FRIEDLINGSTEIN, P.; SITCH, S. Interannual variation of terrestrial carbon cycle: Issues and perspectives. **Global Change Biology**, v. 26, n. 1, p. 300–318, 2020.

QIU, R.; HAN, G.; MA, X.; SHA, Z.; SHI, T.; XU, H.; ZHANG, M. CO2 concentration, a critical factor influencing the relationship between solar-induced chlorophyll fluorescence and gross primary productivity. **Remote Sensing**, v. 12, n. 9, 2020.

QUAN, Q.; TIAN, D.; LUO, Y.; ZHANG, F.; CROWTHER, T. W.; ZHU, K.; CHEN, H. Y. H.; ZHOU, Q.; NIU, S. Water scaling of ecosystem carbon cycle feedback to climate warming. **Science Advances**, v. 5, n. 8, p. 1–8, 2019.

QUÉRÉ, C. LE; MORIARTY, R.; ANDREW, R. M.; PETERS, G. P.; CIAIS, P.; FRIEDLINGSTEIN, P.; JONES, S. D. Global carbon budget 2014. p. 47–85, 2015.

RAHMAN, A. F.; GAMON, J. A.; FUENTES, D. A.; ROBERTS, D. A.; PRENTISS, D. Modeling spatially distributed ecosystem flux of boreal forest using hyperspectral indices from AVIRIS imagery. **Journal of Geophysical Research Atmospheres**, v. 106, n. D24, p. 33579–33591, 2001.

RAMANATHAN, V.; CRUTZEN, P. J.; KIEHL, J. T.; ROSENFELD, D. Aerosols, Climate, and the Hydrological Cycle. **Science (New York, N.Y.)**, v. 294, n. December, p. 2119–2125, 2001.

RODHE, H. A comparison of the contribution of various gases to the greenhouse effect. **Science**, v. 248, n. 4960, p. 1217–1219, 1990.

ROSSI, F. S.; SANTOS, G. A. DE A. Fire dynamics in Mato Grosso State, Brazil: the relative roles of gross primary productivity. **Big Earth Data**, v. 4, n. 1, p. 23–44, 2020.

RYU, Y.; BERRY, J. A.; BALDOCCHI, D. D. What is global photosynthesis? History, uncertainties and opportunities. **Remote Sensing of Environment**, v. 223, n. January, p. 95–114, 2019.

SCHIMEL, D.; STEPHENS, B. B.; FISHER, J. B. Effect of increasing CO2 on the terrestrial carbon cycle. **Proceedings of the National Academy of Sciences of the United States of America**, v. 112, n. 2, p. 436–441, 2015.
SCHNEIDER, S. H. Greenhouse Effect: Science and. **Science Research Articles**, v. 243, n. 7, p. 771–779, 1988.

SCHUUR, E. A. G. *et al.* Climate change and the permafrost carbon feedback. **Nature**, v. 520, n. 7546, p. 171–179, 2015.

SCHWANDNER, F. M. *et al.* Spaceborne detection of localized carbon dioxide sources. **Science**, v. 358, n. 6360, 2017.

SCIENCE. **Special Online Collection: Dealing with Data**. Disponível em: <https://www.sciencemag.org/site/special/data/>. Acesso em: 23 out. 2020.

SEKHAR, C. C.; KUMAR, J. U.; KUMAR, B. K.; SEKHAR, C. Effective use of Big Data Analytics in Crop planning to increase Agriculture Production in India. **International Journal of Advanced Science and Technology**, v. 113, p. 31–40, 2018.

SELLERS, P. J.; SCHIMEL, D. S.; MOORE, B.; LIU, J.; ELDERING, A. Observing carbon cycle–climate feedbacks from space. **Proceedings of the National Academy of Sciences of the United States of America**, v. 115, n. 31, p. 7860–7868, 2018.

SENEVIRATNE, S. I.; CORTI, T.; DAVIN, E. L.; HIRSCHI, M.; JAEGER, E. B.; LEHNER, I.; ORLOWSKY, B.; TEULING, A. J. Earth-Science Reviews Investigating soil moisture – climate interactions in a changing climate : A review. **Earth Science Reviews**, v. 99, n. 3–4, p. 125–161, 2010.

SENEVIRATNE, S. I.; DONAT, M. G.; PITMAN, A. J.; KNUTTI, R.; WILBY, R. L. Allowable CO2 emissions based on regional and impact-related climate targets. **Nature**, v. 529, n. 7587, p. 477–483, 2016.

SERPA, D.; NUNES, J. P.; SANTOS, J.; SAMPAIO, E.; JACINTO, R.; VEIGA, S.; LIMA, J. C.; MOREIRA, M.; CORTE-REAL, J.; KEIZER, J. J.; ABRANTES, N. Science of the Total Environment Impacts of climate and land use changes on the hydrological and erosion processes of two contrasting Mediterranean catchments. **Science of the Total Environment, The**, v. 538, p. 64–77, 2015.

SHANNON, M. **How does NASA use big data?** Disponível em: <https://bigdata-madesimple.com/how-does-nasa-use-big-data/>. Acesso em: 27 out. 2020.

SILVA, B. DE O.; MOITINHO, M. R.; SANTOS, G. A. DE A.; TEIXEIRA, D. D. B.; FERNANDES, C.; SCALA, N. LA. Soil CO2 emission and short-term soil pore class distribution after tillage operations. **Soil and Tillage Research**, v. 186, n. October 2018, p. 224–232, 2019.
SILVA JUNIOR, C.A., Teodoro, P.E., Delgado, R.C., Teodoro, L.P.R., Lima, M., de Andréa Pantaleão, A., Baio, F.H.R., de Azevedo, G.B., Azevedo, G.T.D.O.S., Capristo-Silva, G.F. and Arvor, D., Persistent fire foci in all biomes undermine the Paris Agreement in Brazil. **Scientific Reports**, p. 1–14, 2020.

SILVA JUNIOR, C. A. DA; COSTA, G. DE M.; ROSSI, F. S.; VALE, J. C. E. DO; LIMA, R. B. DE; LIMA, M.; OLIVEIRA-JUNIOR, J. F. DE; TEODORO, P. E.; SANTOS, R. C. Remote

sensing for updating the boundaries between the brazilian Cerrado-Amazonia biomes. **Environmental Science and Policy**, v. 101, n. December 2018, p. 383–392, 2019.

SILVA JUNIOR, C. H. L. *et al.* Persistent collapse of biomass in Amazonian forest edges following deforestation leads to unaccounted carbon losses. **Science Advances**, v. 6, n. 40, p. eaaz8360, 2020.

TAYLOR, T. E. *et al.* Remote Sensing of Environment OCO-3 early mission operations and initial (vEarly) XCO 2 and SIF retrievals. **Remote Sensing of Environment**, v. 251, n. July 2020, p. 112032, 2021.

USSIRI, D. A. N.; LAL, R. **Carbon Sequestration for Climate Change Mitigation and Adaptation**. [s.l: s.n.].

W. C. WANG, Y. L. YUNG, A. A. LACIS, T. MO, J. E. H. SCIE NC : E Greenhouse Effects due to Man-Mad. v. 194, n. 4266, p. 685–690, 1976.

WALLACE, J. M.; HOBBS, P. V. **Atmospheric Science: An Introductory Survey: Second Edition**. [s.l: s.n.].

WH. **FACT SHEET : Big Data Across the Federal Government**. Disponível em: <https://obamawhitehouse.archives.gov/the-press-office/2015/12/04/fact-sheet-big-data-across-federal-government>. Acesso em: 23 out. 2020.

WILLIAMS, R. G.; KATAVOUTA, A.; GOODWIN, P. Carbon-Cycle Feedbacks Operating in the Climate System. **Current Climate Change Reports**, v. 5, n. 4, p. 282–295, 2019.

XAVIER, C. V.; MOITINHO, M. R.; TEIXEIRA, D. D. B.; ARAÚJO SANTOS, G. A. DE; CORÁ, J. E.; SCALA, N. LA. Crop rotation and sequence effects on temporal variation of CO2 emissions after long-term no-till application. **Science of the Total Environment**, v. 709, p. 136107, 2020.

XIAO, J. *et al.* Remote sensing of the terrestrial carbon cycle: A review of advances over 50 years. **Remote Sensing of Environment**, v. 233, n. January, p. 111383, 2019.
XU, Y.; CUI, G. Influence of spectral characteristics of the Earth's surface radiation on the greenhouse effect: Principles and mechanisms. **Atmospheric Environment**, v. 244, n. 516, p. 117908, 2021.

YANG, D.; LIU, Y.; CAI, Z.; CHEN, X.; YAO, L.; LU, D. First Global Carbon Dioxide Maps Produced from TanSat Measurements. p. 1–3, 2018.

YOKOTA, T.; YOSHIDA, Y.; EGUCHI, N.; OTA, Y.; TANAKA, T.; WATANABE, H.; MAKSYUTOV, S. Global concentrations of CO2 and CH4 retrieved from GOSAT: First preliminary results. **Scientific Online Letters on the Atmosphere**, v. 5, n. 1, p. 160–163, 2009.

YOSHIDA, Y.; OSHIO, H.; SOMEYA, Y.; OHYAMA, H.; KAMEI, A.; MORINO, I. **Atmospheric Carbon Dioxide and Methane Observations by** Optical Sensors and Sensing Congress. **Anais**...2019

ZARCO-TEJADA, P. J.; MORALES, A.; TESTI, L.; VILLALOBOS, F. J. Spatio-temporal patterns of chlorophyll fluorescence and physiological and structural indices acquired from hyperspectral imagery as compared with carbon fluxes measured with eddy covariance. **Remote Sensing of Environment**, v. 133, p. 102–115, 2013.

ZHALEH SIABIA, SAMEREH FALAHATKARB, S. J. A. Spatial distribution of XCO 2 using OCO-2 data in growing seasons. **Journal of Environmental Management**, v. 244, n. May, p. 110–118, 2019.

CHAPTER 2 – The role of the vegetation and the weather on the temporal variability of X_{CO2} and SIF: A perspective to biomes and planted forest in Brazil

ABSTRACT – Understanding the dynamics of carbon for detecting sources and sinks in large areas, especially in agricultural or forestry areas, is a challenge to be overcome. Recently, remote sensing techniques have been an alternative in studies aimed at evaluating carbon dynamics. The objective of this study was to characterize the temporal variability of the carbon dioxide (CO_2) column-averaged dry-air mole fraction (X_{CO2}) and Solar Induced Fluorescence (SIF) and its main control factors in biomes and planted forests with eucalyptus in the state of Mato Grosso do Sul, Brazil with the use of remote sensing data. A time series was analyzed from January 2015 to December 2018. The variables X_{CO2}, Solar-induced fluorescence at 757nm and 771nm were extracted from OCO-2. The NDVI, EVI and evapotranspiration data from MODIS and climate variables (precipitation, wind speed, air temperature and relative humidity) as of NASA POWER platform. Data were submitted to regression, correlation, and temporal analysis. In general, the Cerrado biome presents high X_{CO2} between the months of May to October. Similar behavior was observed for the Pantanal. For the Atlantic Forest, this period extended from April to October, while for the eucalyptus macro-region, it was the shortest period, from June to October. Inverse variation to X_{CO2} was observed for SIF. SIF 757 averages were higher when compared to SIF771. The factors that govern the temporal variability of $X_{CO2,}$ SIF771, and NDVI and EVI, were the variables that best represented a dependence in this process. The only control factor that governs the temporal variability of SIF for all study areas is evapotranspiration. However, NDVI, EVI and air temperature are also correlated with SIF, but not in all biomes. Taking these results into account, it is concluded that the carbon sinks (C) created by forests and ecosystems depend on the balance between capturing C (via photosynthesis) and loss through breathing. This balance will vary according to the relative effect of each of these processes' intrinsic environmental factors.

Keywords: Carbon cycle, Climate change, Greenhouse gases, NDVI, OCO-2

2.1 Introduction

With the advent of the industrial revolution in the early XIX century, significant amounts of carbon dioxide (CO_2) began to be emitted into the atmosphere (Xu and Cui, 2021). According to observations made in Mauna Loa Observatory (Hawaii) by the National Oceanic and Atmospheric Administration (NOAA), the atmospheric concentration of CO_2 has increased by about 100ppm in the last 80 years (NOAA, 2020). Human interference has been observed through global warming and climate change (Shi et al., 2021; Xu et al., 2021). Change in rainfall, severe droughts and extreme winds has been observed in various parts of the world (Ramanathan et al., 2001; Farhan et al., 2020).

The effect of anthropogenic activities as a cause of climate change is undeniable (Xie et al., 2020). Several studies point to the burning of fossil fuel (Gaulin and Billon, 2020), land-use change (Ghahramani et al., 2020), deforestation (Junior et al., 2020), forest fires (Silva Junior et al., 2020) and the use of synthetic fertilizers (Pereira et al., 2020) as one of the main sources of emission of effect gases studies GHG for the atmosphere.

The conservation of biomes is still the most efficient for carbon storage since these environments are responsible for capturing an essential portion of the earth's carbon (Jobbagy et al., 2000). Strategies for the conservation of ecosystems and the fight against deforestation were widely discussed at COP21, including where Brazil has committed to reducing emissions of greenhouse gases by 37% by 2025 and 43% in 2030, and one of the main strategies and the fight against deforestation (Lèbre and Rovere, 2016).

Despite this, researchers have been looking for alternatives to mitigate or compensate for greenhouse gas emissions (Ferez et al., 2015; de Araújo Santos et al., 2019). The use of alternatives such as no-tillage, agroforestry systems and planted forests are efficient as agroecosystems can store significant amounts of carbon in plant biomass and soil (Silva et al., 2019; Xavier et al., 2019; Santos et al., 2020). However, it is worth mentioning that the use of these agroecosystems becomes efficient when used to replace agricultural production systems or the recovery of degraded areas.

The use of planted forests has also been presented as an alternative since it prevents deforestation and can increase the soil's carbon stock (Resh et al., 2002; Bhatta et al., 2018). Kumar et al. (2020) observed that in eucalyptus areas, soil carbon stocks were 34.8% increase in 8 years of planting. These authors also observed a total carbon stock (plant + soil) in an 8-year plantation of 114.1 a 118.8 Mg C ha^{-1}. For them, the use of eucalyptus reforestation offers a low-cost strategy for carbon sequestration, in addition to increasing agricultural income.

With the use of remote sensing techniques, Leuning et al. (2005) observed that annual carbon productivity of the 1060 g C m^{-2} $year^{-1}$ in the typical year and 360 g C m^{-2} $year^{-1}$ during the drought in eucalyptus forests in Australia. Recently with advances in remote sensing techniques, studies have shown the variation of atmospheric CO_2 concentration in different land uses, biomes, ecosystems and agricultural areas (Falahatkar et al., 2017; Mousavi et al., 2017; Chhabra and Gohel, 2019). Several of these studies have only become possible under to satellite launches such as Orbiting Carbon Observatory-2 OCO-2 (Crisp et al., 2012), The Greenhouse Gases Observing Satellite (GOSAT) (Yokota et al., 2009) and Scanning Imaging Absorption spectroMeter for Atmospheric CHartographY (SCIAMACHY), among others (Pan et al., 2021).

The use of these satellites has brought numerous advances in understanding the carbon cycle at global and regional scales (Hakkarainen et al., 2016; Eldering et al., 2017). This is due to important variables measured by these, such as the carbon dioxide (CO2) column-averaged dry-air mole fraction (X_{CO2}) (Crisp et al., 2012) and the Solar Induced Fluorescence (SIF) (Frankenberg et al., 2014). X_{CO2} is the average CO_2 concentration in a column that goes from the earth's surface to the top of the atmosphere (Crisp et al., 2012). SIF is considered the most modern in terms of vegetation analysis via remote sensing because SIF is directly related to photosynthesis's internal mechanisms (Xiao et al., 2019). In this sense, the SIF stands out because it can indicate the photosynthetically active vegetation, unlike other more traditional vegetation indicators such as NDVI, which detect only green leaves presence (Mohammed et al., 2019).

Understanding the carbon cycle at regional scales is essential to make a political climate decision. In this sense, sensing techniques emerge as an alternative that

makes it possible to observe this more widely and often quickly. Therefore, knowing the importance of biomes and agricultural production systems, such as forests planted in cycling and carbon storage, our hypothesis is based on the different land uses presenting varied temporal variation and control factors. That said, the objective of this study was to characterize the temporal variability of the carbon dioxide (CO_2) column-averaged dry-air mole fraction (X_{CO2}) and Solar Induced Fluorescence (SIF) and its main control factors in biomes and planted forests with eucalyptus in the state of Mato Grosso do Sul, Brazil with the use of remote sensing data.

2.2 Material and Methods

2.2.1 Study Area

The study was carried out for the state of Mato Grosso do Sul (20.7882° S, 51.7030° W) in the Midwest region of Brazil (Figure 1). The state is formed by the Cerrado, Pantanal and Atlantic Forest biomes. It is also known as being the second largest eucalyptus producer in Brazil. The climate is classified as tropical, being Aw according to Köppen classification, the average temperature is 24. 2ºC and annual precipitation are 1241mm.

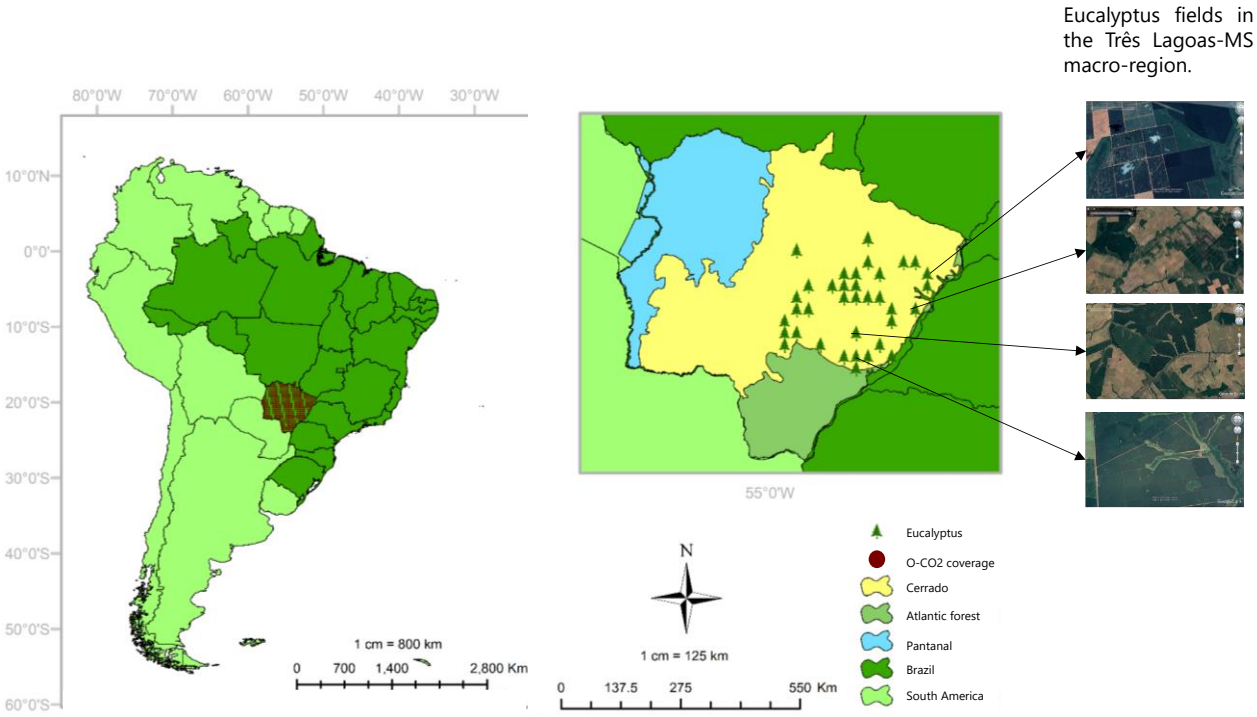

Figure 1. Location of the state of Mato Grosso do Sul with their respective biomes and the points with the presence of Eucalyptus.

2.2.2 Big data remotely sensed acquisition and processing

To reduce the difference between spatial and time resolutions between the orbital sensors used in this study, a process was used, described in Figure 2, which establishes a pattern in the acquisition of data from the coordinates obtained on the OCO-2 platform. We emphasize that studies similar to ours, using satellites with different resolutions, have been conducted by other research groups (Falahatkar et al., 2017; Golkar et al., 2020).

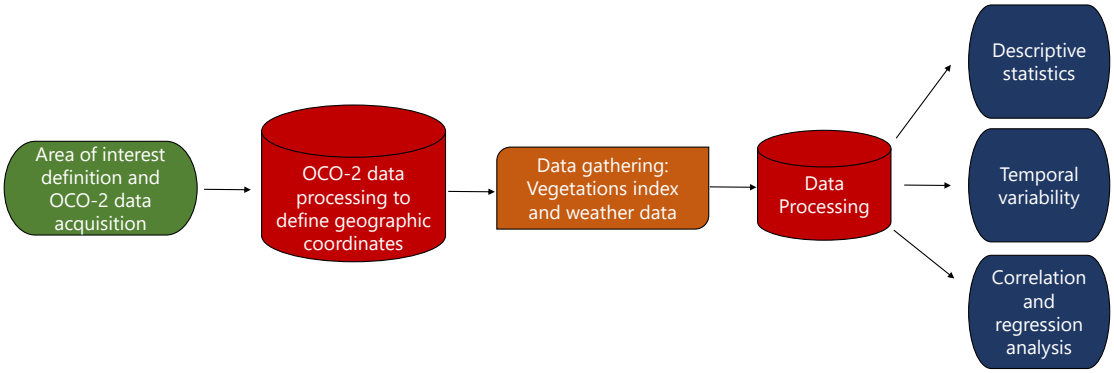

Figure 2. Flowchart of acquisition, processing and data analysis.

2.2.3 Platforms for data extraction

The databases with the acquired variables and their respective resolutions are presented in Table1. We extracted the X_{CO2}, SIF 771, SIF 757, EVI, NDVI and other variables from 2015 to 2018 (timescale with data provided by the OCO-2 when this study was carried).

Table 1. Databases and spatial-temporal resolution of variables used in this study.

	Variable	Data source	Resolution		Reference
			Temporal	Spatial	
CO_2	X_{CO2} (ppm)	OCO-2	16 days	27.75 km	CRISP et al., (2012)
WEATHER	Air Temperature at 2m (ºC)	(NASA/POWER)	Daily	111 km	STACKHOUSE et al., (2015)
	Air moisture (%)	(NASA/POWER)	Daily	111 km	
	Precipitation (mm)	(NASA/POWER)	Daily	111 km	
	Wind speed at 2m (m s^{-1})	(NASA/POWER)	Daily	111 km	
	Wind speed at 10m (m s^{-1})	(NASA/POWER)	Daily	111 km	
VEGETATION	NDVI (0-1)	MOD13C2 MODIS-TERRA	16 days	0.5 km	HUETE et al., (1997)
	EVI (0-1)	MOD13C2 MODIS-TERRA	16 days	0.5 km	ROUSE et al., (1973)
	ET (mm)	MOD16A2.006 V6 MODIS-TERRA	8 days	0.5 km	
	SIF 757 nm (Wm^{-2} sr^{-1} μm^{-1})	OCO-2	16 days	27.75 km	FRANKENBERG et al., (2014)
	SIF 771 nm (Wm^{-2} sr^{-1} μm^{-1})	OCO-2	16 days	27.75 km	

2.2.3.1 Orbiting Carbon Observatory-2 (OCO-2)

The primary product delivered by the Orbiting Carbon Observatory-2 consists of spatially resolved estimates of the column-averaged dry-air mole fraction. This quantity, called X_{CO2} by members of the atmospheric carbon science community, quantifies the average concentration of carbon dioxide in a column of dry air extending from Earth's surface to the top of the atmosphere. Estimates of X_{CO2} derived by taking the column's ratio integrated number densities of carbon dioxide and molecular oxygen along the optical path between the Sun, the surface footprint, and the instrument, and then multiplying these results by the column-averaged oxygen concentration (0.20935 microns). These carbon dioxide and oxygen number densities are estimated from high-resolution spectra of reflected sunlight, collected by the Observatory's instrument at wavelengths (colors) within the 0.765-micron molecular oxygen A-band and two carbon dioxide bands centered at wavelengths near 1.61 and 2.06 microns. The Orbiting Carbon Observatory-2 mission will produce four different levels of data products for the user community that will provide comprehensive mission data results (Crisp et al., 2012).

The OCO-2 SIF Lite files contain bias-corrected SIF (solar-induced fluorescence) and other select fields aggregated as daily files. The OCO-2 spectrometer measures spectra in the O2A-band, with far-red SIF, retrieved at 757 and 771 nm based on the Fraunhofer lines' infilling at 13:36 local time with data commencing on September 6, 2014 (Frankenberg et al., 2014).

We obtained SIF and X_{CO2} data from the OCO-2 Lite version (V7r) with 0.25º Spatial grid resolution from the OCO-2 data archive maintained at NASA (https://co2.jpl.nasa.gov/#mission=OCO-2). To make SIF data more realistic, we deleted SIF values lower than 0.1 W m^{-2} sr^{-1} μm^{-1}, according to Guo et al. (2020). The trend adjustment of the X_{CO2} data was made using the regression method (Gujarati and Porter, 2011).

2.2.3.2 Data extraction on the AρρEEARS platform

This platform provides a simple and efficient way to access and transform geospatial data from various NASA data files. AρρEEARS (https://lpdaacsvc.cr.usgs.gov/appeears/) allows users to obtain subsets of large databases using spatial, time parameters. Two types of sample requests are available: point samples by inserting geographic coordinates and area samples using vector polygons. Sample requests sent to AρρEEARS provide users with not only data values but also associated quality data values.

To analyze vegetation behavior, the Enhanced Vegetation Index (EVI; Huete et al., 1997) and NDVI (Normalized Difference Vegetation Index; Rouse et al., 1973). The MODIS sensor data (Moderate Resolution Imaging Spectroradiometer) Product MOD13Q1 Version 6 (H13V11) was used., with a spatial resolution of 500 m evaluated every 16days. Data from the MODIS sensor allows a regular analysis of vegetation at the global level, thanks to the speed and frequency in which the data is made available (Huete et al., 2002).

2.2.3.3 Weather data from NASA POWER

The data of precipitation (mm), air temperature (ºC), wind speed at 2m (m s^{-1}), wind speed at 10m (m s^{-1}), and air humidity at 2 m (%) were acquired through the NASA Power platform (https://power.larc.nasa.gov) (Stackhouse et al., 2015). This platform consists of a NASA project titled: World Energy Resource Forecast (POWER) and has been started to improve the current renewable energy data set and create new datasets from new satellite systems. The POWER project targets three user communities: (1) Renewable Energy, (2) Sustainable Buildings and (3) Agroclimatology. It compiles information from various data sources directly and those derived from gridded data systems. The air temperature and relative humidity are obtained from the Global Model and Assimilation Office (GEOS-4) system, and precipitation data are obtained from the Global Precipitation Climate Project.

2.2.3 Statistical analysis

The data were initially analyzed using descriptive statistics (mean, standard deviation, minimum, maximum, and standard error). These parameters were used to classify the temporal and spatial variability of the variables studied. Simultaneously, the basic assumptions of variance and regression analyses, normality of errors and homogeneity of variances were tested for all attributes evaluated. The assumptions of homoscedasticity analysis and normality of the residues were tested by the Shapiro-Wilk Tests, respectively, both at a 5% probability. Pearson correlation analyses (Eq. 1) and linear regression (Eq. 2) were performed to understand the variation of X_{CO2} with the other variables. Heatmaps were generated with month means and using the Euclidean distance as the distance method, and this analysis was processed using the package seaborn of the python language. The regressions were made only to variables showed Pearson correlation ≥ r -0.50 or 0.50.

$$r = \frac{\sum_{i=0}^{n}(x_i - \underline{x})(y_i - \underline{y})}{\sqrt{(x_i - \underline{x})}X\sqrt{(y_i - \underline{y})}} \quad \text{(Eq.1)}$$

where: x_i are the observed values of the variable x is the mean of the variable x; y_i is the observed values of the variable y is the mean of the variable y.

$$R^2 adjusted = \left[1 - \frac{(1-R^2)*(n-1)}{N-k-1}\right] \quad \text{(Eq.2)}$$

where: N is the number of points in data sample; K is the number of independent regressors, that is, the number of variables in the model, excluding the constant.

2.3 Results

The mean values and the temporal variation of X_{CO2} for the biomes and the eucalyptus-producing macro-region of Mato Grosso do Sul, Brazil, are shown in Figure 3A and 3B. The means were the same for all study areas (Figure 3A). For the Cerrado biome, the maximum average (401.13 ± 0.38ppm) and minimum (395.66 ± 0.37ppm)

were observed in September 2017 and January 2018. In the Atlantic Forest, it was the months of March (395.58 ± 0.42ppm) and November (401.65 ± 0.40ppm). For the Pantanal, the minimum average was observed in January 2018 (395.12 ± 0. 48ppm) and the highest in July 2016 (401.19 ± 0.22ppm). Finally, in the Eucalyptus fields, the minimum average (395.38 ± 0.97ppm) was in May 2015 and the maximum (401.20 ± 0.38ppm) in June 2016.

In general, the Cerrado biome presents high X_{CO2} between the months of May to October (Figure 3B). Similar behavior was observed for the Pantanal. For the Atlantic Forest, this period extended from April to October, while for Eucalyptus fields, a shorter period was observed, that stayed from June to October. Both the biomes and the eucalyptus macro-region showed the beginning of the fall of X_{CO2} in October, extending until February to March. Inverse behavior was observed for SIF (Figure 3 D and 1F).

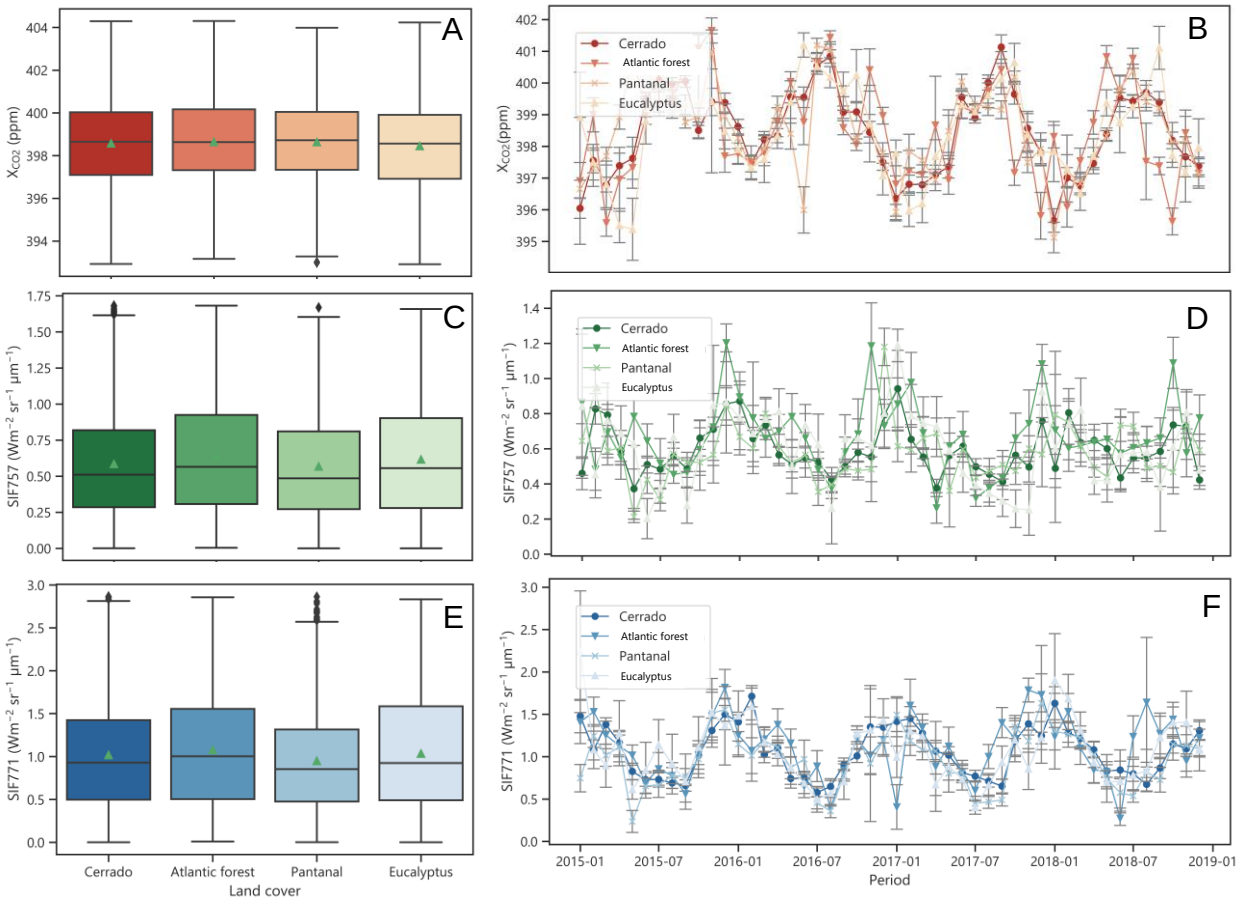

Figure 3. boxplot graph with mean and temporal distribution of X_{CO2} (A and B), SIF 757 (C and D), and SIF 771 (E and F) for biomes and eucalyptus fields of

Mato Grosso do Sul, Brazil. Legend: (— internal) represents the second quartile or median; (□) the first and third quartiles; (⊤ and ⊥) third and first quartiles up to the upper and lower limits; (▲) values of the means; (♦) discrepancies (outliers).

The means of SIF 771 (Figure 3E) was higher when compared to SIF757 (Figure 3C). After observing the study areas, the Pantanal biome presented the lowest averages for both SIF771 (0.94 ± 0.02W m^{-2} sr^{-1} μm^{-1}) as for SIF757 (0.56 ± 0.01W m^{-2} sr^{-1} μm^{-1}). The Atlantic Forest and the Eucalyptus fields presented the highest means of SIF, being, 1. 07 ± 0.03W m^{-2} sr^{-1} m^{-1} (SIF771) and 0.63 ± 0.01 W m^{-2} sr^{-1} μm^{-1} (SIF757) for Atlantic forest and 1. 03 ± 0. 03W m^{-2} sr^{-1} μm^{-1} (SIF771), 0. 61 ± 0. 02W m^{-2} sr^{-1} μm^{-1} (SIF757) for Eucalyptus fields. In the Cerrado the averages were 1.01 ± 0. 06W m^{-2} sr^{-1} μm^{-1} and 0. 58 ± 0. 001 W m^{-2} sr^{-1} μm^{-1} for SIF771 and SIF757, respectively.

In the Cerrado biome, the minimum and maximum averages of SIF 757 ranged from 0.37 ± 0.11W m^{-2} sr^{-1} μm^{-1} to 0.94 ± 0.22W m^{-2} sr^{-1} μm^{-1} for May 2015 and January 2017, respectively (Figure 3D). In the Atlantic Forest, the values of minimum and maximum average were 0.26 ± 0.08W m^{-2} sr^{-1} μm^{-1} to 1.20 ± 0.11W m^{-2} sr^{-1} μm^{-1} in April 2017 and December 2015. In the Pantanal, the minimum average (0.21 ± 0.03W m^{-2} sr^{-1} μm^{-1}) and the maximum (1.18 ± 0.11W m^{-2} sr^{-1} μm^{-1}) were observed in May 2015 and December 2016, respectively. In the Eucalyptus fields, the values of 0.20 ± 0.11 W m^{-2} sr^{-1} μm^{-1} to 1.19 ± 0.09W m^{-2} sr^{-1} μm^{-1} were recorded for June 2016 and January 2017 Figure 3 (C and D).

For SIF771, the maximum and minimum means were 0.57 ± 0.05W m^{-2} sr^{-1} μm^{-1} to 1.71 ± 0.12W m^{-2} sr^{-1} μm^{-1} in July and February of 2016 in the Cerrado biome. To the Atlantic Forest were 0.27 ± 0.08 in June 2018 and 1.81 ± 0.21W m^{-2} sr^{-1} μm^{-1} in December 2015. In the Pantanal, the minimum and maximum means were 0.23 ± 0.12W m^{-2} sr^{-1} μm^{-1} e 1.63 ± 0.34W m^{-2} sr^{-1} μm^{-1} May of 2015 and December of 2017. In Eucalyptus fields, these values were 0.39 ± 0.07 W m^{-2} sr^{-1} μm^{-1} and 2.24 ± 0.72W m^{-2} sr^{-1} μm^{-1} for July of 2017 and January of 2015, respectively (Figure 3E and F).

With the Heatmap of Pearson's correlation matrix, it was observed as the variables that correlated to X_{CO2} (Figure 4). For Cerrado, the significant correlations

($p<0.05$) were found of X_{CO2} with NDVI (-0.8), SIF 771 (-0.75) and EVI (-0.71). In the Atlantic Forest, the variables that best correlated with XCO2 were WS10M (0.46), EVI (-0.46), NDVI (-0.45), SIF 757 (-0.42) and SIF 771 (-0.41). In the Pantanal, the correlations were observed to XCO2 with RH2M (-0.62), WS10M (0,57), EVI (-0.55), WS2M (0.54), SIF 771 (-0,53) and SIF 757 (-0.46), while Eucalyptus fields, which was observed with a significant correction with EVI (-0.67), SIF 771 (-0.45), RH2M (-0.53), WS10M (0.62), WS2M (0.62) and NDVI (-0.66).

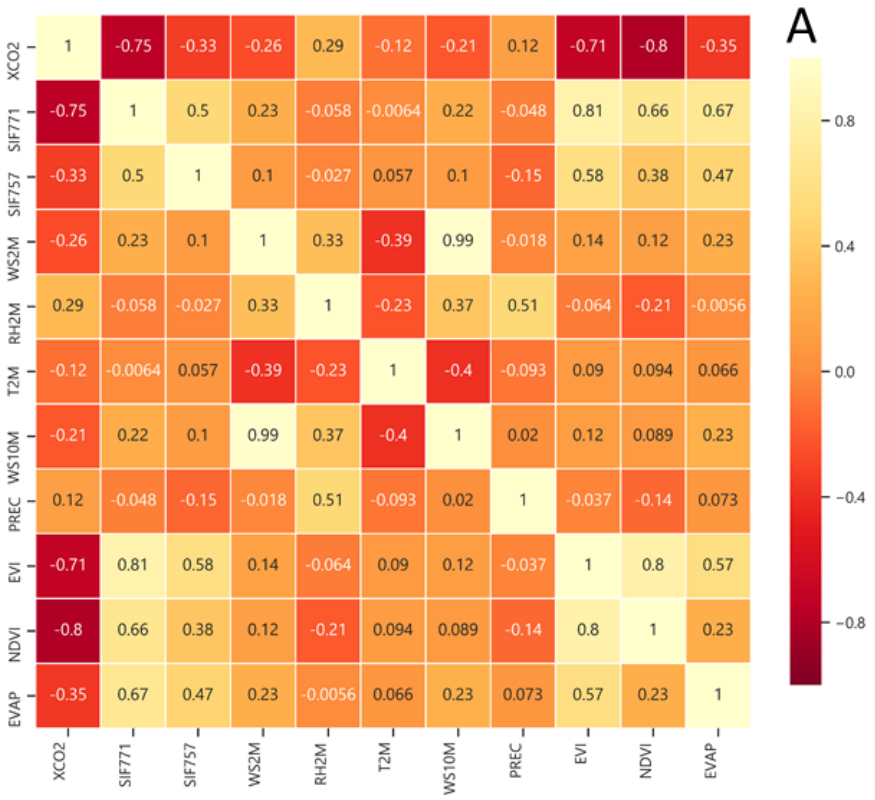
A
XCO2 1 -0.75 -0.33 -0.26 0.29 -0.12 -0.21 0.12 -0.71 -0.8 -0.35
SIF771 -0.75 1 0.5 0.23 -0.058 -0.0064 0.22 -0.048 0.81 0.66 0.67
SIF757 -0.33 0.5 1 0.1 -0.027 0.057 0.1 -0.15 0.58 0.38 0.47
WS2M -0.26 0.23 0.1 1 0.33 -0.39 0.99 -0.018 0.14 0.12 0.23
RH2M 0.29 -0.058 -0.027 0.33 1 -0.23 0.37 0.51 -0.064 -0.21 -0.0056
T2M -0.12 -0.0064 0.057 -0.39 -0.23 1 -0.4 -0.093 0.09 0.094 0.066
WS10M -0.21 0.22 0.1 0.99 0.37 -0.4 1 0.02 0.12 0.089 0.23
PREC 0.12 -0.048 -0.15 -0.018 0.51 -0.093 0.02 1 -0.037 -0.14 0.073
EVI -0.71 0.81 0.58 0.14 -0.064 0.09 0.12 -0.037 1 0.8 0.57
NDVI -0.8 0.66 0.38 0.12 -0.21 0.094 0.089 -0.14 0.8 1 0.23
EVAP -0.35 0.67 0.47 0.23 -0.0056 0.066 0.23 0.073 0.57 0.23 1
XCO2 SIF771 SIF757 WS2M RH2M T2M WS10M PREC EVI NDVI EVAP
0.8
0.4
0.0
−0.4
−0.8

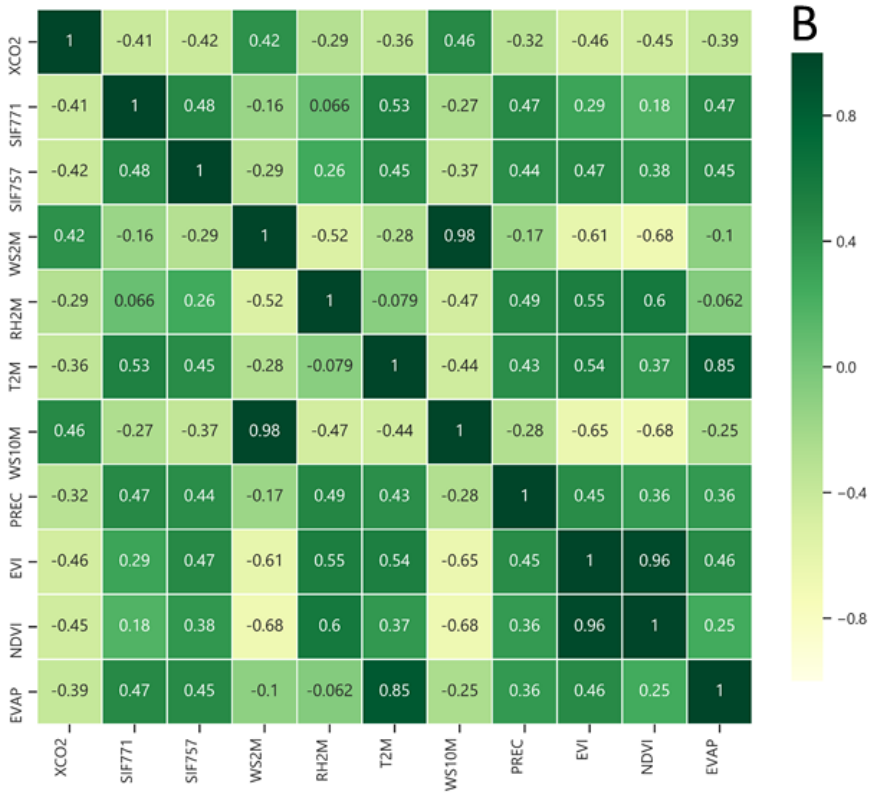
B
XCO2 1 -0.41 -0.42 0.42 -0.29 -0.36 0.46 -0.32 -0.46 -0.45 -0.39
SIF771 -0.41 1 0.48 -0.16 0.066 0.53 -0.27 0.47 0.29 0.18 0.47
SIF757 -0.42 0.48 1 -0.29 0.26 0.45 -0.37 0.44 0.47 0.38 0.45
WS2M 0.42 -0.16 -0.29 1 -0.52 -0.28 0.98 -0.17 -0.61 -0.68 -0.1
RH2M -0.29 0.066 0.26 -0.52 1 -0.079 -0.47 0.49 0.55 0.6 -0.062
T2M -0.36 0.53 0.45 -0.28 -0.079 1 -0.44 0.43 0.54 0.37 0.85
WS10M 0.46 -0.27 -0.37 0.98 -0.47 -0.44 1 -0.28 -0.65 -0.68 -0.25
PREC -0.32 0.47 0.44 -0.17 0.49 0.43 -0.28 1 0.45 0.36 0.36
EVI -0.46 0.29 0.47 -0.61 0.55 0.54 -0.65 0.45 1 0.96 0.46
NDVI -0.45 0.18 0.38 -0.68 0.6 0.37 -0.68 0.36 0.96 1 0.25
EVAP -0.39 0.47 0.45 -0.1 -0.062 0.85 -0.25 0.36 0.46 0.25 1
XCO2 SIF771 SIF757 WS2M RH2M T2M WS10M PREC EVI NDVI EVAP
0.8
0.4
0.0
−0.4
−0.8

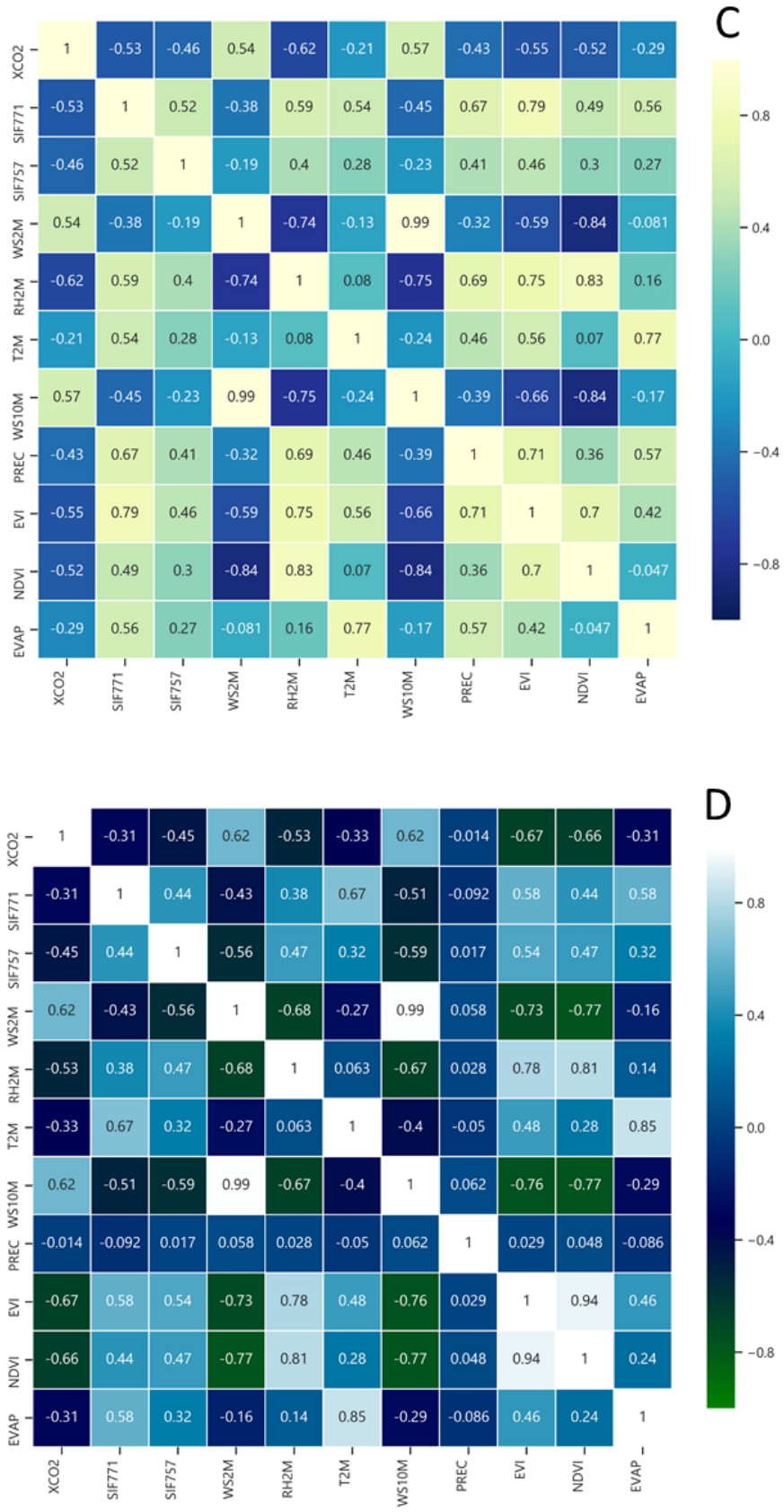

Figure 4. Heatmap with correlation matrix for (A) Cerrado, (B) Atlantic Forest, (C) Pantanal, and (D) Eucalyptus fields in the state of Mato Grosso do Sul.

A linear regression analysis was performed to look the dependence between X_{CO2} and the other variables. Only SIF771, NDVI and EVI showed significant results in all areas studied (Figure 5). For SIF 771 the coefficient of determination adjusted (R^2adj.) were R^2adj = 0.15; $p<0.05$, R^2adj = 0.27; $p<0.05$, R^2adj. = 0.55; $p<0.05$ and R^2adj. = 0.07; $p<0.05$ for Cerrado, Atlantic forest, Pantanal, and Eucalyptus fields, respectively. For EVI were R^2adj = 0.49 for the Cerrado, R^2adj. = 0.20 for Atlantic forest, R^2adj = 0.29 for Pantanal and R^2adj =0.44 for Eucalyptus fields. Finally, for NDVI the values of R^2adj were R^2adj = 0.63, R^2adj. = 0.18, R^2adj =0.26 e R^2adj. = 0.46, for Cerrado, Atlantic Forest, Pantanal, and Eucalyptus fields, respectively.

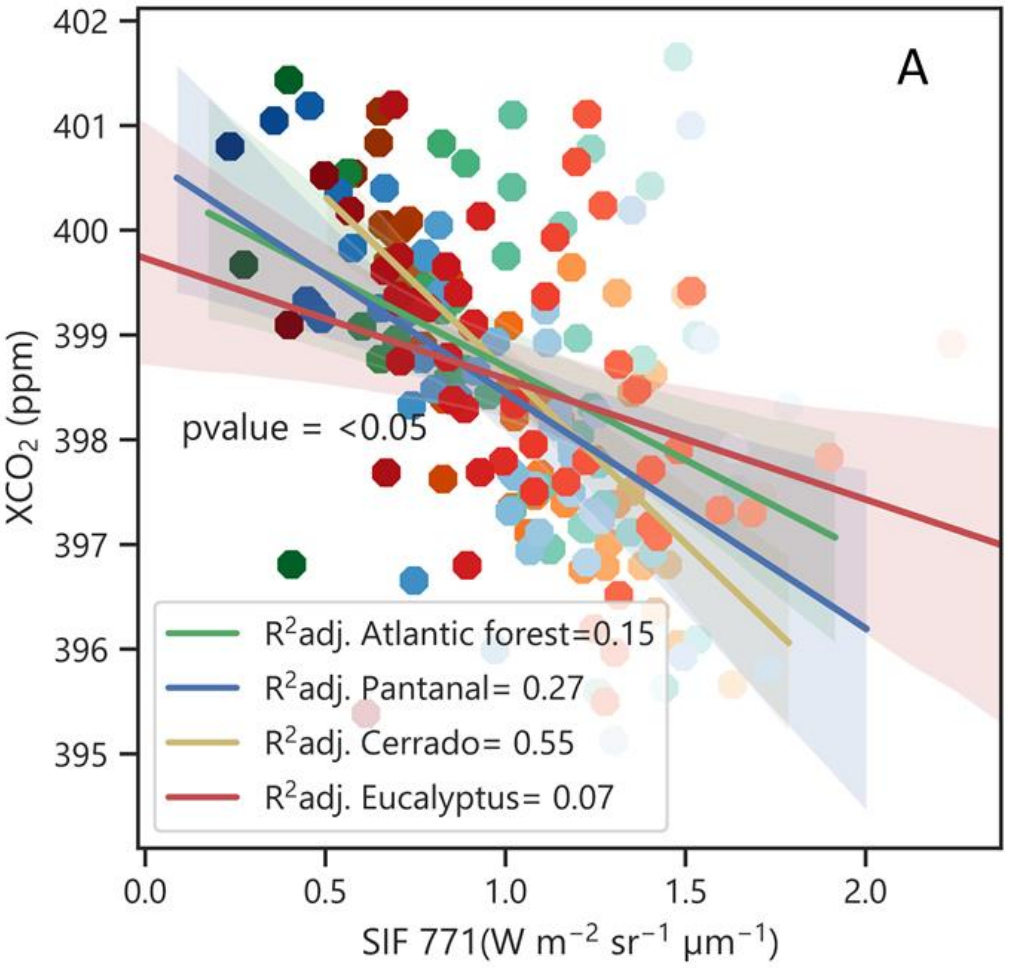
A
402
401
400
399
398
397
396
395
XCO2 (ppm)
pvalue = <0.05
R2adj. Atlantic forest=0.15
R2adj. Pantanal= 0.27
R2adj. Cerrado= 0.55
R2adj. Eucalyptus= 0.07
0.0
0.5
1.0
1.5
2.0
SIF 771(W m−2 sr−1 µm−1)

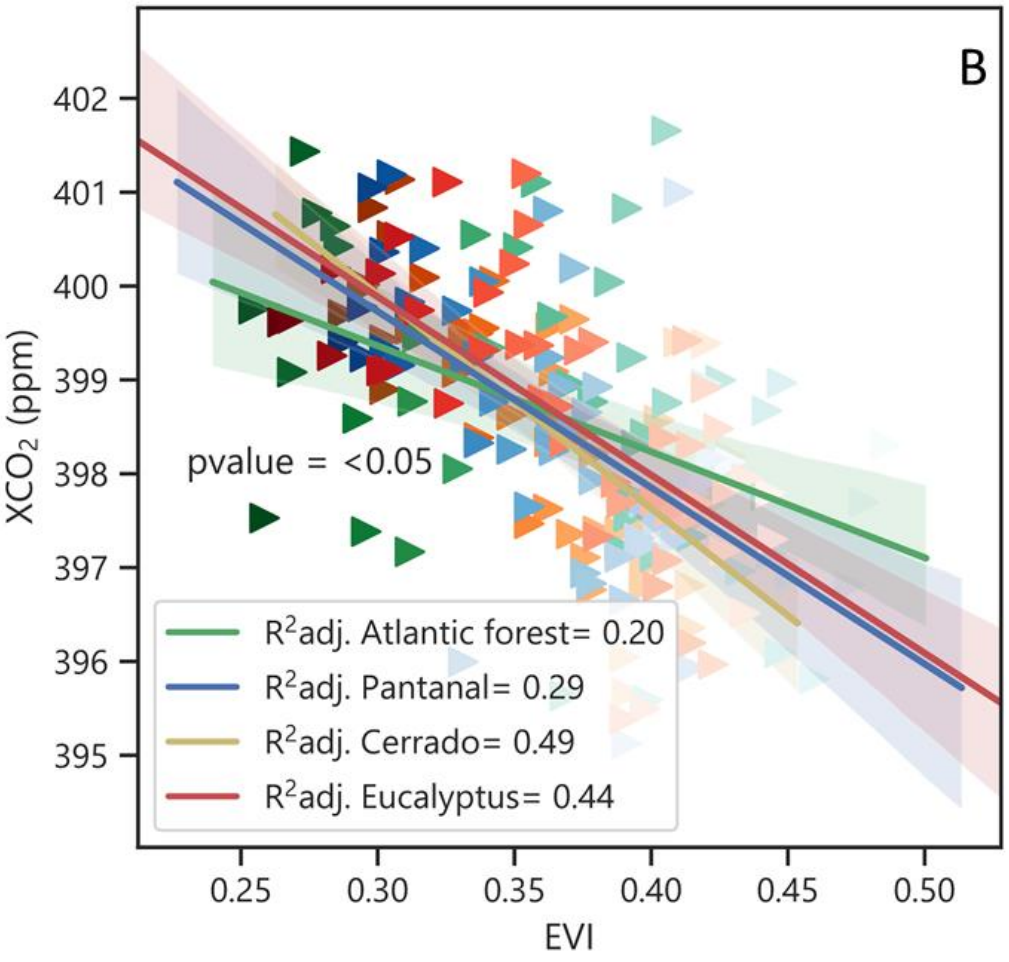
B
402
401
400
399
398
397
396
395
XCO2 (ppm)
pvalue = <0.05
R2adj. Atlantic forest= 0.20
R2adj. Pantanal= 0.29
R2adj. Cerrado= 0.49
R2adj. Eucalyptus= 0.44
0.25
0.30
0.35
0.40
0.45
0.50
EVI

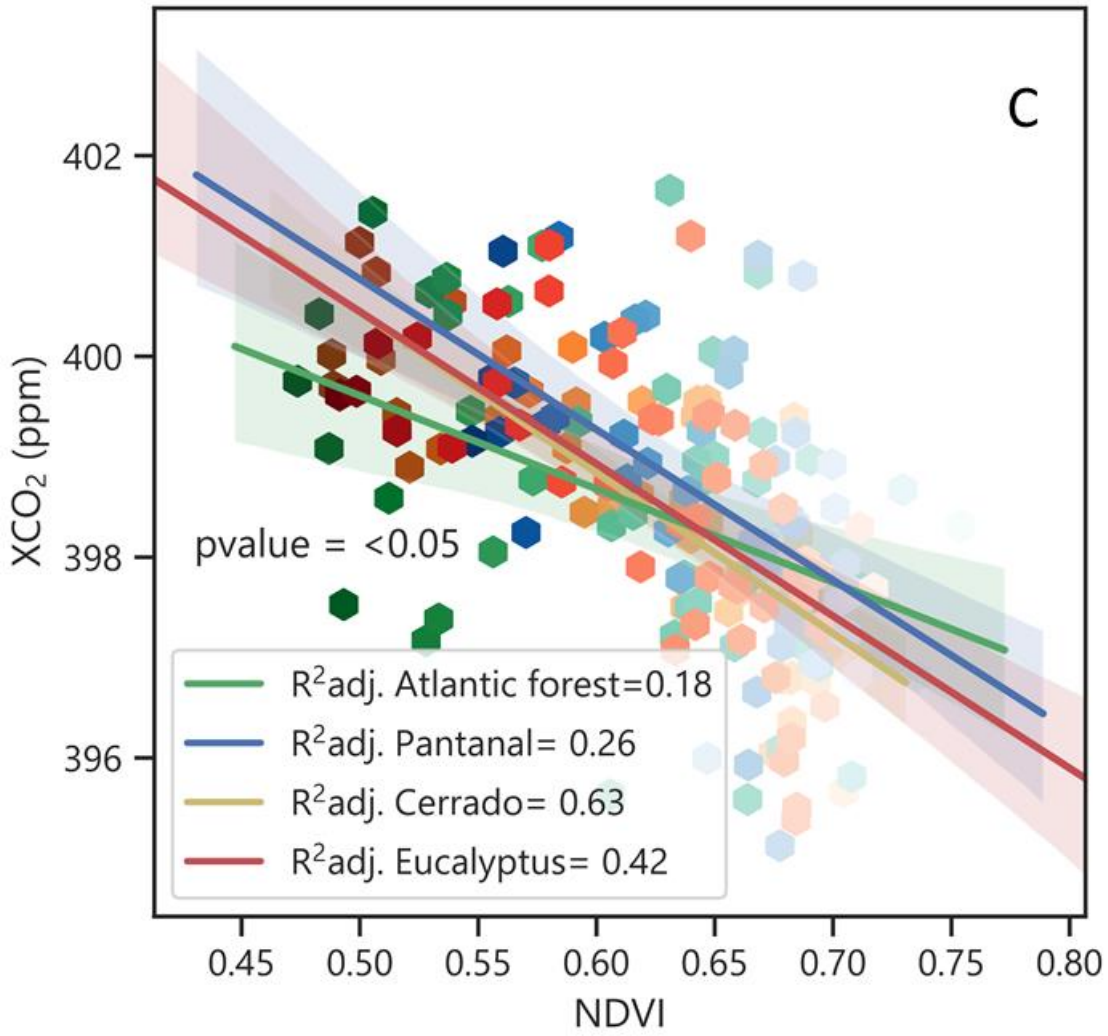

Figure 5. Linear regression between X_{CO2} and SIF771 (A), EVI (B) and NDVI (C).

Among the SIF, the SIF771 was the one that best explained the variation of X_{CO2}. For this reason, regression analysis between SIF771 (Figure 5A) with the other variables was performed (Figure 6). According to, we observed that total evapotranspiration was the only variable that explained the variability of SIF in all biomes and eucalyptus fields (Figure 6A). The coefficient of determination was R^2adj = 0.44, R^2adj =0.20, R^2adj = 0.30 and R^2adj = 0.32, for Cerrado, Atlantic Forest, Pantanal and Eucalyptus, respectively. For NDVI was R^2adj =0.42 in the Cerrado, R^2adj =0.22 for Pantanal and R^2adj = 0.17 for the Eucalyptus fields. For the EVI, in the Cerrado biome, the value was R^2adj = 0.66, while for the Pantanal and e Eucalyptus fields were R^2adj = 0.62 and R^2adj = 0.33, respectively. With air temperature, significant

linear regression was only observed for Pantanal (R^2adj =0.27), Atlantic forest (R^2adj =0.26) and Eucalyptus fields (R^2dj = 0.44).

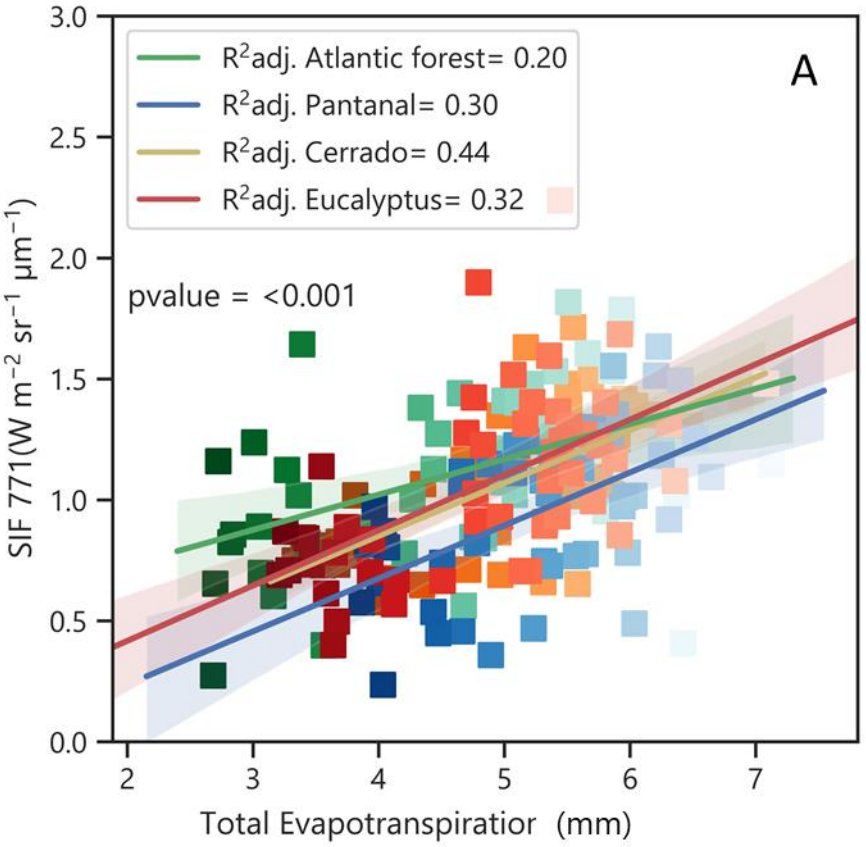
A
R²adj. Atlantic forest= 0.20
R²adj. Pantanal= 0.30
R²adj. Cerrado= 0.44
R²adj. Eucalyptus= 0.32
pvalue = <0.001
SIF 771(W m⁻² sr⁻¹ µm⁻¹)
Total Evapotranspiration (mm)
3.0
2.5
2.0
1.5
1.0
0.5
0.0
2
3
4
5
6
7

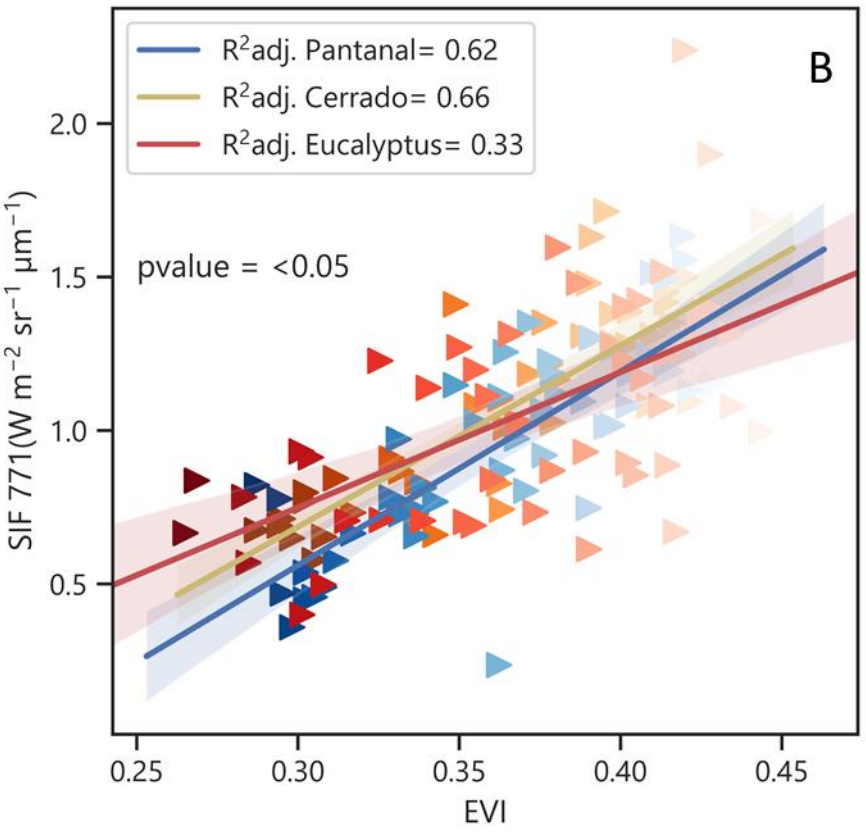
B
R²adj. Pantanal= 0.62
R²adj. Cerrado= 0.66
R²adj. Eucalyptus= 0.33
pvalue = <0.05
SIF 771(W m⁻² sr⁻¹ µm⁻¹)
EVI
2.0
1.5
1.0
0.5
0.25
0.30
0.35
0.40
0.45

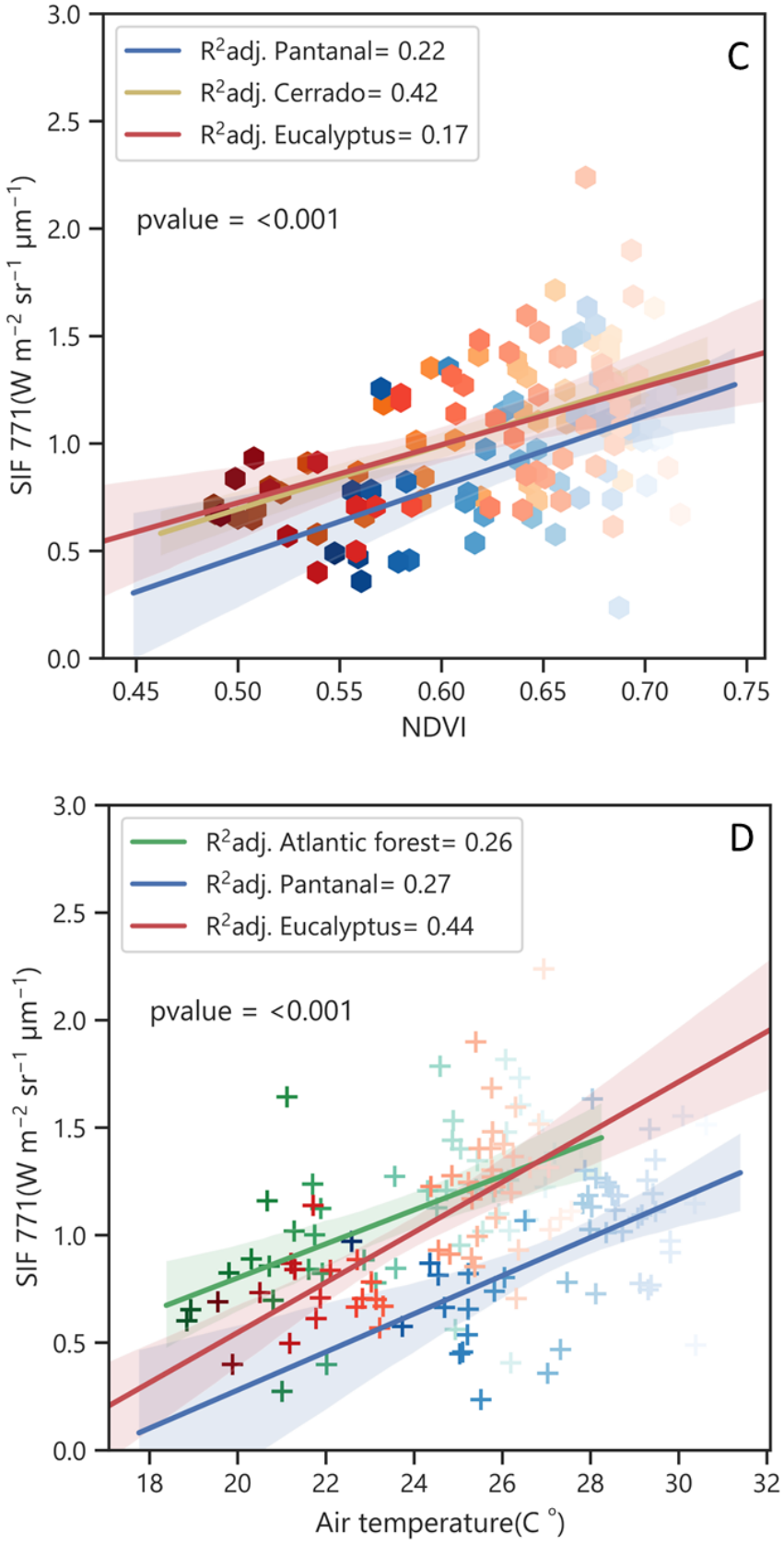

Figure 6. Linear regression of SIF771 with total evapotranspiration (A), EVI (B), NDVI (C) and Air temperature (D).

2.4 Discussion

2.4.1 Temporal variability for X_{CO2}

The dynamics of CO_2 in the atmosphere present variations, which in the literature is reported as the Keeling curve (Keeling, 1958; Uprety and Cao, 2016; Pili and Violanda, 2020). This curve demonstrates the periods of respiration and absorption of CO_2. When the curve is down, photosynthesis is the dominant agent, the contrary means that the breathing of the ecosystem is more significant than photosynthesis.

In this sense, ecosystems play a key role in global carbon cycling and the earth's climate because they absorb and release CO_2 through photosynthesis and respiration, respectively (Schimel et al., 2015). Terrestrial ecosystems have absorbed about 25 to 30% of anthropogenic CO_2 emissions in the last five decades before 2010 (Le Quéré et al., 2009). Much of this absorption occurs through carbon accumulation via photosynthesis by forest biomass (Richard et al., 2011) and soils (de Araújo Santos et al., 2019; Xavier et al., 2019).

Several studies have pointed out the sensitivity of X_{CO2} to vegetation dynamics and the change in photosynthetic rates (Mousavi et al., 2017; Morais Filho, 2018; Chhabra and Gohel, 2019; Golkar et al., 2020). Morais Filho (2018), evaluating the temporal variability of X_{CO2} under different agroecosystems in Brazil, it observed negative relationships between X_{CO2} with NDVI and SIF in areas of soybean and sugarcane production. Their results demonstrate the sensitivity of the temporal variability of X_{CO2} regarding the type of cover since, in areas of agricultural production, this change occurs frequently.

Chhabra and Gohel (2019) also observed a robust negative correction between X_{CO2} and NDVI on different soil cover types. Thus, his study, just like ours, illustrates the significant role of vegetation and different soil cover types in controlling atmospheric concentrations of X_{CO2}. These authors also highlight the supporting role of rainfall in this dynamic since water is one of the main fuels for photosynthesis.

This relationship between the variation in atmospheric CO_2 concentration with rainfall regimes is reported by Wang et al. (2016). According to these authors, the sensitivity of vegetation cover to precipitation can directly affect the variability of atmospheric CO_2. This sensitivity can be observed in our study by analyzing the periods of increase in CO_2 concentration, wherein the region with eucalyptus production happened in a shorter period of 5 months. Another fact that deserves to be highlighted is the beginning of the decrease in $X_{CO2,}$ which was in October for the entire independent state of the biome.

Eucalyptus cultivation is highly technical, with adequate soil management issues (Rocha et al., 2019). Besides, eucalyptus can fetch water at great depths(Dawson and Pate, 1996; Le Maitre et al., 2002) allows its high growth rates and, consequently, high atmospheric carbon absorption. Some studies report the impact of eucalyptus cultivation on carbon accumulation, whether in planted forests (Yu et al., 2020) or integrated systems (Santos et al., 2020). According to Whitehead and Beadle (2004), many eucalyptus species under a wide range of conditions to which they are subjected may present the potential for high carbon absorption rates.

For Cerrado and Pantanal, Rossi and Santos (2020) observed similar values regarding crude primary productivity (GPP) in these two biomes, indicating similarity in carbon cycling. Despite presenting different behaviors regarding the hydrological cycle, these two biomes are composed of large areas of native pastures, which give it some similarity in carbon absorption. Rossi and Santos (2020) observed an increase in GPP rates in these biomes from October. These findings corroborate with our findings that indicate the decrease in X_{CO2} in the same month. It is worth noting that GPP and X_{CO2} present inverse behaviors since GPP represents the absorption of CO_2 by biomes. In Pantanal, the results from Vourlitis et al. (2015) indicates that seasonally flooded forests of the Pantanal are potentially large sinks for CO_2 but strong sources for CH_4, especially during the flood pulse when anaerobic soil conditions concomitantly enhance CH_4 production and limit CO_2 production.

2.4.2 Temporal variability of SIF

The use of solar-induced chlorophyll fluorescence to understand the dynamics of terrestrial carbon via remote sensing is state of the art in this field of

science (Xiao et al., 2019). This is because of the useful information on photosynthetic activities that the SIF is offered (Mohammed et al., 2019). Within this scenario, researchers have been joining forces to understand carbon dynamics in ecosystems using SIF(Merrick et al., 2019; Gao et al., 2020).

The seasonal variability of SIF with NDVI and EVI provides information on vegetation green, linked to the light interception canopy (Chhabra and Gohel, 2020). EVI is a reflectance-based vegetation index widely used to indicate relative vegetables and infer photosynthetic function (Huete et al., 2002). In summary, the vegetation indices provide a more static view of vegetation activity when compared to SIF derived from remote sensing since its sensitivity to environmental factors is as much as that of the reflectance of the top of the canopy.

Several studies have reported positive linear correlations of SIF with EVI and NDVI (Li et al., 2018; Wei et al., 2019; Qiu et al., 2020), corroborating our results. Chhabra e Gohel (2020) founded Pearson correlation coefficients between SIF757 derived from OCO-2 and NDVI and EVI derived from MODIS of 0.63 and 0.72. Using GOSAT SIF data. Frankenberg et al. (2011) reported plant fluorescence patterns observed by GOSAT with GPP derived from MODIS and Normalized SIF with vegetation indices such as NDVI, EVI and LAI. Therefore, it is observed that data from the MODIS sensor, already widely used in the literature (de Oliveira Souza et al., 2018; Rossi and Santos, 2020), are essential tools for understanding the dynamics of SIF.

In this study, SIF showed a correlation with evapotranspiration and air temperature, and evapotranspiration was the only variable that presented a strong relationship under all the studied environments. According to Maes et al. (2020), SIF is closely linked to the transpiration of the ecosystem; they came to this fact because they observed that the relationship between SIF and photosynthesis (GPP) is mainly controlled by the biochemical properties of the leaf and plant structure and the SIF-T ratio (transpiration) seems determined mainly by air temperature and intrinsic efficiency of water use.

Gonsamo et al. (2019), evaluating the sensitivity of SIF to soil moisture, they also observed a positive relationship between SIF and air temperature. According to these authors, the day's temperature and duration are the main limiting factors of plant growth during the beginning and end of the growing season in some latitudes. Besides,

for arid and cultivated lands, the impact of temperature on photosynthetic activities is manifested through soil moisture and steam pressure deficit, showing that air temperature can also have adverse effects on photosynthesis. A positive correlation between SIF and air temperature for Atlantic Forest was also observed. In this same study, the authors also did not observe this relationship for the Pantanal biome. According to Delgado et al. (2018) the Atlantic Forest regions have relevant capacity of atmospheric carbon absorption. These authors also observed the highest values of GPP in the rainy season, corroborating with our results related to SIF on the Atlantic Forest.

2.5 Conclusions

In the State of Mato Grosso do Sul, in general, the periods of high CO_2 concentration are between April and June. Pantanal, Atlantic Forest, and Eucalyptus fields show the beginning of X_{CO2} in October, extending until February/March. The Eucalyptus fields have a shorter period (5 months) of high for $X_{CO2\ on}$ an annual scale. Inverse behavior is observed for SIF to temporal variation. The Eucalyptus fields have a photosynthetic activity like that of the Atlantic Forest.

Likely the factors that govern the temporal variability of $X_{CO2,}$ SIF771, together with NDVI and EVI, were the variables that best represented a dependence in this process and all variables that govern the temporal variability of X_{CO2} have an inverse relationship. These observations were observed in Cerrado, Pantanal, Atlantic Forest, and the eucalyptus fields. Thus, we could observe that this region's photosynthetic activity plays a fundamental role in the absorption of atmospheric carbon.

The only control factor that governs the temporal variability of SIF for all study areas is evapotranspiration. However, NDVI, EVI and air temperature are also correlated with SIF, but not in all biomes. All these variables have positive relationships with SIF. Therefore, it is evident that vegetation behavior's comparability about its sensitivity to biotic and abiotic factors present in each ecosystem. Understanding such relationships is essential in the search for carbon sinks. In this sense, we emphasize that the carbon sinks created by forests and ecosystems depend on the balance between capturing C (via photosynthesis) and loss through breathing. This balance will

vary according to the intrinsic environmental factors' relative effect in each of these processes (photosynthesis and respiration).

Finally, we reinforce that climate change and changes induced by the disturbance of ecosystems can affect photosynthesis and respiration processes differently and, therefore, resulting in the change in the balance of carbon exchange in ecosystems. An unwanted reduction in carbon capture intensity by ecosystems and forests will bring positive feedback in the carbon cycle, which results in the increased greenhouse effect and worsening climate change.

References

BHATTA, S. P.; SHARMA, K. P.; BALAMI, S. Variation in carbon storage among tree species in the planted forest of Kathmandu , Central. **Current science**, [s. l.], v. 115, n. 2, p. 274–282, 2018.

CHHABRA, A.; GOHEL, A. Dynamics of atmospheric carbon dioxide over different land cover types in India. **Environmental Monitoring and Assessment**, [s. l.], v. 191, n. July 2014, 2019.

CHHABRA, A.; GOHEL, A. Elucidating space based observations of solar induced chlorophyll fluorescence over terrestrial vegetation of India. **Tropical Ecology**, [s. l.], v. 61, n. 1, p. 32–41, 2020. https://doi.org/10.1007/s42965-020-00074-w

CRISP, D.; FISHER, B. M.; O'DELL, C.; FRANKENBERG, C.; BASILIO, R.; BÖSCH, H.; BROWN, L. R.; CASTANO, R.; CONNOR, B.; DEUTSCHER, N. M.; ELDERING, A.; GRIFFITH, D.; GUNSON, M.; KUZE, A.; MANDRAKE, L.; MCDUFFIE, J.; MESSERSCHMIDT, J.; MILLER, C. E.; MORINO, I.; NATRAJ, V.; NOTHOLT, J.; O'BRIEN, D. M.; OYAFUSO, F.; POLONSKY, I.; ROBINSON, J.; SALAWITCH, R.; SHERLOCK, V.; SMYTH, M.; SUTO, H.; TAYLOR, T. E.; THOMPSON, D. R.; WENNBERG, P. O.; WUNCH, D.; YUNG, Y. L. The ACOS CO 2 retrieval algorithm – Part II: Global X CO2 data characterization. **Atmospheric Measurement Techniques**, [s. l.], v. 5, n. 4, p. 687–707, 2012.

DAWSON, T. E.; PATE, J. S. 10.1007-BF00582230.pdf. [s. l.], p. 13–20, 1996.

DE ARAÚJO SANTOS, G. A.; MOITINHO, M. R.; DE OLIVEIRA SILVA, B.; XAVIER, C. V.; TEIXEIRA, D. D. B.; CORÁ, J. E.; JÚNIOR, N. L. S. Effects of long-term no-tillage systems with different succession cropping strategies on the variation of soil CO<inf>2</inf> emission. **Science of the Total Environment**, [s. l.], v. 686, 2019.

DE OLIVEIRA SOUZA, T. C.; DELGADO, R. C.; MAGISTRALI, I. C.; DOS SANTOS, G. L.; DE CARVALHO, D. C.; TEODORO, P. E.; DA SILVA JÚNIOR, C. A.; CAÚLA, R. H. Spectral trend of vegetation with rainfall in events of El Niño-Southern Oscillation for Atlantic Forest biome, Brazil. **Environmental Monitoring and Assessment**, [s. l.], v. 190, n. 11, 2018.

DELGADO RC, PEREIRA MG, TEODORO PE, DOS SANTOS GL, DE CARVALHO DC, MAGISTRALI IC, VILANOVA RS. Seasonality of gross primary production in the Atlantic Forest of Brazil. **Glob Ecol Conserv**.14:e00392. 2018 https://doi.org/10.1016/j.gecco.2018.e00392

ELDERING, A.; WENNBERG, P. O.; CRISP, D.; SCHIMEL, D. S.; GUNSON, M. R.; CHATTERJEE, A.; LIU, J.; SCHWANDNER, F. M.; SUN, Y.; O'DELL, C. W.; FRANKENBERG, C.; TAYLOR, T.; FISHER, B.; OSTERMAN, G. B.; WUNCH, D.; HAKKARAINEN, J.; TAMMINEN, J.; WEIR, B. The Orbiting Carbon Observatory-2 early science investigations of regional carbon dioxide fluxes. **Science**, [s. l.], v. 358, n. 6360, 2017.

FALAHATKAR, S.; MOUSAVI, S. M.; FARAJZADEH, M. Spatial and temporal distribution of carbon dioxide gas using GOSAT data over IRAN. **Environmental Monitoring and Assessment**, [s. l.], v. 189, n. 12, 2017.

FARHAN, M.; MOAZZAM, U.; LEE, B. G.; RAHMAN, G.; WAQAS, T. Spatial Rainfall Variability and an Increasing Threat of Drought , According to Climate Change in Uttaradit Province , Thailand. **Atmospheric and Climate Sciences**, [s. l.], v. 10, n. June, p. 357–370, 2020.

FEREZ, A. P. C.; CAMPOE, O. C.; MENDES, J. C. T.; STAPE, J. L. Silvicultural opportunities for increasing carbon stock in restoration of Atlantic forests in Brazil. **Forest Ecology and Management**, [s. l.], v. 350, p. 40–45, 2015.

FILHO, L. F. F. M. **Variabilidade temporal da concentração atmosférica de co2, fluorescência da clorofila induzida pelo sol e ndvi em áreas com diferentes usos agrícolas no centro-sul do Brasil**. 2018. UNIVERSIADE ESTATUAL PAULISTA – UNESP, [s. l.], 2018.

FRANKENBERG, C.; FISHER, J. B.; WORDEN, J.; BADGLEY, G.; SAATCHI, S. S.; LEE, J. E.; TOON, G. C.; BUTZ, A.; JUNG, M.; KUZE, A.; YOKOTA, T. New global observations of the terrestrial carbon cycle from GOSAT: Patterns of plant fluorescence with gross primary productivity. **Geophysical Research Letters**, [s. l.], v. 38, n. 17, p. 1–6, 2011.

FRANKENBERG, C.; O'DELL, C.; BERRY, J.; GUANTER, L.; JOINER, J.; KÖHLER, P.; POLLOCK, R.; TAYLOR, T. E. Prospects for chlorophyll fluorescence remote sensing from the Orbiting Carbon Observatory-2. **Remote Sensing of Environment**, [s. l.], v. 147, p. 1–12, 2014. http://dx.doi.org/10.1016/j.rse.2014.02.007

GAO, Y.; WANG, S.; GUAN, K.; WOLANIN, A.; YOU, L.; JU, W.; ZHANG, Y. The ability of sun-induced chlorophyll fluorescence from OCO-2 and MODIS-EVI to monitor spatial variations of soybean and maize yields in the midwestern USA. **Remote Sensing**, [s. l.], v. 12, n. 7, 2020.

GAULIN, N.; BILLON, P. Le. Climate change and fossil fuel production cuts : assessing global supply-side constraints and policy implications. [s. l.], 2020.

GHAHRAMANI, A.; KINGWELL, R. S.; NARAYAN, T. Land use change in Australian mixed crop-livestock systems as a transformative climate change adaptation. **Agricultural Systems**, [s. l.], v. 180, n. January, p. 102791, 2020. https://doi.org/10.1016/j.agsy.2020.102791

GOLKAR, F.; AL-WARDY, M.; SAFFARI, S. F.; AL-AUFI, K.; AL-RAWAS, G. Using OCO-2 satellite data for investigating the variability of atmospheric CO2 concentration

in relationship with precipitation, relative humidity, and vegetation over Oman. **Water (Switzerland)**, [s. l.], v. 12, n. 1, 2020.

GONSAMO, A.; CHEN, J. M.; HE, L.; SUN, Y.; ROGERS, C.; LIU, J. Exploring SMAP and OCO-2 observations to monitor soil moisture control on photosynthetic activity of global drylands and croplands. **Remote Sensing of Environment**, [s. l.], v. 232, n. July, p. 111314, 2019. https://doi.org/10.1016/j.rse.2019.111314

GUO, M.; LI, J.; HUANG, S.; WEN, L. Feasibility of using MODIS products to simulate sun-induced chlorophyll fluorescence (SIF) in boreal forests. **Remote Sensing**, [s. l.], v. 12, n. 4, 2020.

HAKKARAINEN, J.; IALONGO, I.; TAMMINEN, J. Direct space-based observations of anthropogenic CO2 emission areas from OCO-2. **Geophysical Research Letters**, [s. l.], v. 43, n. 21, p. 11,400-11,406, 2016.

HUETE, A.; DIDAN, K.; MIURA, T.; RODRIGUEZ, E. P.; GAO, X.; FERREIRA, L. G. Overview of the radiometric and biophysical performance of the MODIS vegetation indices. **Remote Sensing of Environment**, [s. l.], v. 83, n. 1–2, p. 195–213, 2002.

JOBBAGY, E. G.; JACKSON, R. B.; APPLICATIONS, S. E.; APR, N. The Vertical Distribution of Soil Organic Carbon and Its Relation to Climate and Vegetation THE VERTICAL DISTRIBUTION OF SOIL ORGANIC CARBON AND ITS. **Ecological Applications**, [s. l.], v. 10, n. 2, p. 423–436, 2000.

JUNIOR, C. H. L. S.; ARAGÃO, L. E. O. C.; ANDERSON, L. O.; FONSECA, M. G.; SHIMABUKURO, Y. E.; VANCUTSEM, C.; ACHARD, F.; BEUCHLE, R.; NUMATA, I.; SILVA, C. A.; MAEDA, E. E.; LONGO, M.; SAATCHI, S. S. Persistent collapse of biomass in Amazonian forest edges following deforestation leads to unaccounted carbon losses. [s. l.], n. I, p. 1–10, 2020.

KEELING, D. The concentration and isotopic abundances of atmospheric carbon dioxide in rural areas. [s. l.], v. 13, 1958.

KUMAR, P.; MISHRA, A. K.; CHAUDHARI, S. K.; SHARMA, K.; RAI, A. K.; SINGH, K.; RAI, P. Carbon Sequestration and Soil Carbon Build-Up under Eucalyptus Plantation in Semi-Arid Regions of North-West India Carbon Sequestration and Soil Carbon Build-Up under. **Journal of Sustainable Forestry**, [s. l.], v. 00, n. 00, p. 1–13, 2020. Disponível em: https://doi.org/10.1080/10549811.2020.1749856

LE MAITRE, D. C.; VAN WILGEN, B. W.; GELDERBLOM, C. M.; BAILEY, C.; CHAPMAN, R. A.; NEL, J. A. Invasive alien trees and water resources in South Africa: Case studies of the costs and benefits of management. **Forest Ecology and Management**, [s. l.], v. 160, n. 1–3, p. 143–159, 2002.

LE QUÉRÉ, C.; RAUPACH, M. R.; CANADELL, J. G.; MARLAND, G.; BOPP, L.; CIAIS, P.; CONWAY, T. J.; DONEY, S. C.; FEELY, R. A.; FOSTER, P.; FRIEDLINGSTEIN, P.; GURNEY, K.; HOUGHTON, R. A.; HOUSE, J. I.; HUNTINGFORD, C.; LEVY, P. E.; LOMAS, M. R.; MAJKUT, J.; METZL, N.; OMETTO, J. P.; PETERS, G. P.; PRENTICE, I. C.; RANDERSON, J. T.; RUNNING, S. W.; SARMIENTO, J. L.; SCHUSTER, U.; SITCH, S.; TAKAHASHI, T.; VIOVY, N.; VAN DER WERF, G. R.; WOODWARD, F. I. Trends in the sources and sinks of carbon dioxide. **Nature Geoscience**, [s. l.], v. 2, n. 12, p. 831–836, 2009.

LÈBRE, E.; ROVERE, L. Low-carbon development pathways in Brazil and ‘ Climate Clubs ’. **WIREs Climate Change**, [s. l.], v. 8, n. 1, 2016.

LEUNING, R.; CLEUGH, H. A.; ZEGELIN, S. J.; HUGHES, D. Carbon and water fluxes over a temperate Eucalyptus forest and a tropical wet / dry savanna in Australia : measurements and comparison with MODIS remote sensing estimates. **Agricultural and Forest Meteorology**, [s. l.], v. 129, n. 3–4, p. 151–173, 2005.

LI, X.; XIAO, J.; HE, B.; ALTAF ARAIN, M.; BERINGER, J.; DESAI, A. R.; EMMEL, C.; HOLLINGER, D. Y.; KRASNOVA, A.; MAMMARELLA, I.; NOE, S. M.; ORTIZ, P. S.; REY-SANCHEZ, A. C.; ROCHA, A. V.; VARLAGIN, A. Solar-induced chlorophyll fluorescence is strongly correlated with terrestrial photosynthesis for a wide variety of biomes: First global analysis based on OCO-2 and flux tower observations. **Global Change Biology**, [s. l.], v. 24, n. 9, p. 3990–4008, 2018.

MAES, W. H.; PAGÁN, B. R.; MARTENS, B.; GENTINE, P.; GUANTER, L.; STEPPE, K.; VERHOEST, N. E. C.; DORIGO, W.; LI, X.; XIAO, J.; MIRALLES, D. G. Remote Sensing of Environment Sun-induced fl uorescence closely linked to ecosystem transpiration as evidenced by satellite data and radiative transfer models. **Remote**

Sensing of Environment, [s. l.], v. 249, n. August, p. 112030, 2020. https://doi.org/10.1016/j.rse.2020.112030

MERRICK, T.; PAU, S.; JORGE, M. L. S. P.; SILVA, T. S. F.; BENNARTZ, R. Spatiotemporal patterns and phenology of tropical vegetation solar-induced chlorophyll fluorescence across 76razilian biomes using satellite observations. **Remote Sensing**, [s. l.], v. 11, n. 15, 2019.

MOHAMMED, G. H.; COLOMBO, R.; MIDDLETON, E. M.; RASCHER, U.; VAN DER TOL, C.; NEDBAL, L.; GOULAS, Y.; PÉREZ-PRIEGO, O.; DAMM, A.; MERONI, M.; JOINER, J.; COGLIATI, S.; VERHOEF, W.; MALENOVSKÝ, Z.; GASTELLU-ETCHEGORRY, J. P.; MILLER, J. R.; GUANTER, L.; MORENO, J.; MOYA, I.; BERRY, J. A.; FRANKENBERG, C.; ZARCO-TEJADA, P. J. Remote sensing of solar-induced chlorophyll fluorescence (SIF) in vegetation: 50 years of progress. **Remote Sensing of Environment**, [s. l.], v. 231, n. February, p. 111177, 2019. https://doi.org/10.1016/j.rse.2019.04.030

MOUSAVI, S. M.; FALAHATKAR, S.; FARAJZADEH, M. Assessment of seasonal variations of carbon dioxide concentration in Iran using GOSAT data. **Natural Resources Forum**, [s. l.], v. 41, n. 2, p. 83–91, 2017.

PAN, G.; XU, Y.; MA, J. The potential of CO 2 satellite monitoring for climate governance : A review. **Journal of Environmental Management**, [s. l.], v. 277, n. September 2020, p. 111423, 2021. https://doi.org/10.1016/j.jenvman.2020.111423

PEREIRA, B. D. J.; BERNARDES, A.; FILHO, C.; LA, N.; JR, S. Greenhouse gas emissions and carbon footprint of cucumber, tomato and lettuce production using two cropping systems. **Journal of Cleaner Production**, [s. l.], n. xxxx, p. 124517, 2020. https://doi.org/10.1016/j.jclepro.2020.124517

PILI, U. B.; VIOLANDA, R. R. Extracting Earth's orbital period from atmospheric CO2concentrations using the Fourier transform based on Matlab. **Physics Education**, [s. l.], v. 55, n. 5, p. 1V, 2020.

QIU, R.; HAN, G.; MA, X.; SHA, Z.; SHI, T.; XU, H.; ZHANG, M. CO2 concentration, a critical factor influencing the relationship between solar-induced chlorophyll fluorescence and gross primary productivity. **Remote Sensing**, [s. l.], v. 12, n. 9, 2020.

RAMANATHAN, V.; CRUTZEN, P. J.; KIEHL, J. T.; ROSENFELD, D. Aerosols, Climate, and the Hydrological Cycle. **Science (New York, N.Y.)**, [s. l.], v. 294, n. December, p. 2119–2125, 2001.

RESH, S. C.; BINKLEY, D.; PARROTTA, J. A. Greater Soil Carbon Sequestration under Nitrogen-fixing Trees Compared with Eucalyptus Species. **Ecosystems**, [s. l.], v. 5, n. 3, p. 217–231, 2002.

RICHARD, A.; PEKKA, E.; WERNER, A.; OLIVER, L.; SIMON, L.; JOSEP, G.; ROBERT, B.; STEPHEN, W.; DAVID, A. A large and persistent carbon sink in the world's forests. **Science**, [s. l.], v. 333, n. August, p. 988–993, 2011.

ROCHA, J. H. T.; MENEGALE, M. L. C.; RODRIGUES, M.; GONÇALVES, J. L. de M.; PAVINATO, P. S.; FOLTRAN, E. C.; HARRISON, R.; JAMES, J. N. Impacts of timber harvest intensity and P fertilizer application on soil P fractions. **Forest Ecology and Management**, [s. l.], v. 437, n. December 2018, p. 295–303, 2019. https://doi.org/10.1016/j.foreco.2019.01.051

ROSSI, F. S.; SANTOS, G. A. de A. Fire dynamics in Mato Grosso State, Brazil: the relative roles of gross primary productivity. **Big Earth Data**, [s. l.], v. 4, n. 1, p. 23–44, 2020. https://doi.org/10.1080/20964471.2019.1706832

SANTOS, M. V.; DA FONSECA, D. M.; DA SILVA, L. D.; DE SOUZA, W. F.; DE OLIVEIRA, T. S.; FERREIRA, L. R.; DE OLIVEIRA NETO, S. N.; PACIULLO, D. S. C. Integrated crop–forage–forestry for sustainable agricultural systems: productive performance. **Agroforestry Systems**, [s. l.], v. 94, n. 2, p. 417–427, 2020.

SCHIMEL, D.; STEPHENS, B. B.; FISHER, J. B. Effect of increasing CO2 on the terrestrial carbon cycle. **Proceedings of the National Academy of Sciences of the United States of America**, [s. l.], v. 112, n. 2, p. 436–441, 2015.

SHI, S.; YU, J.; WANG, F.; WANG, P.; ZHANG, Y.; JIN, K. Science of the Total Environment Quantitative contributions of climate change and human activities to vegetation changes over multiple time scales on the Loess Plateau. **Science of the Total Environment**, [s. l.], v. 755, p. 142419, 2021. https://doi.org/10.1016/j.scitotenv.2020.142419

SILVA, B. de O.; MOITINHO, M. R.; SANTOS, G. A. de A.; TEIXEIRA, D. D. B.; FERNANDES, C.; LA SCALA, N. Soil CO2 emission and short-term soil pore class distribution after tillage operations. **Soil and Tillage Research**, [s. l.], v. 186, n. October 2018, p. 224–232, 2019. https://doi.org/10.1016/j.still.2018.10.019

SILVA JUNIOR, C.; TEODORO, P. E.; DELGADO, R. C.; PEREIRA, L.; TEODORO, R.; LIMA, M.; PANTALEÃO, A. D. A.; HENRIQUE, F.; BAIO, R.; AZEVEDO, G. B. De; TAÍS, G.; SOUSA, D. O. Persistent fire foci in all biomes undermine the Paris Agreement in Brazil. **Scientific Reports**, [s. l.], p. 1–14, 2020. https://doi.org/10.1038/s41598-020-72571-w

UPRETY, S.; CAO, C. Radiometric comparison of 1.6-μm CO2 absorption band of Greenhouse Gases Observing Satellite (GOSAT) TANSO-FTS with Suomi-NPP VIIRS SWIR band. **Journal of Atmospheric and Oceanic Technology**, [s. l.], v. 33, n. 7, p. 1443–1453, 2016.

VOURLITIS, G.L., DALMAGRO, H.J., ARRUDA, P.H.Z.D., LATHUILLIERE, M.J., PINTO-JR, O.B., LOBO, F.D.A., COUTO, E.G., NOGUEIRA, J.D.S. AND JOHNSON, M.S., 2015. Ecosystem-scale CH 4 and CO2 fluxes in a seasonally flooded scrub forest of the Brazilian Pantanal. **AGUFM**, pp.B13F-0698, 2015.

WANG, J.; ZENG, N.; WANG, M. Interannual variability of the atmospheric CO2 growth rate: Roles of precipitation and temperature. **Biogeosciences**, [s. l.], v. 13, n. 8, p. 2339–2352, 2016.

WEI, J.; TANG, X.; GU, Q.; WANG, M.; MA, M.; HAN, X. Using solar-induced chlorophyll fluorescence observed by OCO-2 to predict autumn crop production in China. **Remote Sensing**, [s. l.], v. 11, n. 14, p. 1–14, 2019.

WHITEHEAD, D.; BEADLE, C. L. Physiological regulation of productivity and water use in Eucalyptus: A review. **Forest Ecology and Management**, [s. l.], v. 193, n. 1–2, p. 113–140, 2004.

XAVIER, C. V.; MOITINHO, M. R.; DE BORTOLI TEIXEIRA, D.; ANDRÉ DE ARAÚJO SANTOS, G.; DE ANDRADE BARBOSA, M.; BASTOS PEREIRA MILORI, D. M.; RIGOBELO, E.; CORÁ, J. E.; LA SCALA JÚNIOR, N. Crop rotation and succession in a no-tillage system: Implications for CO<inf>2</inf> emission and soil attributes. **Journal of Environmental Management**, [s. l.], v. 245, 2019.

XIAO, J.; CHEVALLIER, F.; GOMEZ, C.; GUANTER, L.; HICKE, J. A.; HUETE, A. R.; ICHII, K.; NI, W.; PANG, Y.; RAHMAN, A. F.; SUN, G.; YUAN, W.; ZHANG, L.; ZHANG, X. Remote sensing of the terrestrial carbon cycle: A review of advances over 50 years. **Remote Sensing of Environment**, [s. l.], v. 233, n. January, p. 111383, 2019. Disponível em: https://doi.org/10.1016/j.rse.2019.111383

XIE, S.; MO, X.; HU, S.; LIU, S. Agricultural and Forest Meteorology Contributions of climate change, elevated atmospheric CO 2 and human activities to ET and GPP trends in the Three-North Region of China. **Agricultural and Forest Meteorology**, [s. l.], v. 295, n. October, p. 108183, 2020. https://doi.org/10.1016/j.agrformet.2020.108183

XU, X.; LI, F.; LIN, Z.; SONG, X. Science of the Total Environment Holocene fi re history in China : Responses to climate change and human activities. **Science of the Total Environment**, [s. l.], v. 753, p. 142019, 2021. Disponível em: https://doi.org/10.1016/j.scitotenv.2020.142019

XU, Y.; CUI, G. Influence of spectral characteristics of the Earth's surface radiation on the greenhouse effect: Principles and mechanisms. **Atmospheric Environment**, [s. l.], v. 244, n. 516, p. 117908, 2021. https://doi.org/10.1016/j.atmosenv.2020.117908

YOKOTA, T.; YOSHIDA, Y.; EGUCHI, N.; OTA, Y.; TANAKA, T.; WATANABE, H.; MAKSYUTOV, S. Global concentrations of CO2 and CH4 retrieved from GOSAT: First preliminary results. **Scientific Online Letters on the Atmosphere**, [s. l.], v. 5, n. 1, p. 160–163, 2009.

YU, Z.; ZHOU, G.; LIU, S.; SUN, P.; AGATHOKLEOUS, E. Impacts of forest management intensity on carbon accumulation of China's forest plantations. **Forest Ecology and Management**, [s. l.], v. 472, n. June, p. 118252, 2020. Disponível em: https://doi.org/10.1016/j.foreco.2020.118252

CHAPTER 3 – Space-time variability of X_{CO2} and SIF from OCO-2: A case study in the Mato Grosso State, Brazil

ABSTRACT – The use of geostatistics in the analysis of space-time processes is widely used in several knowledge areas. In recent years it has been applied to detect space-time variability of atmospheric CO_2 concentration in some parts of the world. Thus, the objective with this study was to detect the seasonal spatial variability of X_{CO2} and SIF using Ordinary Kriging to Mato Grosso State, Brazil. The study comprises the period from January 2015 to December 2018. Remote sensing data (X_{CO2} and SIF) were collected on the OCO-2 platform. The dataset was separated into the dry and wet season, and then submitted to descriptive statistical analysis and ordinary kriging's spatial variability. The mean for X_{CO2} in the wet season ranged from 393.96 ± 0.10 to 394.14 ± 0.10 ppm between 2015 and 2018, and no variation in the means of X_{CO2} was observed between these years for the dry period. In the wet season, the SIF was higher about the dry period. A significant, more substantial negative relation ($r= -0.84$ $p <0.01$) was observed between X_{CO2} and SIF. Higher X_{CO2} and SIF values were observed in the state's northern region, under the Amazon biome. Therefore, we conclude that in Mato Grosso, Brazil, the seasonal variability of X_{CO2} is positively related to Solar-Induced chlorophyll Fluorescence (SIF). This indicates that under these regional conditions, photosynthesis plays an essential role in this process. High values of SIF and X_{CO2} under the Amazon may be indicating an imbalance. This means that the rainforest may be releasing all the carbon it absorbs into the atmosphere.

Keywords: Carbon cycle, carbon-climate-feedbacks, geostatistics, OCO-2

3.1 Introduction

The use of geostatistics in the analysis of the processes that evolve in space and time is widely used in various areas of knowledge, such as medicine (Kleinschmidt et al., 2000; Langkulsen et al., 2020), environmental sciences (García-santos et al., 2020; Wu et al., 2021), climatology (Haylock et al., 2008; Alvares et al., 2014), hydrology (Rivas-tabares et al., 2020), agricultural sciences (Kazama et al. , 2020; Morlin et al., 2020), soil science (La Scala Jr et al., 2000; Panosso et al., 2009; Terçariol et al., 2016), social sciences (Luukkainen et al., 2020) and transport (Kumar et al., 2020).

With the advance of remote sensing techniques in the detection of greenhouse gas concentration (Yokota et al., 2009; Eldering et al., 2017; Schwandner et al., 2017), studies using kriging techniques are essential in the mapping of CO_2 and CH_4 (Falahatkar et al., 2017; Liu et al., 2018; Mousavi and Falahatkar, 2020). Liu et al. (2018) observed that the concentration of X_{CO2} is higher in winter and spring, and the concentration of X_{CH4} changed significantly with latitude in East Asia.

In Brazil, Kriging techniques are used in several areas of knowledge, especially agricultural sciences (Moitinho et al., 2015; Terçariol et al., 2016) and climate (Alvares et al., 2014). This method's application for mapping the atmospheric concentration of CO_2 and fluorescence of sun-induced chlorophyll is summarized in a few studies (He et al., 2020).

The presence of the sun-induced chlorophyll fluorescence (SIF) is significant In studies involving the variability of X_{CO2} (Meneses, 2018; Morais Filho, 2018) since SIF carries useful information on photosynthetic activities. Thus, the understanding of carbon dynamics in ecosystems has been explored in recent years (Gao et al., 2020; Merrick et al., 2019; Mohammed et al., 2019).

Recent studies have shown the sensitivity of SIF to periods of drought (Castro et al., 2020; Lee et al., 2013) and that this can affect the dynamics of CO_2 in the atmosphere (Morais Filho, 2018). Therefore, this study was developed for Mato Grosso, Brazil, due to its large territorial extension, which covers three national biomes (Pantanal, Amazonia and Cerrado), which gives it special attention due to agricultural expansion on these biomes. Knowing that ecosystems (biomes) play a fundamental

role in carbon cycling, the objective with this study was to detect the seasonal spatial variability of X_{CO2} and SIF for the state of Mato Grosso, Brazil, through Ordinary Kriging using OCO-2 data to find potential carbon sources and sinks.

3.2 Material and Methods

3.2.1 Study area

The study was developed for the state of Mato Grosso (9º09'S – 61º19' W and 17º49' S – 53º19'W) located in the Midwest region of Brazil. The area occupies 92,547,100 ha, bordering the northern states of Pará and Amazonas, to the south with the state of Mato Grosso do Sul, to the east and west with the states of Goiás, Tocantins and with the states of Rondônia and Bolivia. The climate is classified as tropical with concentrated rains in the summer period. The classification is Aw, according to the classification of Köppen and Geiger. The mean air temperature is 26.5 °C, and the annual precipitation is 2000 mm $year^{-1}$ and may vary between the regions of the state. The state is divided into three domains: the Amazonia, Cerrado and Pantanal (Figure 1). The values of accumulated precipitation and average air temperature for the study are presented in Figure 2.

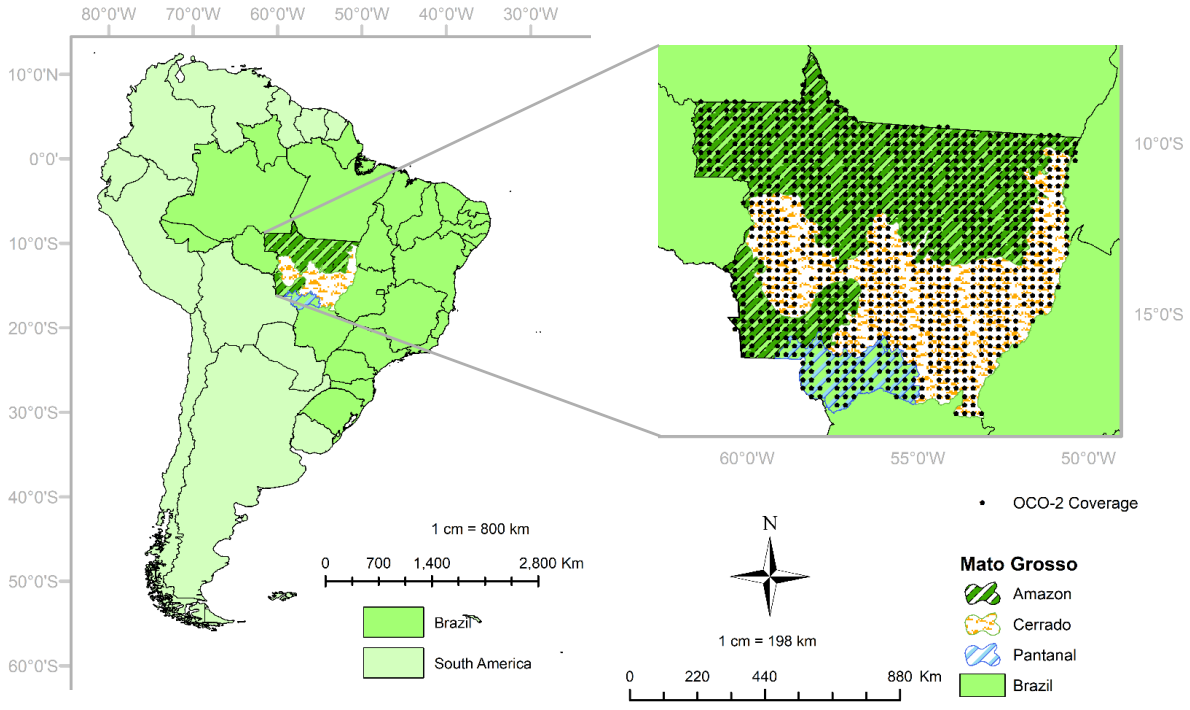

Figure 1. Characterization biomes in Mato Grosso state, Midwest of Brazil.

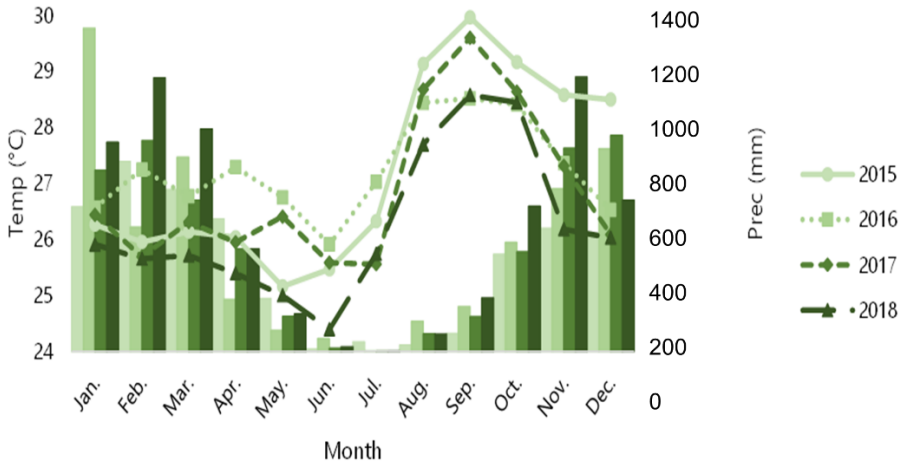

Figure 2. Temporal variation of accumulated precipitation (bars) and average air temperature (lines) for the state of Mato Grosso, Brazil-based on data extracted from the NASA/POWER platform (Stackhouse et al., 2015).

3.2.2 Data acquisition

Data were obtained from January 2015 to December 2018 and after stratified in the dry and rainy season. The dry season corresponds to April to September and the rainy season from October to March. The database used to perform all the analyses present in this article can be accessed at https://github.com/gustavoanndre/OK_MT_XCO2_SIF. Those were treated following the flowchart presented in Figure 3.

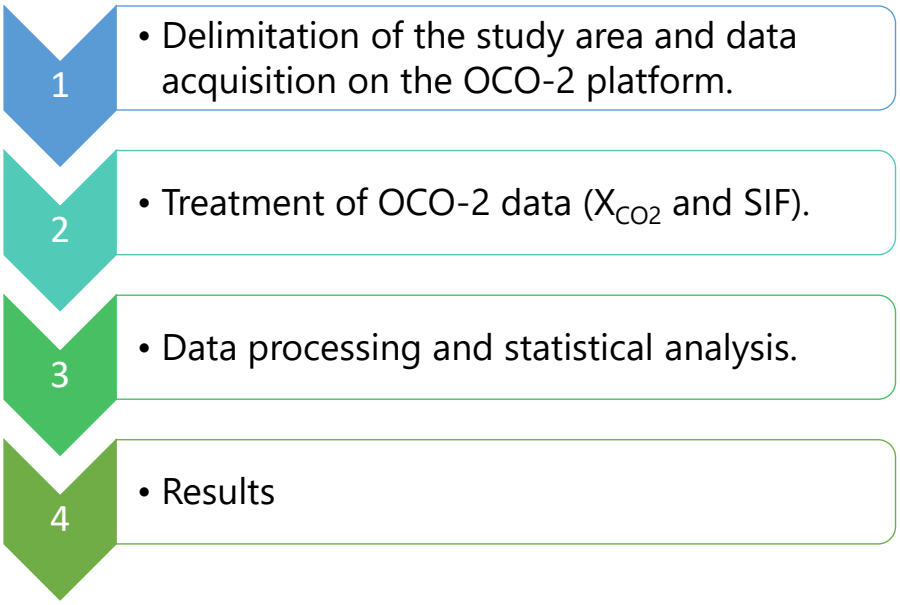

Figure 3. Flowchart of the data acquisition and processing.

3.2.2.1 Orbiting carbon observatory-2 (OCO-2)

The primary product delivered by the Orbiting Carbon Observatory-2 consists of spatially resolved estimates of the column-averaged dry-air mole fraction. This quantity, called X_{CO2} by members of the atmospheric carbon science community, quantifies the average concentration of carbon dioxide in a column of dry air extending from Earth's surface to the top of the atmosphere. Estimates of X_{CO2} derived by taking the ratio of the column integrated number densities of carbon dioxide and molecular oxygen along the optical path between the Sun, the surface footprint, and the instrument, and then multiplying these results by the column-averaged oxygen

concentration (0.20935). These carbon dioxide and oxygen number densities are estimated from high-resolution spectra of reflected sunlight, collected by the Observatory's instrument at wavelengths (colors) within the 0.765-micron molecular oxygen A-band and two carbon dioxide bands centered at wavelengths near 1.61 and 2.06 microns. The Orbiting Carbon Observatory-2 mission will produce four different levels of data products for the user community that will provide comprehensive mission data results. (CRISP et al., 2012).

The OCO-2 SIF Lite files contain bias-corrected SIF (solar-induced fluorescence) and other select fields aggregated as daily files. The OCO-2 spectrometer measures spectra in the O2A-band, with far-red SIF, retrieved at 757 and 771 nm based on the infilling of the Fraunhofer lines at 13:36 local time with data commencing on September 6, 2014 (Frankenberg et al., 2014).

We obtained SIF and X_{CO2} data from the OCO-2 Lite version (V7r) with 0.25º Spatial grid resolution from the OCO-2 data archive maintained at NASA (https://co2.jpl.nasa.gov/#mission=OCO-2). To make SIF771 data more realistic, we deleted SIF values lower than 0.1 W m^{-2} sr^{-1} μm^{-1}, according to Guo et al. (2020). The trend adjustment of the X_{CO2} data was made using the regression method (Gujarati and Porter, 2011).

3.2.3 Statistical analysis and temporal variation of data

Data used to consist of quarterly averages for each geographic coordinate evaluated in the study area. The descriptive statistics (mean, standard error of the mean, minimum, maximum, and Kurtosis) was used to classify the variability of the variables. Simultaneously, the basic assumptions of the analysis of variance and normality of errors and homogeneity of variances were tested for all variables evaluated. Pearson correlation analysis (Eq. 1) was performed to understand the variation of X_{CO2} with the SIF.

$$r = \frac{\sum_{i=0}^{n}(x_i - \underline{x})(y_i - \underline{y})}{\sqrt{(x_i - \underline{x})X\sqrt{(y_i - \underline{y})}}} \qquad \text{(Eq.1)}$$

where: x_i are the observed values of the variable x is the mean of the variable x; y_i is the observed values of the variable y is the mean of the variable y.

The code used to perform this analysis can be accessed at https://github.com/gustavoanndre/OK_MT_XCO2_SIF/blob/master/pearsoncorrelation.

3.2.4 Spatial variability (ordinary kriging)

In this study, spherical, exponential and gaussian models were tested. The choice of the model and parameters adjusted to the experimental variogram was based on the residual sum of squares (RSS) and largest coefficient of determination (R^2) obtained during the adjustment of the theoretical model to the experimental variogram.

The spatial variability of the attributes evaluated was determined by calculating and modeling the experimental variogram, based on the theory of regionalized variables and the principles of an intrinsic hypothesis (ISAAKS and SRIVASTAVA, 1989). The variogram describes the spatial continuity of the variables as a function of the distances between two locations, is estimated by:

$$\hat{\gamma}(h) = \frac{1}{2\,N\,(h)} \times \sum_{i=1}^{N(h)} [z(x_i) - z(x_i + h)]^2 \qquad \text{(Eq.02)}$$

in which γ (h) is the experimental semivariance for a separation distance h, z(xi) is the property value at the point I, and N(h) is the number of pairs of points separated by distance h. During the modeling of the experimental variogram, the coefficients of the model are estimated: nugget effect (C0), level (C0+C1), and range (a).

The Ordinary kriging (OK) estimation at the unsampled point x_0 is given by Equation (3):

$$\hat{z}(x_0) = \sum_{i=1}^{N} \lambda_i \, Z\,(x_i) \qquad \text{(Eq.03)}$$

where $\hat{z}(x_0)$is the OK estimation at the unsampled point x_0, $Z(x_i)$ is the neighboring value at the location x_i, with i= 1, 2, …, n, and λ_i is the weight of observations

associated with the neighbouring values, which are estimated based on the adjusted variogram.

The construction of spatial pattern maps interpolated by OK was performed using GS$^+$ 9.0 (Gamma Design Software, LLC, Plainwell, MI, USA)

3.3 Results

3.3.1 Temporal variation

The descriptive statistic for X_{CO2} and SIF is presented in Table S1 (Appendices). The average for X_{CO2} in the rainy season ranged from 393.96±0.10 ppm to 394.14±0.10ppm between 2015 and 2018 (Figure 4a). No considerable variation was observed in the means of X_{CO2} between these years for the dry period. In general, the variation of X_{CO2} between years was around 1 ppm. The median was close to the average for all observed periods. The kurtosis values for X_{CO2} ranged from -0. 29 to 1.84.

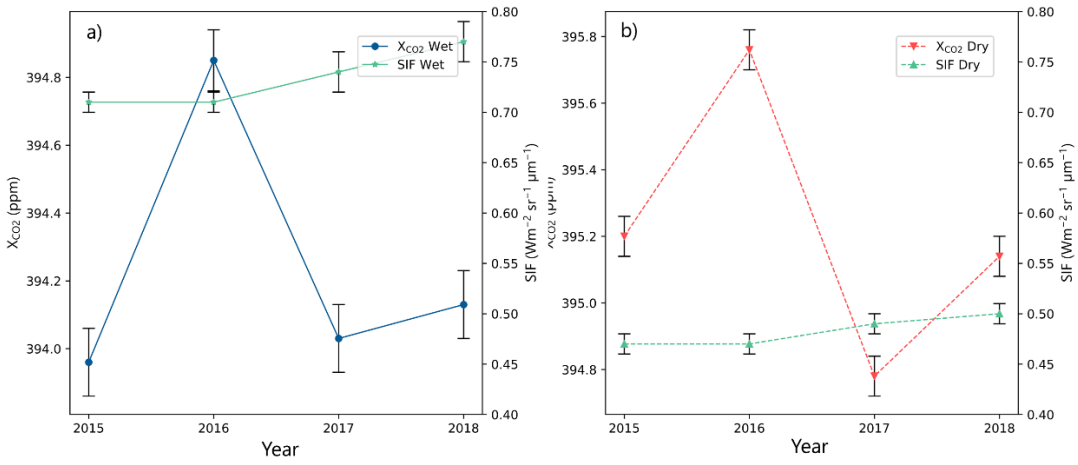

Figure 4. Temporal variation for X_{CO2} ppm and SIF to wet (a) and dry (b) period of Mato Grosso State, Brazil.

The wet season presented higher values in the dry period (Figure 4). The averages between 2015 and 2018 for SIF in the rainy season were 0.71 ± 0.01 m^{-2} sr^{-1} μm^{-1} and 0.77 ± m^{-2} sr^{-1} μm^{-1}. On the other hand, in the dry period were 0.47 ± 0.01 m^{-2} sr^{-1} μm^{-1} and 0.50 ± 0.01 m^{-2} sr^{-1} μm^{-1}. Like X_{CO2}, the median presented values close to the average for SIF. The kurtosis values were like those of X_{CO2}, ranging from -0.60 to 1.79 (Table 1).

The Pearson correlation analysis was performed (Figure 5) to X_{CO2} with SIF demonstrated the sensibility of X_{CO2} to photosynthetic activity through chlorophyll fluorescence. A significant negative relationship was observed ($p < 0.01$) SIF with a correlation coefficient of the $r = -0.84$.

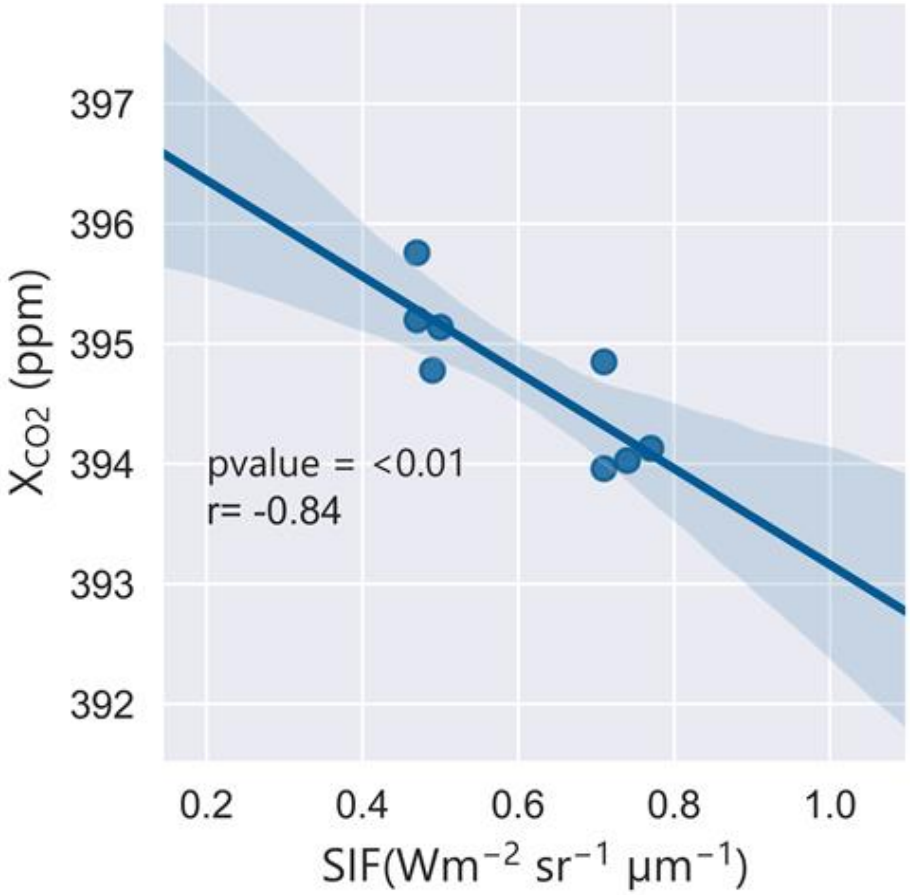

Figure 5. Pearson correlation to X_{CO2} with SIF considering the averages of the dry and rainy periods of each year studied (N=8).

3.3.2 Spatial variability

Regarding the parameters of the semivariograms (Table 2), the spherical model was the one that best adjusted for most of the variables studied. The exponential model adjusted better in both 2017 and the rainy season in 2018 for X_{CO2}.

The estimated ranges from the models adjusted to the semivariograms for X_{CO2} in the dry period ranged from 0.783º to 1.483º for 2015 and 2017, respectively, while in the rainy season, this variation was from 0.738º to 1,111º observed in the same years of the dry periods. For the SIF, the years 2015 and 2018 presented the lowest (0.56º) and the highest (1.328º) and range value in the dry period, respectively. In the

rainy season, higher (0.926º) and lower (0.623º) reach value was for the years 2017 and 2018.

Table 2. Models, parameters of the estimated semivariograms, degree of spatial variability, coefficient of determination, and the sum of squares of residues for X_{CO2}, SIF757 e SIF 771, in the state of Mato Grosso, Brazil.

Target			Model	Patamar	Alcance	SDD[1]			
				C0	C0+C1	A	C0/[C0+C1]	R^2	RSS[2]
2015	wet	X_{CO2}	Spherical	1.67	0.58	0.73	0.58	0.68	3.24
		SIF	Spherical	0.05	0.42	0.74	0.42	0.72	1.45E^{-04}
	dry	X_{CO2}	Spherical	0.86	0.55	0.78	0.55	0.62	0.18
		SIF	Spherical	0.01	0.38	0.56	0.38	0.26	2.87E^{-04}
2016	wet	X_{CO2}	Spherical	1.34	0.60	0.75	0.60	0.83	0.61
		SIF	Spherical	0.05	0.30	0.79	0.30	0.55	1.98E^{-04}
	dry	X_{CO2}	Spherical	0.96	0.50	0.94	0.50	0.53	0.24
		SIF	Spherical	0.02	0.44	0.80	0.44	0.5	1.47E^{-04}
2017	wet	X_{CO2}	Exponential	0.39	0.90	1.11	0.90	0.8	0.67
		SIF	Spherical	0.05	0.38	0.92	0.38	0.71	1.66E^{-04}
	dry	X_{CO2}	Exponential	0.69	0.63	1.48	0.63	0.66	0.22
		SIF	Spherical	0.03	0.24	1.03	0.24	0.43	4.55E^{-05}
2018	wet	X_{CO2}	Exponential	0.88	0.75	0.77	0.75	0.54	2.03
		SIF	Spherical	0.06	0.31	0.62	0.31	0.48	1.11E^{-04}
	dry	X_{CO2}	Spherical	0.99	0.48	1.14	0.48	0.48	0.33
		SIF	Spherical	0.03	0.23	1.32	0.23	0.27	1.51E^{-01}

Where: (1) degree of spatial dependence (strong with % ≤ 25%, moderate with 25 to 75%, and weak >75%); (2) Sum of squares of waste.

The degree of spatial dependence (DSD) for X_{CO2} was higher concentrated in the dry period for the years 2016 (0.83) and 2017 (0.80). For the other periods, the DSD of X_{CO2} presented median values. In general, the SIF presented values of degree of spatial dependence between 0.25 and 0.75.

Considering that the variables did not present high kurtosis values, the distribution of data considered close to normal, and the geostatistical analysis was performed. When analyzing the spatial distribution of X_{CO2} (Figure 6a) and SIF (Figure 6b), we observed that the variables presented uneven dynamics. The periods did not present a predictable variation concerning the dynamics of hot spots and cold spots between dry and rainy months. The variations between subsequent years also did not demonstrate a defined pattern, varying independently for each year analyzed.

However, for the spatial variability of hot spots and cold spots of X_{CO2}, it was observed that the southern region (Pantanal) of the state presented lower

concentrations in most periods, and the north (Amazon) and center (Cerrado) of the state presented higher concentrations during most of the years analyzed.

The values of SIF indicated a standardization over the years, evidenced by the decrease in the color amplitude present in the maps, where the yellow and orange shades (higher values) increased in the area over the years, and the shades of green (higher values) decreased. The SIF showed intensely the yellow and orange shades that were predominant at the end of the last year. However, there was a significant presence of readings that turned green on the maps. The highest values of SIF were concentrated in the northern region of Mato Grosso, while the lower value readings were concentrated in the southeast region of the state map. This dynamic tended to homogenize over the years, decreasing the variety of readings between the north and south regions of the state.

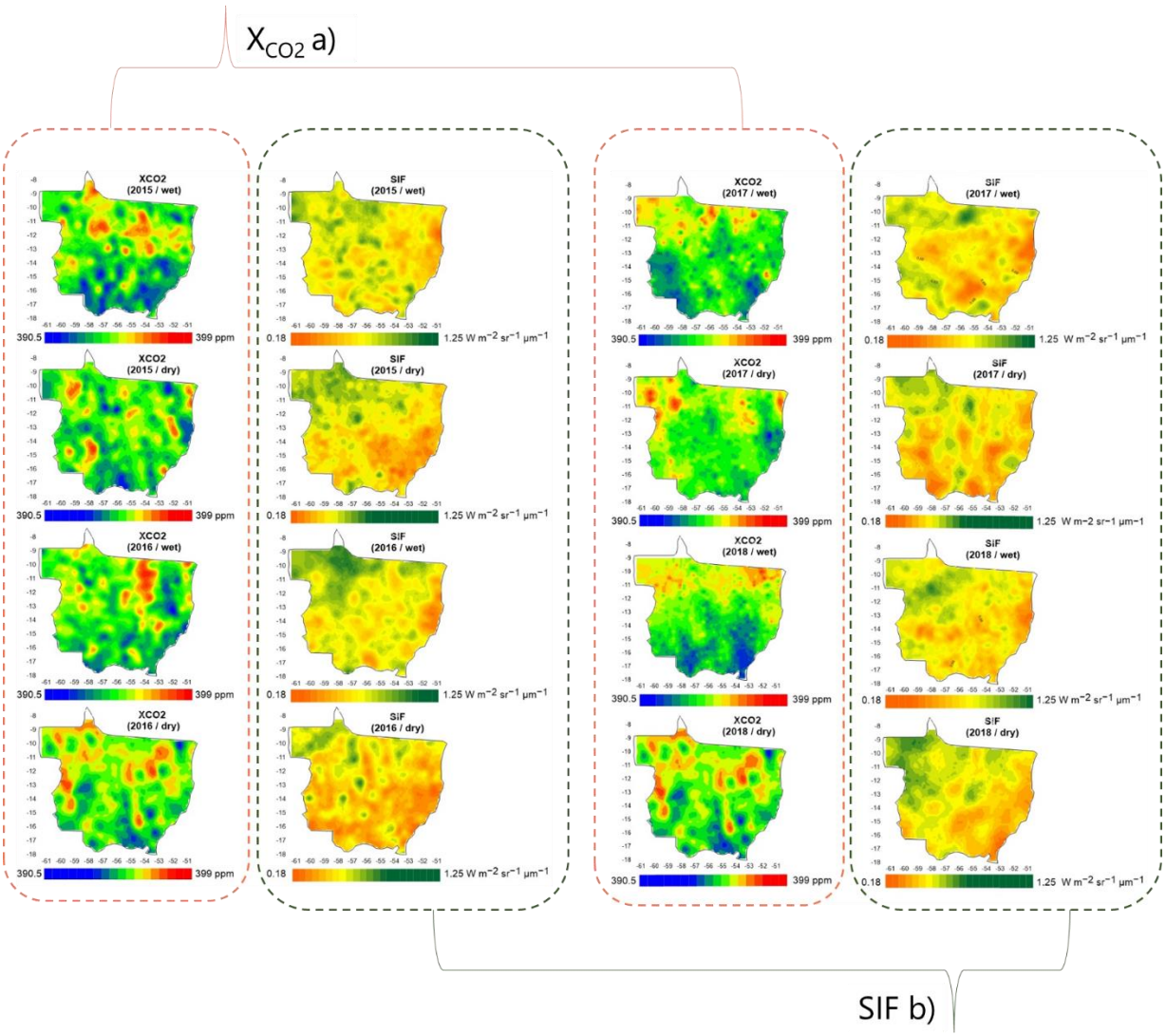

Figure 6. Spatial distribution of X_{CO2} (a) and SIF (b) in the state of Mato Grosso, Brazil considering the seasons.

3.4 Discussion

The response of X_{CO2} and SIF to the dynamics of the rainfall regime was already expected since, in studies of temporal variability, this response has already been reported (MENESES, 2018; MORAIS FILHO, 2018). In our study, the correlation between X_{CO2} and SIF was considered high according to Mukaka, (2012). This demonstrates the relationship between X_{CO2} variation and photosynthetic activity. The seasonal carbon balance in southern Amazonia, Parazoo et al. (2013) observed that SIF is inversely correlated with X_{CO2} in southern Amazonia (r = -0.53), indicating, according to the authors, that the increase in X_{CO2} variability is driven by changes effects on gross primary productivity by vegetation.

The fluorescence of sun-induced chlorophyll (SIF) carries useful information on photosynthetic activities. For this reason, SIF has been explored in the understanding of carbon dynamics in ecosystems in recent years (Gao et al., 2020; Merrick et al., 2019; Mohammed et al., 2019). When investigating the seasonal fluorescence patterns of high-resolution of SIF to assess the extreme vulnerability to drought in the Amazonian ecoregions, observed the variability of SIF in the Amazonian ecoregions. These same authors found responses to SIF to drought on an ecoregional scale, which indicates that there are different levels of drought resilience in the Amazon ecosystem than currently. Analyzing three years of SIF data for vegetation classes within and among the six Brazilian biomes showed that SIF satellite measurements can distinguish important functions and phenological differences in vegetation classes and, therefore, can improve our understanding of productivity seasonality in the tropics.

Regarding this seasonality, in the state of Mato Grosso, Rossi and Santos (2020) observed that the variation of carbon assimilation (gross primary production) by biomes in the state of Mato Grosso is governed by rain. Lee et al. (2013) and Castro et al. (2020) also observed falls in photosynthetic activity during the dry season are lower than during the rainy season. According to Lee et al. (2013), plants can maintain

their chlorophyll content during the dry season but photosynthesize less due to stomatic closure (except early in the morning, when soil water potentials had time to recover).

Given the sensitivity of SIF to the canopy and rain dynamics, the highest values of kurtosis compared to X_{CO2} are justified. The kurtosis index reflects the extent to which the density of observations differs from the probability density of the normal curve (Kots and Johnson, 1982). According to the values of asymmetry and shortness between -2 and +2 are considered acceptable to prove the normal univariate distribution (George & Mallery, 2010). Although the short for SIF values were higher than $X_{CO2,}$ the values of kurtosis were close to 0 and below -2/2, demonstrate the normality of data. Liu et al. (2011) observed the same results.

The spherical, exponential, and Gaussian models are the ones that explain most spatial phenomena, according to Yakamoto and Landim (2013). In our study, the spheric and exponential models were best adjusted, especially the spheric models that explained for all variables.

Less erratic phenomena without significant variations are best described by spherical and Gaussian models (Isaaks and Srivatava 1989). According to Webster and Oliver (2007), the spherical model seems the most obvious to describe the variation in three-dimensional bodies; however, the spherical function is one of the most used geostatistics models to two and three dimensions. As for the exponential model, Isaacks and Srivatava (1989) claim that, just as the spherical is linear at very short distances near the origin, however, it rises more abruptly and then flattens more gradually.

For the mapping of $X_{CO2,}$ the application of spherical models was also made by Liu et al. (2011); Zeng et al. (2012); Falahatkar et al. (2017). The spatial distribution of the X_{CH4} also presented spherical models in a study based on Mousavi and Falahatkar (2020). CO_2 emissions in agricultural soils is a carbon source for the atmosphere (Santos et al., 2019; Xavier et al., 2019). Within this perspective, studies have been pointing out spherical and exponential models such as those that best map the emission of CO_2. For SIF, although there are studies using kriging in its spatial interpolation (Tadic et al., 2015; Tadić et al., 2017), the discussion of model adjustment is not yet well infused.

In addition to the adjustment of models, in geostatistics, the range (a) is an essential parameter in the study of the semivariogram because it represents the distance in which there is no spatial correlation between the points of the same variable (Panosso et al., 2009).

Another critical parameter for geostatistics is the degree of spatial dependence (DSD) according to the classification made by Cambardella et al. (1994). The DSD for X_{CO2} was considered weak in the dry period for the years 2016 and 2017. For the other periods, the DSD of X_{CO2} was considered moderate. The only variables that presented strong DSD were the SIF in the dry period of 2018. In other periods, the SIF presented a degree of moderate spatial dependence. Falahatkar et al. (2017), in a study conducted for Iran with GOSAT data, found a degree of spatial dependence from 0.15 to 0.25 for X_{CO2}, considered strong. Liu et al. (2012) found a moderate degree of spatial dependence for X_{CO2}, corroborating our results.

According to Parazoo et al. (2013), the strong gradients in the annual exclusion, duration of the dry season and type of vegetation caused a great deal of spatial heterogeneity in the Amazon carbon cycle. Because of this spatial and temporal variability, as a carbon exchange link on normal scales and continents, we should only improve our understanding of the role of the Amazon in the global carbon cycle with data acquisition on a broad temporal scale. In the study to Mato Grosso with the objective to measure patterns of aboveground wood C stocks (Cw) and rates of wood C storage (ΔCw) over a 7^{-year} period for Cerrado forests and woodlands of southern Mato Grosso, Brazil, arrayed across hydrological and soil fertility gradients, the Vourlitis et al. (2019) looked the Rates of wood C storage increased as nutrient availability increased, and C storage declined during drought years for both seasonally flooded and non-flooded forests and woodlands.

3.5 Conclusions

Our findings indicate that in the state of Mato Grosso, the seasonal variation of X_{CO2} is highly related to Solar-Induced chlorophyll Fluorescence (SIF). This shows that photosynthesis is the most important key when looking for carbon uptake. The SIF is responsive to the dry and rainy season, being the lowest values always observed in

the dry season, thus being an essential variable in studies aimed at seeing the effects of extreme droughts in Amazon, Cerrado, and Pantanal ecosystems. The difference of X_{CO2} between the dry and rainy season for the state of Mato Grosso, Brazil, is up to 1 ppm.

The spatial distribution of X_{CO2} demonstrates that the southern region (Pantanal) of the state presents lower concentrations in most periods, and the north (Amazon) and center (Cerrado) of the state shows the higher concentrations during most of the years studied.

References

CASTRO, A. O.; CHEN, J.; ZANG, C. S.; SHEKHAR, A.; JIMENEZ, J. C.; BHATTACHARJEE, S.; KINDU, M.; MORALES, V. H.; RAMMIG, A. OCO-2 solar-induced chlorophyll fluorescence variability across ecoregions of the Amazon basin and the extreme drought effects of El Niño (2015-2016). **Remote Sensing**, [s. l.], v. 12, n. 7, 2020.

DE ARAÚJO SANTOS, G. A.; MOITINHO, M. R.; DE OLIVEIRA SILVA, B.; XAVIER, C. V.; TEIXEIRA, D. D. B.; CORÁ, J. E.; JÚNIOR, N. L. S. Effects of long-term no-tillage systems with different succession cropping strategies on the variation of soil CO<inf>2</inf> emission. **Science of the Total Environment**, [s. l.], v. 686, 2019.

ELDERING, A.; WENNBERG, P. O.; CRISP, D.; SCHIMEL, D. S.; GUNSON, M. R.; CHATTERJEE, A.; LIU, J.; SCHWANDNER, F. M.; SUN, Y.; O'DELL, C. W.; FRANKENBERG, C.; TAYLOR, T.; FISHER, B.; OSTERMAN, G. B.; WUNCH, D.; HAKKARAINEN, J.; TAMMINEN, J.; WEIR, B. The Orbiting Carbon Observatory-2 early science investigations of regional carbon dioxide fluxes. **Science**, [s. l.], v. 358, n. 6360, 2017.

FALAHATKAR, S.; MOUSAVI, S. M.; FARAJZADEH, M. Spatial and temporal distribution of carbon dioxide gas using GOSAT data over IRAN. **Environmental Monitoring and Assessment**, [s. l.], v. 189, n. 12, 2017.

GAO, Y.; WANG, S.; GUAN, K.; WOLANIN, A.; YOU, L.; JU, W.; ZHANG, Y. The ability of sun-induced chlorophyll fluorescence from OCO-2 and MODIS-EVI to monitor

spatial variations of soybean and maize yields in the midwestern USA. **Remote Sensing**, [s. l.], v. 12, n. 7, 2020.

GARCÍA-SANTOS, G.; SCHEIBER, M.; PILZ, J. Chemosphere Spatial interpolation methods to predict airborne pesticide drift deposits on soils using knapsack sprayers. **Chemosphere**, [s. l.], v. 258, p. 127231, 2020. Disponível em: https://doi.org/10.1016/j.chemosphere.2020.127231

GUO, M.; LI, J.; HUANG, S.; WEN, L. Feasibility of using MODIS products to simulate sun-induced chlorophyll fluorescence (SIF) in boreal forests. **Remote Sensing**, [s. l.], v. 12, n. 4, 2020.

HARUNA, E.; ROUVERSON, K. Methodology for selective coffee harvesting in management zones of yield and maturation. **Precision Agriculture**, [s. l.], n. 0123456789, 2020. https://doi.org/10.1007/s11119-020-09751-1

HAYLOCK, M. R.; HOFSTRA, N.; TANK, A. M. G. K.; KLOK, E. J.; JONES, P. D.; NEW, M. A European daily high-resolution gridded data set of surface temperature and precipitation for 1950 – 2006. [s. l.], v. 113, 2008.

HE, Z.; LEI, L.; ZHANG, Y.; SHENG, M.; WU, C.; LI, L.; ZENG, Z. C.; WELP, L. R. Spatio-temporal mapping of multi-satellite observed column atmospheric CO2 using precision-weighted kriging method. **Remote Sensing**, [s. l.], v. 12, n. 3, p. 1–24, 2020.

IZIDORIO, R.; MARTINS FILHO, M. V.; MARQUES JÚNIOR, J.; DE SOUZA, Z. M.; PEREIRA, G. T. Perdas de nutrientes por erosão e sua distribuiçao espacial em área sob cana-de-açúcar. **Engenharia Agricola**, [s. l.], v. 25, n. 3, p. 660–670, 2005.

LA SCALA, N., J. M.; PEREIRA, G. T.; CORA, J. E. Short-term temporal changes in the spatial variability model of CO 2 emissions from a Brazilian bare soil. [s. l.], v. 32, p. 0–3, 2000.

KLEINSCHMIDT, I.; BAGAYOKO, M.; CLARKE, G. P. Y.; CRAIG, M.; SUEUR, D. Le. A spatial statistical approach to malaria mapping. [s. l.], p. 355–361, 2000.

KUMAR, A.; KUMAR, R.; SARMA, K. Mapping spatial distribution of traffic induced criteria pollutants and associated health risks using kriging interpolation tool in Delhi. **Journal of Transport & Health**, [s. l.], v. 18, n. July, p. 100879, 2020. https://doi.org/10.1016/j.jth.2020.100879

LANGKULSEN, U.; PROMSAKHA, K.; SAKOLNAKHON, N.; JAMES, N. Climate change and dengue risk in central region of Thailand. **International Journal of Environmental Health Research**, [s. l.], v. 30, n. 3, p. 327–335, 2020. https://doi.org/10.1080/09603123.2019.1599100

LEE, J. E.; FRANKENBERG, C.; VAN DER TOL, C.; BERRY, J. A.; GUANTER, L.; BOYCE, C. K.; FISHER, J. B.; MORROW, E.; WORDEN, J. R.; ASEFI, S.; BADGLEY, G.; SAATCHI, S. Forest productivity and water stress in Amazonia: Observations from GOSAT chlorophyll fluorescence. **Tohoku Journal of Experimental Medicine**, [s. l.], v. 230, n. 1, 2013.

LIU, Y.; WANG, X.; GUO, M.; TANI, H. Mapping the FTS SWIR L2 product of XCO2 and XCH4 data from the GOSAT by the Kriging method - a case study in East Asia. **International Journal of Remote Sensing**, [s. l.], v. 33, n. 10, p. 3004–3025, 2012.

LIU, Y.; WANG, X.; TANI, H.; GUO, M. Analysis of relationship between NDVI and GHG in Daxing'an mountain region, China. **Proceedings for ISPRS workshop on Dynamic and Multi-dimensional GIS**, [s. l.], n. January 2014, p. 40–43, 2011.

LIU, Y.; YUE, T.; ZHANG, L.; ZHAO, N.; ZHAO, M.; LIU, Y. Simulation and analysis of XCO2 in North China based on high accuracy surface modeling. **Environmental Science and Pollution Research**, [s. l.], v. 25, n. 27, p. 27378–27392, 2018.

LUUKKAINEN, H. H.; VETTENRANTA, J.; WANG, J.; GARVIS, S. Family related variables effect on later educational outcome : a further geospatial analysis on TIMSS 2015 Finland. **Large-scale Assessments in Education**, [s. l.], 2020.https://doi.org/10.1186/s40536-020-00081-2

M.M MUKAKA. Statistics Corner: A Guide to Appropriate Use of Correlation Coefficient in Medical Research. **Malawi Medical Journal**, [s. l.], v. 24, n. 3, p. 69–71, 2012. https://pubmed.ncbi.nlm.nih.gov/23638278/

MERRICK, T.; PAU, S.; JORGE, M. L. S. P.; SILVA, T. S. F.; BENNARTZ, R. Spatiotemporal patterns and phenology of tropical vegetation solar-induced chlorophyll fluorescence across brazilian biomes using satellite observations. **Remote Sensing**, [s. l.], v. 11, n. 15, 2019.

MOHAMMED, G. H.; COLOMBO, R.; MIDDLETON, E. M.; RASCHER, U.; VAN DER TOL, C.; NEDBAL, L.; GOULAS, Y.; PÉREZ-PRIEGO, O.; DAMM, A.; MERONI, M.; JOINER, J.; COGLIATI, S.; VERHOEF, W.; MALENOVSKÝ, Z.; GASTELLU-ETCHEGORRY, J. P.; MILLER, J. R.; GUANTER, L.; MORENO, J.; MOYA, I.; BERRY, J. A.; FRANKENBERG, C.; ZARCO-TEJADA, P. J. Remote sensing of solar-induced chlorophyll fluorescence (SIF) in vegetation: 50 years of progress. **Remote Sensing of Environment**, [s. l.], v. 231, n. February, p. 111177, 2019. https://doi.org/10.1016/j.rse.2019.04.030

MORLIN, F.; CARLOS, C.; ANGELI, E.; ZERBATO, C.; CANDIDA, P.; LUCAS, D. M.; GÍRIO, S. Comparison between vegetation indices for detecting spatial and temporal variabilities in soybean crop using canopy sensors. **Precision Agriculture**, [s. l.], v. 21, n. 5, p. 979–1007, 2020. https://doi.org/10.1007/s11119-019-09704-3

MOUSAVI, S. M.; FALAHATKAR, S. Spatiotemporal distribution patterns of atmospheric methane using GOSAT data in Iran. **Environment, Development and Sustainability**, [s. l.], v. 22, n. 5, p. 4191–4207, 2020. https://doi.org/10.1007/s10668-019-00378-5

MOUSAVI, S. M.; FALAHATKAR, S.; FARAJZADEH, M. Assessment of seasonal variations of carbon dioxide concentration in Iran using GOSAT data. **Natural Resources Forum**, [s. l.], v. 41, n. 2, p. 83–91, 2017.

PANOSSO, A. R.; EDUARDO, C.; RIBEIRO, R.; ZANINI, J. R.; PAVANI, L. C.; PEREIRA, G. T.; LA, N.; JÚNIOR, S. Variabilidade espacial da emissão de CO 2 , da temperatura e umidade de um latossolo desprovido de vegetação sob diferentes lâminas de molhamento Spatial variability of co 2 emission , temperature and moisture of a bare oxisol submitted to different wetti. [s. l.], p. 1017–1034, 2009. a.

PANOSSO, A. R.; JR, J. M.; PEREIRA, G. T.; JR, N. L. S. Soil & Tillage Research Spatial and temporal variability of soil CO 2 emission in a sugarcane area under green and slash-and-burn managements. [s. l.], v. 105, p. 275–282, 2009. b.

PARAZOO, N. C.; BOWMAN, K.; FRANKENBERG, C.; LEE, J. E.; FISHER, J. B.; WORDEN, J.; JONES, D. B. A.; BERRY, J.; COLLATZ, G. J.; BAKER, I. T.; JUNG, M.; LIU, J.; OSTERMAN, G.; O'DELL, C.; SPARKS, A.; BUTZ, A.; GUERLET, S.; YOSHIDA, Y.; CHEN, H.; GERBIG, C. Interpreting seasonal changes in the carbon balance of southern Amazonia using measurements of XCO2 and chlorophyll fluorescence from GOSAT. **Geophysical Research Letters**, [s. l.], v. 40, n. 11, p. 2829–2833, 2013.

RIVAS-TABARES, D.; MIGUEL, Á. De; WILLAARTS, B.; TARQUIS, A. M. Self-organizing map of soil properties in the context of hydrological modeling. **Applied Mathematical Modelling**, [s. l.], v. 88, p. 175–189, 2020. https://doi.org/10.1016/j.apm.2020.06.044

SCHWANDNER, F. M.; GUNSON, M. R.; MILLER, C. E.; CARN, S. A.; ELDERING, A.; KRINGS, T.; VERHULST, K. R.; SCHIMEL, D. S.; NGUYEN, H. M.; CRISP, D.; O'DELL, C. W.; OSTERMAN, G. B.; IRACI, L. T.; PODOLSKE, J. R. Spaceborne detection of localized carbon dioxide sources. **Science**, [s. l.], v. 358, n. 6360, 2017.

STAPE, L.; SENTELHAS, P. C.; ALVARES, C. A.; GONC, L. D. M. Ko ¨ ppen ' s climate classification map for Brazil. [s. l.], v. 22, n. 6, p. 711–728, 2014.

TADIĆ, J. M.; QIU, X.; MILLER, S.; MICHALAK, A. M. Spatio-temporal approach to moving window block kriging of satellite data v1.0. **Geoscientific Model Development**, [s. l.], v. 10, n. 2, p. 709–720, 2017.

TADIC, J. M.; QIU, X.; YADAV, V.; MICHALAK, A. M. Mapping of satellite Earth observations using moving window block kriging. **Geoscientific Model Development**, [s. l.], v. 8, n. 10, p. 3311–3319, 2015.

TERÇARIOL, M. C.; BRANCAGLIONI, V. A.; ARTÊNCIO JÚNIOR, J. P.; MONTANARI, R.; TEIXEIRA FILHO, M. C. M.; BOLONHEZI, A. C.; LA SCALA JÚNIOR, N.; CHAVARETTE, F. R.; PANOSSO, A. R. Spatial Variability of Soil Co2 Emission in Soybean and Sugarcane Areas in Mato Grosso Do Sul Cerrado, Brazil. **Journal of Geospatial Modelling**, [s. l.], v. 2, n. 1, p. 45, 2016.

VOURLITIS GL, ZAPPIA A, BORGES PINTO O, ZANELLA DE ARRUDA PH, SANTANNA FB, DALMAGRO HJ, LOBO F DE A, NOGUEIRA J DE S. Spatial and Temporal Variations in Aboveground Woody Carbon Storage for Cerrado Forests and Woodlands of Mato Grosso, Brazil. **J Geophys Res Biogeosciences**.;124:3252-68. 2019. https://doi.org/10.1029/2019JG005201

WU, Z.; LIU, Y.; HAN, Y.; ZHOU, J.; LIU, J.; WU, J. Science of the Total Environment Mapping farmland soil organic carbon density in plains with combined cropping system extracted from NDVI time-series data. **Science of the Total Environment**, [s. l.], v. 754, p. 142120, 2021. https://doi.org/10.1016/j.scitotenv.2020.142120

XAVIER, C. V.; MOITINHO, M. R.; DE BORTOLI TEIXEIRA, D.; ANDRÉ DE ARAÚJO SANTOS, G.; DE ANDRADE BARBOSA, M.; BASTOS PEREIRA MILORI, D. M.; RIGOBELO, E.; CORÁ, J. E.; LA SCALA JÚNIOR, N. Crop rotation and succession in a no-tillage system: Implications for CO<inf>2</inf> emission and soil attributes. **Journal of Environmental Management**, [s. l.], v. 245, 2019.

YOKOTA, T.; YOSHIDA, Y.; EGUCHI, N.; OTA, Y.; TANAKA, T.; WATANABE, H.; MAKSYUTOV, S. Global concentrations of CO2 and CH4 retrieved from GOSAT: First preliminary results. **Scientific Online Letters on the Atmosphere**, [s. l.], v. 5, n. 1, p. 160–163, 2009.

ZENG, Z.; LEI, L.; HOU, S.; LI, L. A spatio-temporal interpolation approach for the FTS SWIR product of XCO2 data from GOSAT. **International Geoscience and Remote Sensing Symposium (IGARSS)**, [s. l.], p. 852–855, 2012.

CHAPTER 4 – Hot spots and anomalies of CO_2 over eastern Amazonia, Brazil

ABSTRACT – The easternmost part of the Amazonia, located in Maranhão in Brazil, has suffered major deforestation over the last years, which led to the devastation of almost 80% of the original vegetation. Here we aim to characterize the hot spots, hot moments, anomalies of column-averaged carbon dioxide in the atmosphere (X_{CO2}, ppm) and their interactions with climate and vegetation indices in eastern Amazonia using the Orbiting Carbon Observatory-2 (OCO-2) data from Nasa. The study was carried out for Amazonia Oriental present in the state of Maranhão, northeast Brazil. The variables X_{CO2}, Solar-induced chlorophyll fluorescence at 757 nm and 771 nm (SIF 757 and SIF 771, respectively) were extracted from OCO-2. The NDVI data from MODIS and climate variables as of NASA POWER platform was used to explain X_{CO2} variability. The study comprised the period from January 2015 to December 2018. Data were submitted to regression, correlation, and temporal analysis, identifying hot/cold moments and spatial hot/cold spots. In addition, anomalies were calculated to identify CO_2 potential sources and sinks. Temporal changes indicate atmospheric X_{CO2} in the range from 362.2 to 403.4 ppm. Higher X_{CO2} values (hot moments) were concentrated from May to September, with some peaks in December. The lower values (cold moments) were concentrated in November to April. The SIF 771 W m^{-2} sr^{-1} μm^{-1} explained temporal changes of X_{CO2} in 58% (R^2Adj. = 0.58; $p < 0.001$) and the precipitation into 27% (R^2Adj. = 0.27; $p < =0.001$). The spatial hot spots with 90% confidence were more representative in 2016. The X_{CO2} anomaly (ppm) maximum and minimum were 6.19 ppm (source) and - 6.29 ppm (sink), respectively. We conclude that the hot moments of X_{CO2} to the Eastern Amazon forest are concentrated in the year's droughts season. The spatial hot spots of X_{CO2} and the anomalies are also concentrated in the southern region and near Amazon forest protected areas.

Keywords: Carbon Cycle; OCO-2, Climate-carbon-feedbacks; Tropical forest; Remote sensing

4.1 Introduction

Amazonia biome is a key part of the global carbon cycle (Longo et al., 2020). In 2000 the amount of carbon stored in its Amazon biomass was approximately 93 ± 23 PgC (Malhi et al., 2006). In addition to the carbon cycle, Amazonia also plays a significant role in the hydrological cycle, with significant precipitation effects throughout South America (Ruiz-Vásquez et al., 2020). Recent estimations of ecosystem services provided by the Amazonia rainforest reach the highest values from US$ 56.72 ± 10 ha^{-1} yr^{-1} to US$ 737 ± 134 ha^{-1} yr^{-1} but are restricted to only 12% of the remaining forest (Strand et al., 2018) having 8.8 M hectares.

Despite the numerous benefits provided by the intact Amazonia rainforest, this does not deprive it of degradation. The Amazonia Rainforest has lost about 20% of its native vegetation in recent decades (INPE, 2020). The effects of deforestation are diverse, among them the loss of biodiversity (Barlow et al., 2016), reduction of ecosystem services (Strand et al., 2018), increased incidence of diseases such as malaria (Bauhoff and Busch, 2020), deregulation of rain cycles (Casagrande et al., 2018), increase in periods of extreme droughts (Souza et al., 2019) and increased CO_2 emissions into the atmosphere (Walker et al., 2020). In recent years, fires are the result of uncontrolled deforestation (De Oliveira Silva et al., 2021), which mischaracterizes the forest canopy resulting in an environment conducive to forest fires (Rossi and Santos, 2020).

Some regions of Amazonia have already been quite deforested, as is the case of the eastern Amazon in Maranhão. In this region, about 74% of the Amazonia rainforest has already been deforested, the remaining 23,967 km^2 unforested (Silva Junior et al., 2020), having no more forest centers outside protected areas (Santos de Lima et al., 2018). Such devastation directly impacts the effects that the Amazonia has on the hydrological cycle and carbon dynamics (Longo et al., 2020). The effects of deforestation under Amazonia have changed the functional structure (Silva Junior et al., 2019; Sales et al., 2020). Using vegetation indexes to detect the change in land use between the Amazonia and the Cerrado, Silva Júnior et al. (2019) observed a new frontier that delimits biomes transition is different from the official limit of the government.

Deforestation in Brazil is the leading sector associated with greenhouse gas emissions. Changes in land use of Amazonia accounts for about 66.7% of carbon emissions into the atmosphere during non-drought years, according to a study by Aragão et al. (2014) using mathematical modeling. These same authors point out that drought-related carbon emissions from tree mortality and forest fires during extreme drought events become critically important, contributing 48.3% of total emissions from the Brazilian Amazonia.

In addition to models that estimate greenhouse gas (GHG) fluxes, remote sensing emerges as essential ferments in understanding GHG dynamics (Esteves et al., 2016). More recently, the scientific community has joined efforts into developing satellites capable of measuring atmospheric GHG concentrations. Two significant projects within this perspective are Greenhouse gases Observing Satellite- GOSAT (Yokota et al., 2009) launched in 2009 by JAXA (Japan Aerospace Exploration Agency) e o Orbiting Carbon Observatory-2 OCO-2 (Crisp et al., 2017) launched in 2014 by NASA. These satellites were developed to characterize sources and sinks around the planet and fill some gaps related to the global carbon cycle.

Using OCO-2 data Patra et al. (2017) derived that during the 2014-2016 El Niño, about 2-3 pentagrams of carbon from the Earth's surface (land + ocean) were emitted into the atmosphere. Some researchers have been using satellite data to estimate emissions in forest fires (Guo et al., 2017, 2012; Villalobos et al., 2020) and others to relate the dynamics of vegetation cover with the atmospheric concentration of greenhouse gases (Falahatkar et al., 2017; Mousavi et al., 2017).

The data disposable from these platforms are essential to better understand the regional or global carbon cycle, which is uncertain in the tropics, where land-use change is a severe problem (Cox et al., 2000; Anderegg et al., 2015; Schimel et al., 2015). Even knowing the importance of understanding the carbon cycle, the characterization of potential carbon sources and sinks, and the advances in data use from these satellites worldwide, studies in the Amazonia region using these satellite data are practically non-existent.

This Eastern Amazonia region could be greatly impacted if protection policies are not taken seriously about forest conservation. While the government does not implement forest restoration policies, this region of the Amazon serves as a laboratory

for studies aimed at predicting the impacts of deforestation for other forest regions, or even for the biome as a whole, since the hostility to which the Eastern Amazon in Maranhão State has been submitted cannot be seen in other regions of the Amazon biome. Therefore, knowing the importance of the Amazon in the global carbon cycle and the scarcity of studies under the Amazonia areas that are highly deforested, our study hypothesis is that climatological variables and photosynthetic activity influence the hot moments of XCO2. Therefore, we aimed to identify the hot spots, hot moments, anomalies of X_{CO2} and their interactions with climate and vegetation index in the eastern Amazon using the OCO-2 data.

4.2 Material and Methods

4.2.1 Study area

The easternmost part of the Amazon biome reaches the State of Maranhão in Brazil (Fig. 1). The Maranhense Amazon has 81,208.40 $km^{2,}$ representing 24.46% of the state territory (IBGE, 2002), in which it is located 62 municipalities. Climate characterization was made by the climatic classification described by Thornwaite (1948). For Imperatriz Subregion, the climate is sub-humid type C2. In Zé Doca, the climate is humid type B1. For Turiaçu and São Luis regions, the Climate is humid type B2. All this information can be found at Martins e Oliveira (2011).

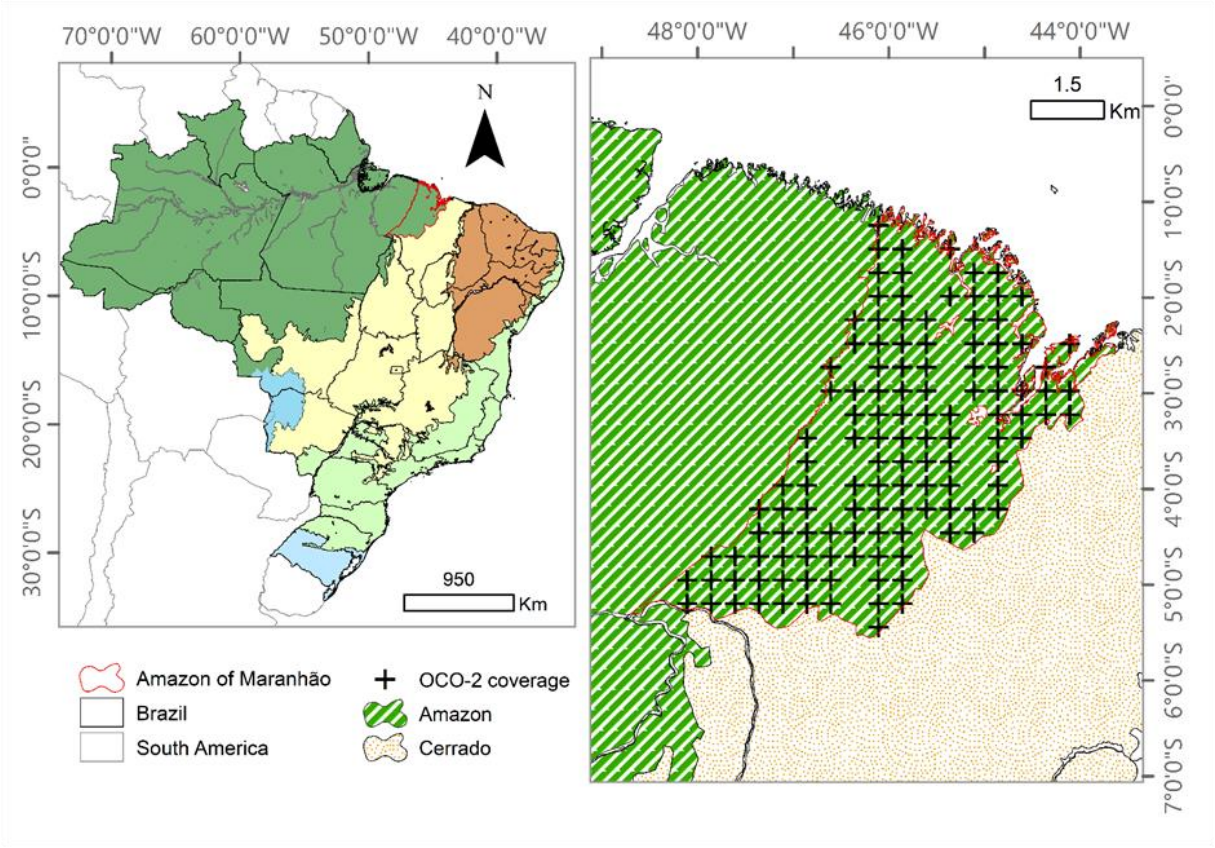

Figure 1. Location of the Eastern Amazonia region in Maranhão State, Brazil.

4.2.2 Remotely sensed and meteorological data

The data of X_{CO2}, SIF 757 and 771 from the OCO-2 system were obtained from January 2015 to December 2018 and after stratified monthly. Those were treated following the flowchart presented in Figure 2.

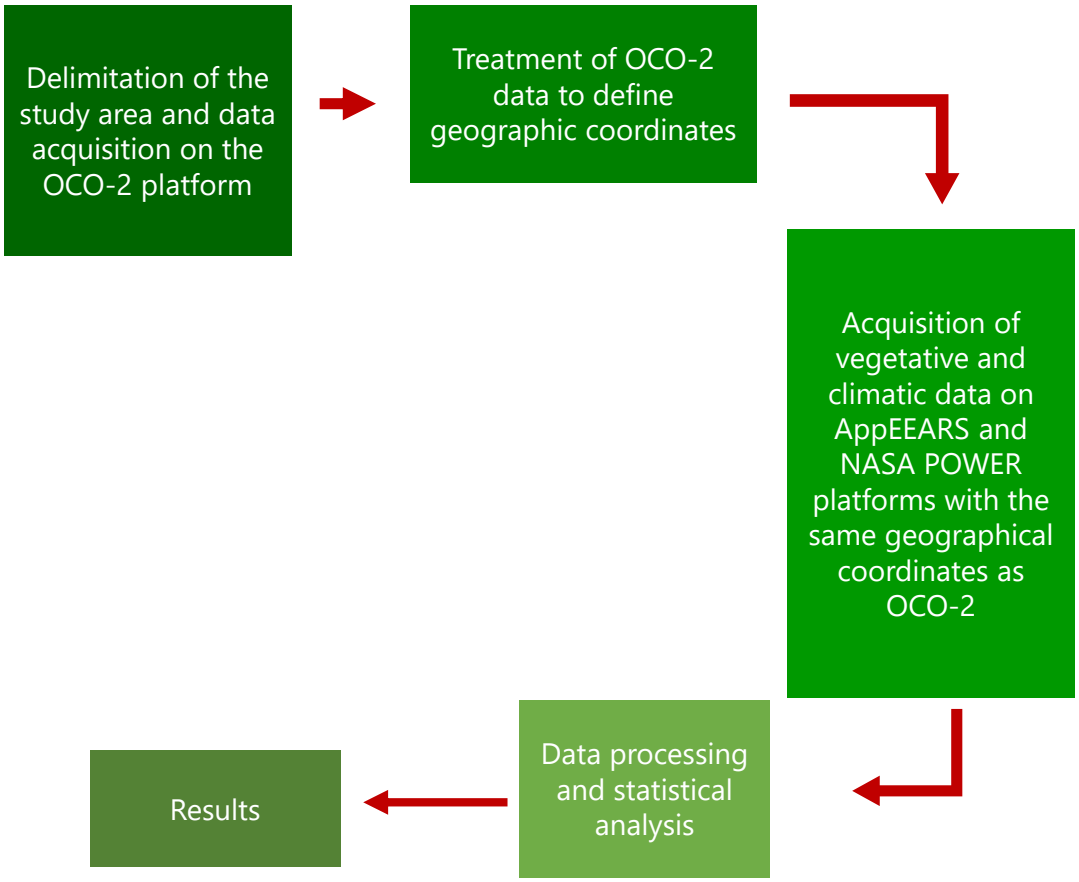

Figure 2. Flowchart of the data acquisition and processing.

4.2.2.1 Orbiting Carbon Observatory-2 (OCO-2)

The primary product delivered by the Orbiting Carbon Observatory-2 consists of spatially resolved estimates of the column-averaged dry air mole fraction. This quantity, called X_{CO2} by members of the atmospheric carbon science community, quantifies the average concentration of carbon dioxide in a column of dry air extending from Earth's surface to the top of the atmosphere. Estimates of X_{CO2} derived by taking the ratio of the column integrated number densities of carbon dioxide and molecular oxygen along the optical path between the Sun, the surface footprint, and the instrument, and then multiplying these results by the column-averaged oxygen concentration (0.20935-micron). These carbon dioxide and oxygen number densities are estimated from high-resolution spectra of reflected sunlight, collected by the Observatory's instrument at wavelengths (colors) within the 0.765-micron molecular

oxygen. A band and two carbon dioxide bands centered at wavelengths near 1.61 and 2.06 microns. The Orbiting Carbon Observatory-2 mission will produce four different levels of data product for the user community that will provide comprehensive mission data results (Crisp et al., 2012).

The OCO-2 SIF Lite files contain bias-corrected SIF (solar-induced fluorescence) and other select fields aggregated as daily files. The OCO-2 spectrometer measures spectra in the O2A-band, with far-red SIF, retrieved at 757 and 771 nm based on the infilling of the Fraunhofer lines at 13:36 local time with data commencing on September 6, 2014 (Frankenberg et al., 2014).

We obtained SIF and X_{CO2} data from the OCO-2 Lite version (V7r) with Spatial grid resolution from the OCO-2 data archive maintained at NASA (https://co2.jpl.nasa.gov/#mission=OCO-2). We deleted SIF values lower than 0.1 W m^{-2} sr^{-1} μm^{-1}, according to Guo et al. (2020). The temporal trend adjustment of the X_{CO2} data was made using the regression method (Gujarati e Porter, 2011). For this reason, after the adjustment, the X_{CO2} is the call of $X_{CO2adjusted}$.

4.2.2.2 Meteorological data

The data of precipitation (mm), wind speed at 10m (m s^{-1}), wind direction and air humidity at 2 m (%) were acquired through the NASA Power platform (https://power.larc.nasa.gov) (Stackhouse et al., 2015). This platform consists of a NASA project titled: World Energy Resource Forecast (POWER) and has been started to improve the current renewable energy data set and create new datasets from new satellite systems. The POWER project targets three user communities: (1) Renewable Energy, (2) Sustainable Buildings and (3) Agroclimatology. It compiles information from various data sources directly and those derived from gridded data systems. The air temperature and relative humidity are obtained from the Global Model and Assimilation Office (GEOS-4) system, and precipitation data are obtained from the Global Precipitation Climate Project.

4.2.2.3 MODIS data

The NDVI (Normalized Difference Vegetation Index) was used; (Rouse et al., 1973). We used data from the MODIS-Terra sensor-system (Moderate Resolution Image Spectroradiometer) Product MOD13A1 with a spatial resolution of 500 m evaluated every 16 days that were downloaded through Nasa AρρEEARS platform (https://lpdaacsvc.cr.usgs.gov/appeears/). Data were obtained for the same time series as OCO-2 for tile h13v09. These data are generally used to evaluate vegetation phenological aspects and detect land-use changes and land cover (Huete et al., 2002). NDVI is known to be more sensitive to chlorophyll and other pigments responsible for the absorption of solar radiation in the red band. (Gao et al., 2000; Huete et al., 2002).

NDVI values were calculated from the equation (Eq.1) described below:

$$NDVI = \frac{\rho NIR - \rho R}{\rho NIR + \rho R} \quad \text{(Eq.1)}$$

where: ρNIR and ρR: reflectance in the spectral bands of near-infrared and red, respectively.

4.2.3 Statistical analysis

4.2.3.1 Descriptive data statistics to hot moments

The data were initially analyzed using descriptive statistics (mean, standard deviation, minimum, maximum, and standard error). These parameters were used to classify the temporal and spatial variability of the variables studied. The assumptions of homoscedasticity analysis and normality of the residues were tested by the Shapiro-Wilk Tests, respectively, both at a 5% probability. Pearson correlation analyses (Eq. 2) and linear regression (Eq. 3) were performed to understand the variation of X_{CO2} with the other variables.

$$r = \frac{\sum_{i=0}^{n}(x_i - \underline{x})(y_i - \underline{y})}{\sqrt{(x_i - \underline{x})X\sqrt{(y_i - \underline{y})}}} \quad \text{(Eq.2)}$$

where: x_i are the observed values of the variable *x* is the mean of the variable *x*; y_i is the observed values of the variable *y* is the mean of the variable *y*.

$$R^2 adjusted = \left[1 - \frac{(1-R^2)*(n-1)}{N-k-1}\right] \quad \text{(Eq.3)}$$

where: *N* is the number of points in the data sample; *K* is the number of independent regressors, that is, the number of variables in the model, excluding the constant.

Code developed for data analyses is available at a public repository (https://github.com/gustavoanndre/Eastern-Amazon_SANTOSETAL2020).

4.2.3.2 Hot Spot analysis (Getis-Ord Gi*)

The hot spot analysis tool calculates the Statistics of Getis-Ord Gi * (ORD and GETIS 1992) for each feature in the dataset. The resulting z-scores and p-values inform where resources with high or low values are spatially grouped. This tool works by looking at each resource within the context of neighboring resources. A high-value feature is interesting, but it may not be a statistically significant access point. To be a statistically significant hot spot, a resource will have a high value and will be surrounded by other features with high values. The local sum of a resource and its neighbors is compared proportionally to the sum of all resources; when the local sum is very different from the expected local sum, and when this difference is too large to be the result of the random chance, a statistically significant result in z scores results.

The sample mean ($\overline{X}$) and the variance of the sample (S) of variable X was defined as:

$$\overline{X} = \frac{\sum_{j=1}^{n} x_j}{n} \quad \text{(Eq. 4)}$$

$$S = \sqrt{\frac{\sum_{j=1}^{n} x_j^2}{n} - (\overline{X})^2} \quad \text{(Eq. 5)}$$

Getis-Ord Gi * is given by:

$$G_i^* = \frac{\sum_{j=1}^{n} w_{i,j}x_j - \overline{X}\sum_{j=1}^{n} w_{i,j}}{S\sqrt{\left[\frac{n\sum_{j=1}^{n} w_{i,j}^2 - \left(\sum_{i=0}^{n} w_{i,j}\right)^2}{n-1}\right]}} \quad \text{(Eq. 6)}$$

where Gi * describes the spatial dependence of incident i on all n events, xj is the magnitude of variable X at the site of the j incident on tod the observations (n) (j can be equal to i) and wij is the value of the weight between the event i and j representing its spatial interrelationship. Usually, the wij is calculated based on the spatial concept relationship and about d. So, it is often written as wij (d). The value of d (for example, Cartesian distance) is a limit specified by the user. However, argument d can be omitted depending on the spatial relationship specification. Gi* statistics may vary depending on the selection of d (SONGCHITRUKSA and ZENG, 2010).

4.2.3.3 X_{CO2} anomaly model

The anomaly model adopted (Eq.7) is based on the one described by Hakkarainen et al. (2016), where anomaly values greater than zero is characterized as carbon emission sources and, for values less than zero, is assigned as a source of carbon absorption. These two characterizations are attributed to anthropic activities such as burning fossil fuels, and when it comes to an emissions source and absorption are attributed to biosphere activities such as forest growth and photosynthetic activities.

$$\mathrm{XCO2\ (anomaly)} = \mathrm{XCO2\ (observation)} - \mathrm{XCO2\ (total\ median)} \qquad \text{(Eq.7)}$$

The calculation of the anomaly occurs by the difference between observation and the daily median of observations. Considering that this study is at the regional level, unlike the basic study that considers global data, there is not enough data to follow the exact model, but it is possible to adapt it using the total median rather than the daily rate. Adaptations in the anomaly model were also carried out by Labzovskii et al. (2019).

4.3 Results

4.3.2 Hot and cold moments

The temporal analysis indicates atmospheric $X_{CO2adjusted}$ in the range from 362.24 to 403.38 ppm (Fig. 3a), with the annual averages of 393.13 ± 0.11 ppm, 393.34 ± 0.10 ppm, 393.13 ± 0.15 ppm and 393 ± 0.14 ppm in 2015, 2016, 2017 and 2018, respectively (Fig. 3b). Higher $X_{CO2adjusted}$ values were concentrated from May to September, with some increases in December. On the other hand, the lower values were concentrated in November to April (Fig. 3c). Observing only the annual averages, it was not possible to notice an increase in $X_{CO2\ adjusted}$ over the years for this region, but when observed the months and seasonal trends, it is seen hot and cold moments for regional $X_{CO2\ adjusted}$.

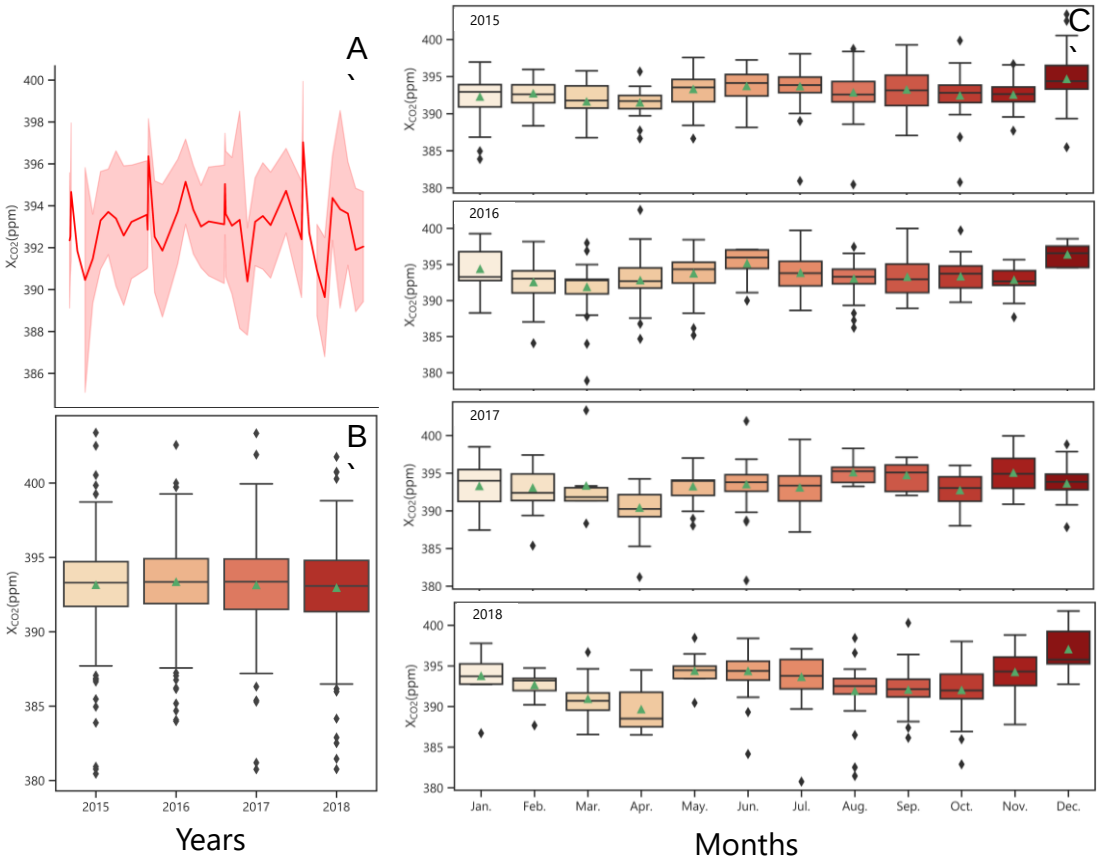

Figure 3. Temporal series of $X_{CO2adjusted}$ to daily observations (A), annual average (B) and monthly averages (C) between 2015 and 2018 for Amazon biome in the Maranhão State of Brazil. Legend: (— internal) represents the second quartile or median; (□) the first and third quartiles; (⊤ and ⊥) third and first quartiles up to the upper and lower limits; (▲) values of the means; (♦) discrepancies (outliers).

The correlation analysis was performed using the monthly averages of X_{CO2}, vegetation spectral index and meteorological variables (Fig 4). The positive correlations for X_{CO2} were founded with wind speed at 2 meters ($r = 0.26$; $p < 0.05$) and 10 meters ($r = 0.37$; $p<0.05$) and wind direction at 50 meters ($r = 0.41$; $p < 0.05$), these relationships are considered medium to low correlated. Stronger and significant ($p<0.05$) negative correlations were observed between X_{CO2} against SIF 757 ($r = -0.54$), SIF771 ($r = -0.72$) and precipitation ($r = -0.52$).

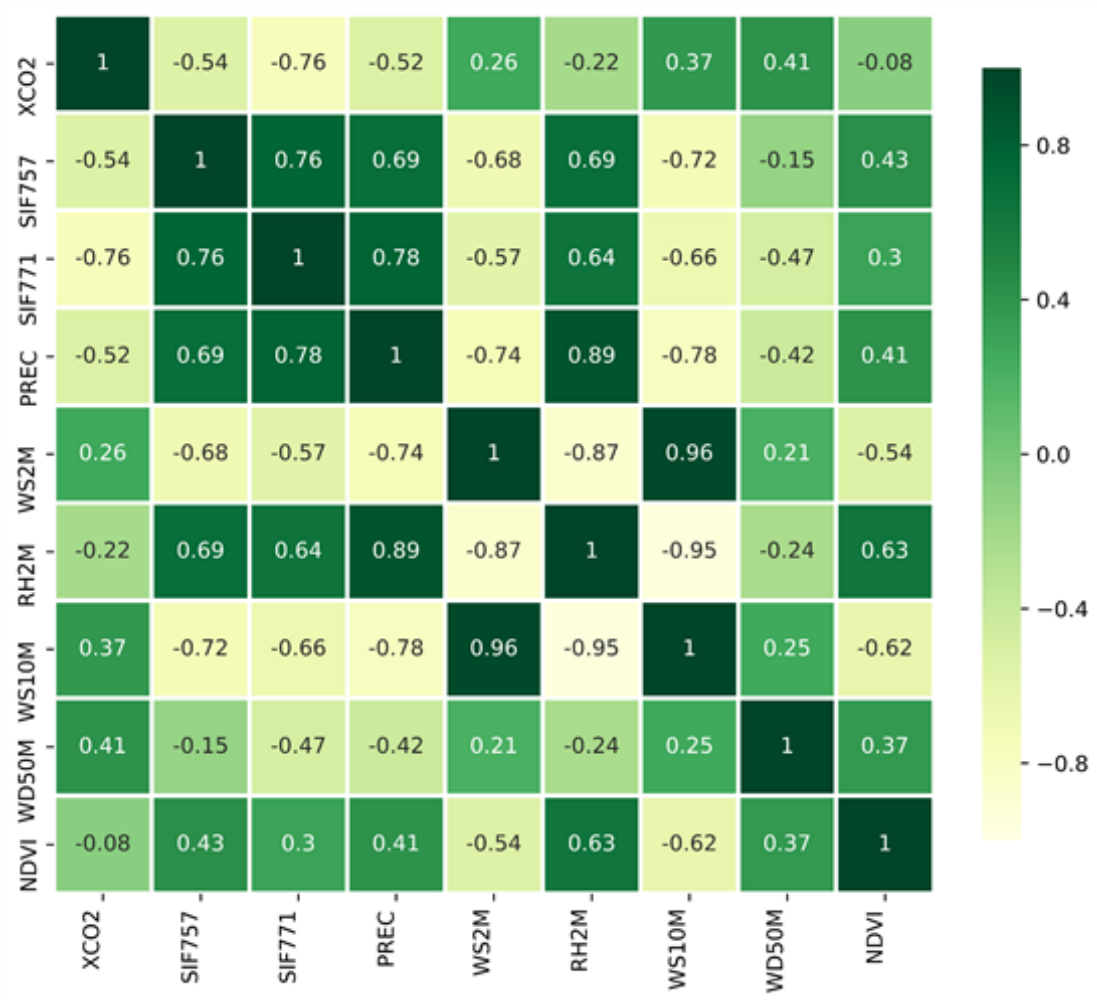

Figure 4. Heatmap of Pearson correlation matrix for X_{CO2} with SIF 757, SIF 771, precipitation, wind speed at 2 meters, wind speed at 10 meters, relative humidity at 2 meters, wind direction at 2 meters and NDVI for Amazon biome in the Maranhão, State of Brazil.

Linear regression analysis was performed only with variables having higher r value (Figure 5). Thus the SIF 771 ($y=-6.559x+398.1$) and 757 ($y= -5.383x+395.86$)

W m^{-2} sr^{-1} μm^{-1} explained changes of X_{CO2} in 58% (R^2Adj. = 0.58; p =0.001) and 28% (R^2Adj. = 0.29 p; =0.001) (Fig 5a). The precipitation (y= -0.000173x +393.8) (Figure 5b) was able to explain the X_{CO2} by 27% (R^2Adj. = 0.27 p=0.001).

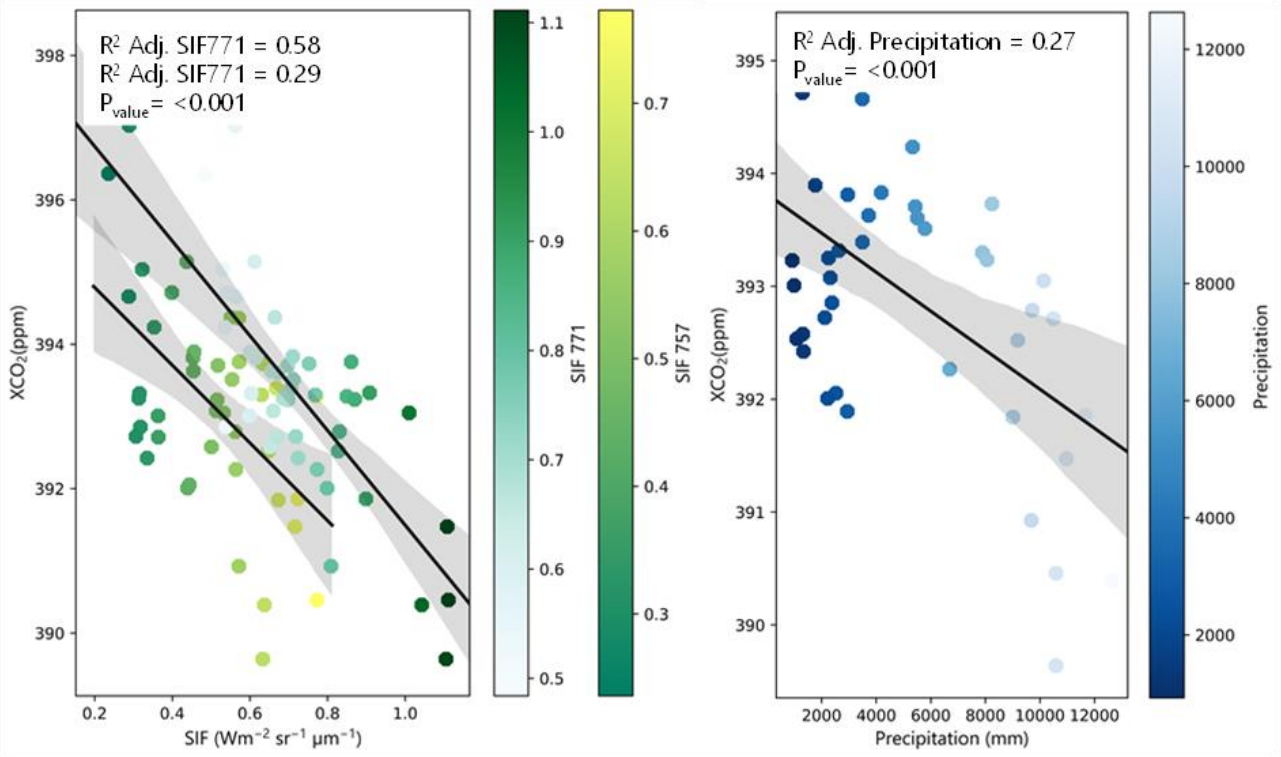

Figure 5. Linear regression analysis of X_{CO2} (ppm) with SIF 757 (W m^{-2} sr^{-1} μm^{-1}), SIF 771 (W m^{-2} sr^{-1} μm^{-1}) and precipitation (mm) for Amazon biome in the Maranhão State of Brazil.

4.3.3 Spatial hot and cold spots to X_{CO2} and SIF 771

The hot spot analysis identified the higher and lower values of the X_{CO2} and SIF 771 clustering, with a z-score returned for each X_{CO2} and SIF771 values in the dataset in the statistical hot spot analysis. The positive z-scores occur, the larger the z-score is, the clustering of high X_{CO2} and SIF values will be more intense. On the other hand, the significant negative z-scores result in a more intense clustering of low values.

The spatial distribution of the X_{CO2} hot spots was concentrated in the south of the region, more specifically in the southwest and southeast (Figure 6a), while SIF hotspots were concentrated in the east of the region (Fig. 6b). In 2017, an inversion was observed between X_{CO2} and SIF (X_{CO2} HOT SPOTS X SIF COLD SPOTS). However, in general, X_{CO2} hot spots are usually shifted from SIF hotspots, not overlapping. An important aspect is that the X_{CO2} hotspots were concentrated near an indigenous and preserved natural forested area.

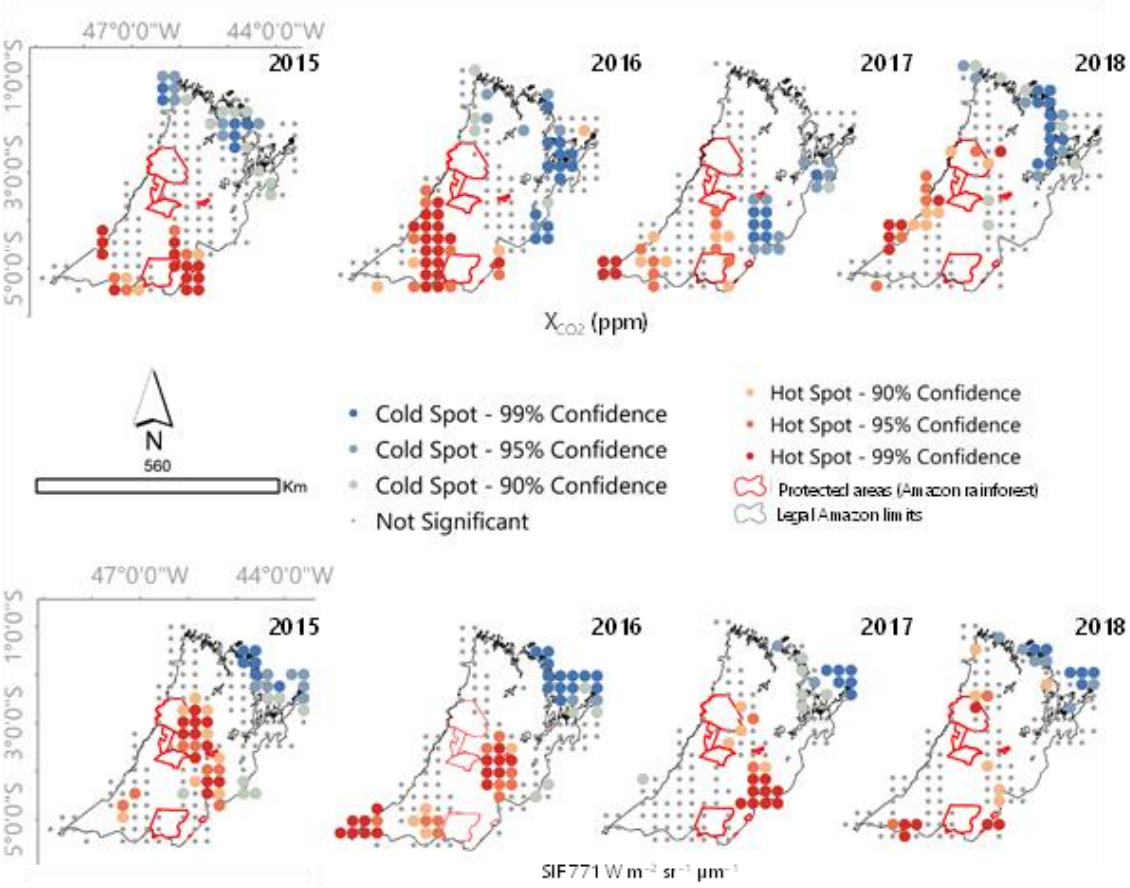

Figure 6. Spatial hot and cold spots to X_{CO2} and SIF 771 for Amazon biome in the Maranhão State of Brazil.

The ratio of hot, cold, and non-significant spots of X_{CO2} and SIF were also calculated (Figure 7). The number of non-significant spots was always more representative in all years for the two variables. The years with more hot spots (99% confidence) numbers were in 2018 with 6.87% to X_{CO2} and 5.12% to SIF. The hotspots with 90% confidence were more representative in 2016, with 13.55% to X_{CO2} and 18.34% to SIF. About the cold spots, the points with 99% of confidence were more evident in 2016, with 13.21% for X_{CO2} and 13.94 for SIF.

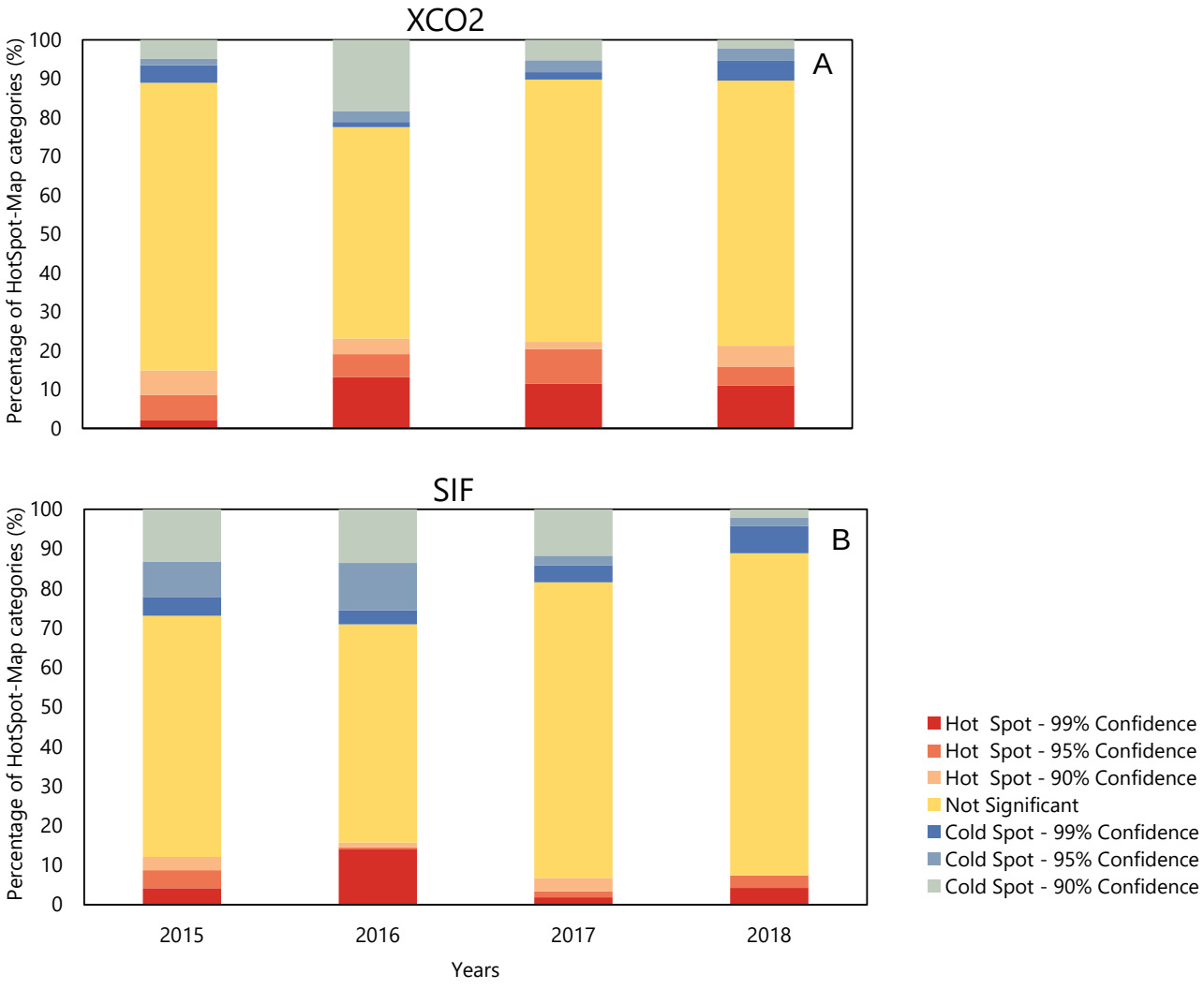

Figure 7. Timeline variation of hot and cold spots of A) X_{CO2} and B) SIF 771 for Amazon biome in the Maranhão State of Brazil.

4.3.4 X_{CO2} anomalies

The data of the X_{CO2} anomaly showed a normal distribution (Figure 8b). The X_{CO2} anomaly (ppm) maximum and minimum were 6.19 and -6.29, respectively, during all the years studied. Figure 8a presents the means of the X_{CO2} anomalies calculated for the Amazon biome on the Maranhão. The elevated values were observed in the southwest and southeast of the studied area, while the lowest values were concentrated in the north. Despite those different analyses, this spatial distribution is quite similar, as observed in the hotspot's analysis (Figure 8). This behavior is more evident when observed in the X_{CO2} distribution on the latitude (Figure 8c). The south region with higher latitude presents more and increased anomalies implying emissions sources close to protected areas.

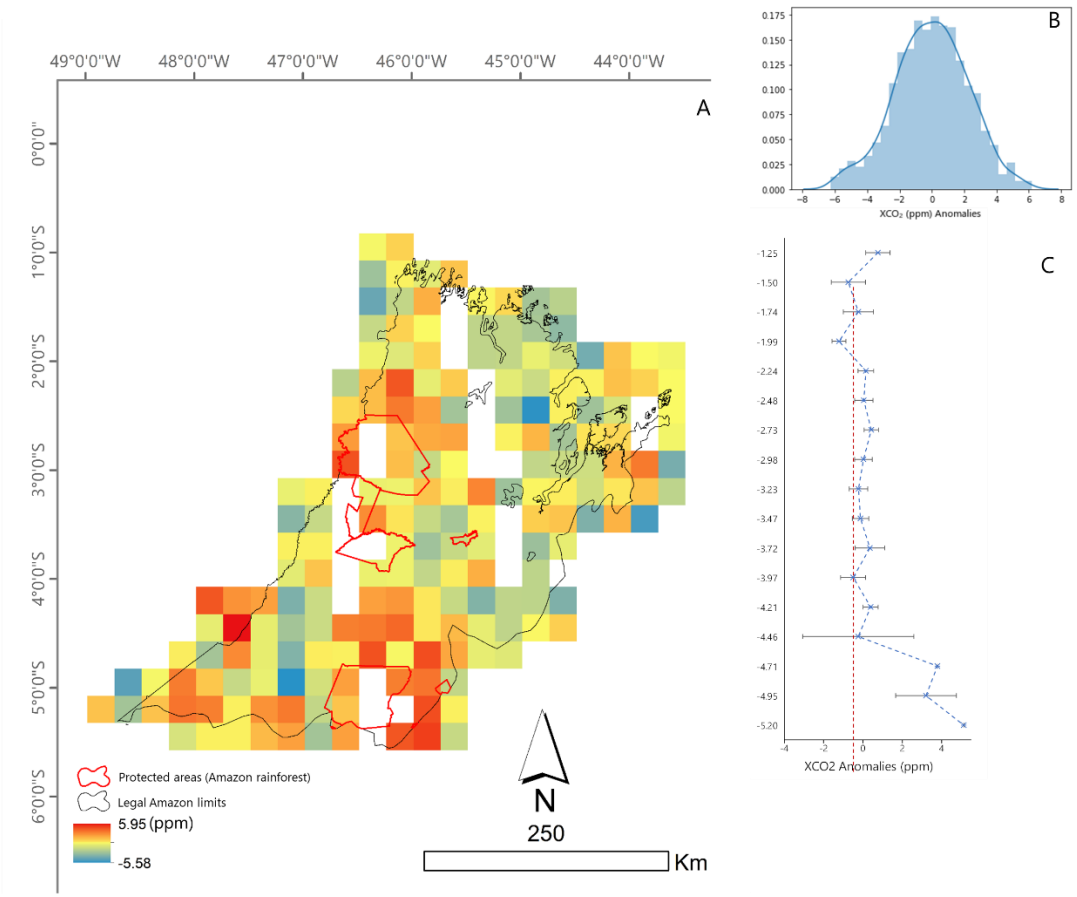

Figure 8. Spatial distribution of X_{CO2} anomalies (a), anomalies data distribution (b) and latitude distribution (c).

4.4 Discussion

X_{CO2} from OCO-2 helps understand spatial and temporal changes of CO_2 in regional scales (Eldering et al., 2017). According to Schwandner et al. (2017), this is possible due to OCO-2 unprecedented kilometer-scale resolution, and high sensitivity enables detection of CO_2 from natural and anthropogenic localized emission sources.

Studies have been conducted at regional scales indicate how X_{CO2} varies, and it is surface relations (Falahatkar et al., 2017; Golkar et al., 2020; Mousavi et al., 2017). Our study detected the seasonal variability during the year, which is essential as the Amazonia region has two seasons, dry and rainy. Hence, differently from what happens in the northern hemisphere, in the Brazilian Amazonia, the climatic seasons are not well defined as a function of mean temperatures (Levine et al., 2019).

In general, in Maranhão, the wettest months are February, March and April, while the driest months are July, August and September (UEMA, 2015). According to Reschke et al. (2010), the highest rainfall indices occur in the north of the region in the first quarter and the third quarter for the South region, generally speaking, according to the authors, in the northern region of the study area is where annual rainfall totals are concentrated.

Thus, when observing the dry and rainy season, we detected a relationship between the temporal variation of precipitation and X_{CO2}. This is much more evident in our study when we observe the correlation analyses (Fig.4) and regression (Fig. 5) between X_{CO2} and precipitation. The negative correlation observed in our study indicates that CO_2 in the atmosphere decreases as precipitation increases. Work carried by Wang et al. (2016); Chhabra and Gohel (2019); Golkar et al. (2020) corroborate with our findings. Wang et al. (2016) reinforce that the sensitivity of the growth rate of atmospheric CO_2 about precipitation is always negative. The response varies according to the type of soil cover since vegetation precipitation sensitivity could affect the variability of atmospheric CO_2.

Regarding vegetation, the sensitivity of X_{CO2} to photosynthetic activity was very evident through the fluorescence of sun-induced chlorophyll (SIF). In summary, SIF consists of the energy that escapes from the chlorophyll of the plant during photosynthetic activity, with a wavelength ranging from 600 to 800nm (Baker, 2008).

In this study, SIF at wavelengths 757 and 771nm were used. This negative relationship observed between X_{CO2} and SIF was already expected since photosynthesis is the main path responsible for the absorption of CO_2 from the atmosphere. Some studies have already identified a positive linear relationship between SIF and crude primary production, which is an important variable in studies evaluating carbon dynamics (Frankenberg et al., 2014; Guo et al., 2020; Qiu et al., 2020).

In studies conducted by Li et al. (2018) and Wei et al. (2019), a correlation of SIF757 with GPP and NDVI was observed. Wei et al. (2019) attributed the fact that the 771mn band is farther from the peak emission in the SIF spectrum. In our study, SIF757 also presented a better correlation with NDVI. However, for X_{CO2}, it was SIF771 that presented a better performance in regression analysis and correlation with relation. A similar effect was also observed with precipitation. This indicates a higher sensitivity of SIF771 to precipitation in our study region, sensitivity, and X_{CO2} and precipitation.

Precipitation events are closely linked to El Niño events (Almeida Silva et al., 2020). In this sense, the powerful El Niño of 2015-2016 had a significant impact on the Earth's natural climate system, which affected the earth's ecosystem (Patra et al., 2017). For this reason, the highest peak in the number of X_{CO2} hot spots in 2016 may be related to El Niño in 2015-2016. According to Liu et al. (2017), with respect to 2011-2016, El Niño in the pantropical biosphere released about 2.5 ± 0.34 gigatons more carbon into the atmosphere.

On a global scale for Patra et al. (2017), estimates were that El Niño provided an excessive release of CO_2 into the atmosphere in the 2.23-2.55 PgC July 2015 to June 2016 compared to the 2014 reference period. This excess flow of CO_2 into the atmosphere is mainly due to the reduction in carbon absorption due to drought and, on a smaller scale, by increasing biomass burning (Patra et al., 2017). Effects of El Niño on photosynthetic activity in the Amazon using SIF were also observed by Castro et al. (2020).

As previously reported, some studies point to the effects of X_{CO2} anomalies with El Niño events. In our study, the anomaly of X_{CO2} was calculated for the entire period studied, according to Wang et al. (2018). The higher density of positive anomaly

values that indicate emission were concentrated to the south of the region and close to reserve areas.

Carbon dioxide exchange has been measured directly over Amazon basin showing contrasting values at dry (0.48 ± 0.18 Pg Cyr-1) and wet (0.06 ± 0.1 Pg Cyr-1) years (Gatti et al., 2014), suggesting a suppression of photosynthesis during drought as the primary cause for the wet years sink neutralization, this effect has been pointed as Amazon could become an carbon emitter instead of sinker, due to fires and the suppression of net biome exchange by drought season.

Some studies have indicated the danger of deforestation in the Amazon in this region (Celentano et al., 2017; Vedovato et al., 2016) has already lost more than 75% of its original coverage. Recently, Silva Junior et al. (2020) warned that the Maranhão Amazon is on the verge of collapse, according to these authors, almost half of all deforested areas in the region (36,060 km^2) are considered a hotspot of global restoration, however, secondary vegetation remains unprotected and 8,294 km^2 were deforested between 2014 and 2018.

Deforestation is one of the main sources of CO_2 emissions for the atmosphere (Achard et al., 2013), especially in Brazil (Sanquetta et al., 2020). In addition to deforestation, the Amazon has been suffering from recurrent fires that only occur due to deforestation. For the region where this study was carried out, the Amazon was clearly replaced by pasture and this is clear when observing the results reported by Parente et al. (2019). Through the digital platform (http://pastagem.org) made available by the authors, it was observed that for the State of Maranhão, pasture is mainly concentrated in the Amazon region. Between 2015 and 2018 (our study period) the pasture areas went from 175.907.959 Ha^{-1} $year^{-1}$ to 183.090.997 Ha^{-1} $year^{-1}$. Another important fact is about degraded

pastures, they are concentrated further south of our study area, which corroborates with our findings of anomalies and hot spots. The disturbance caused by deforestation has increased the incidence of fires, which has as a consequence the decrease in carbon assimilation by biomes present in the state of Mato Grosso, among them, the Amazon (Rossi and Santos, 2020).

4.5 Conclusions

Our findings show that the hot moments of X_{CO2} to Eastern Amazonia in Maranhão, Brazil, are concentrated in May to September and with some peaks in December. The cold moments indicating the decrease of X_{CO2} are from October to April. The spatial distribution of X_{CO2} hot spots is concentrated in the south of the region, while SIF hot spots are concentrated east of the Eastern Amazon of the Maranhão State. In most of the cases, X_{CO2} hot spots present where there are no significant spots for SIF. The year 2016 stood out as the year with the highest peak of hot spots of X_{CO2} coinciding with El Niño. Like spatial hot spots, X_{CO2} anomalies are also concentrated in the southern region and near Amazonia forest protected areas.

Knowing the uncertainties of the mechanisms governing carbon circulation in the tropics (Cox et al., 2000; Anderegg et al., 2015; Schimel et al., 2015), our results bring interesting conclusions in this aspect, once the, in the Eastern Amazon, the X_{CO2} presents significant sensitivity with photosynthetic activity through solar-induced chlorophyll fluorescence (SIF771) and precipitation. Even the X_{CO2} presented interesting responses to these variables. We emphasize that for future studies, variables related to the hydrological cycle responsible for photosynthetic activity such as soil moisture, relative air humidity and evapotranspiration can bring interesting answers to understand the carbon cycle in very degraded ecosystems, such as the Eastern Amazon of Maranhão.

Finally, with the advancement of science in remote sensing detection of greenhouse gas concentration, such as the Carbon Observatory 3 (OCO-3) launch, more data from X_{CO2} and SIF have been collected around the planet, helping the knowledge around the carbon cycle. Therefore, we reinforce that the use of this data is more widespread and implemented by the scientific community to bring new

"climate-carbon-feedbacks" that will help better understand the carbon cycle on a global and regional scale. Such solutions are of paramount importance for mitigating climate change and for generating a sustainable society.

References

ACHARD, F.; EVA, H. D.; MAYAUX, P.; GALLEGO, J.; RICHARDS, T. Determination of Deforestation Rates of the World ' s Humid Tropical Forests. [s. l.], v. 999, n. 2002, 2013.

ALMEIDA SILVA, K.; DE SOUZA ROLIM, G.; BORGES VALERIANO, T. T.; DA SILVA CABRAL DE MORAES, J. R. Influence of El Niño and La Niña on coffee yield in the main coffee-producing regions of Brazil. **Theoretical and Applied Climatology**, [s. l.], v. 139, n. 3–4, p. 1019–1029, 2020.

ANDEREGG, W. R. L.; BALLANTYNE, A. P.; SMITH, W. K.; MAJKUT, J.; RABIN, S.; BEAULIEU, C.; BIRDSEY, R.; DUNNE, J. P.; HOUGHTON, R. A.; MYNENI, R. B.; PAN, Y.; SARMIENTO, J. L.; SEROTA, N.; SHEVLIAKOVA, E.; TANS, P.; PACALA, S. W. Tropical nighttime warming as a dominant driver of variability in the terrestrial carbon sink. **Proceedings of the National Academy of Sciences of the United States of America**, [s. l.], v. 112, n. 51, p. 15591–15596, 2015.

ARAGÃO, L. E. O. C.; POULTER, B.; BARLOW, J. B.; ANDERSON, L. O.; MALHI, Y.; SAATCHI, S.; PHILLIPS, O. L.; GLOOR, E. Environmental change and the carbon balance of Amazonian forests. **Biological Reviews**, [s. l.], v. 89, n. 4, p. 913–931, 2014.

BAKER, N. R. Chlorophyll fluorescence: A probe of photosynthesis in vivo. **Annual Review of Plant Biology**, [s. l.], v. 59, p. 89–113, 2008.

BARLOW, J.; LENNOX, G. D.; FERREIRA, J.; BERENGUER, E.; LEES, A. C.; NALLY, R. Mac; THOMSON, J. R.; FERRAZ, S. F. D. B.; LOUZADA, J.; OLIVEIRA, V. H. F.; PARRY, L.; RIBEIRO DE CASTRO SOLAR, R.; VIEIRA, I. C. G.; ARAGAÕ, L. E. O. C.; BEGOTTI, R. A.; BRAGA, R. F.; CARDOSO, T. M.; JR, R. C. D. O.; SOUZA, C. M.; MOURA, N. G.; NUNES, S. S.; SIQUEIRA, J. V.; PARDINI, R.; SILVEIRA, J. M.; VAZ-DE-MELLO, F. Z.; VEIGA, R. C. S.; VENTURIERI, A.; GARDNER, T. A. Anthropogenic disturbance in tropical forests can double biodiversity loss from

deforestation. **Nature**, [s. l.], v. 535, n. 7610, p. 144–147, 2016. Disponível em: http://dx.doi.org/10.1038/nature18326

BAUHOFF, S.; BUSCH, J. Does deforestation increase malaria prevalence? Evidence from satellite data and health surveys. **World Development**, [s. l.], v. 127, p. 104734, 2020. Disponível em: https://doi.org/10.1016/j.worlddev.2019.104734

CASAGRANDE, E.; RECANATI, F.; MELIÀ, P. Assessing the Influence of Vegetation on the Water Budget of Tropical Areas. **IFAC-PapersOnLine**, [s. l.], v. 51, n. 5, p. 1–6, 2018. Disponível em: https://doi.org/10.1016/j.ifacol.2018.06.190

CASTRO, A. O.; CHEN, J.; ZANG, C. S.; SHEKHAR, A.; JIMENEZ, J. C.; BHATTACHARJEE, S.; KINDU, M.; MORALES, V. H.; RAMMIG, A. OCO-2 solar-induced chlorophyll fluorescence variability across ecoregions of the Amazon basin and the extreme drought effects of El Niño (2015-2016). **Remote Sensing**, [s. l.], v. 12, n. 7, 2020.

CELENTANO, D.; ROUSSEAU, G. X.; MUNIZ, F. H.; VARGA, I. van D.; MARTINEZ, C.; CARNEIRO, M. S.; MIRANDA, M. V. C.; BARROS, M. N. R.; FREITAS, L.; NARVAES, I. da S.; ADAMI, M.; GOMES, A. R.; RODRIGUES, J. C.; MARTINS, M. B. Towards zero deforestation and forest restoration in the Amazon region of Maranhão state, Brazil. **Land Use Policy**, [s. l.], v. 68, n. August, p. 692–698, 2017.

CHHABRA, A.; GOHEL, A. Dynamics of atmospheric carbon dioxide over different land cover types in India. **Environmental Monitoring and Assessment**, [s. l.], v. 191, n. July 2014, 2019.

COX, P. M.; BETTS, R. A.; JONES, C. D.; SPALL, S. A.; TOTTERDELL, I. J. Acceleration of global warming due to carbon-cycle feedbacks in a coupled climate model. **Nature**, [s. l.], v. 408, n. 6809, p. 184–187, 2000.

CRISP, D.; POLLOCK, H.; ROSENBERG, R.; CHAPSKY, L.; LEE, R.; OYAFUSO, F.; FRANKENBERG, C.; DELL, C.; BRUEGGE, C.; DORAN, G.; ELDERING, A.; FISHER, B.; FU, D.; GUNSON, M.; MANDRAKE, L.; OSTERMAN, G.; SCHWANDNER, F.; SUN, K.; TAYLOR, T.; WENNBERG, P.; WUNCH, D. The on-orbit performance of the Orbiting Carbon Observatory-2 (OCO-2) instrument and its radiometrically calibrated products. **Atmospheric Measurement Techniques**, [s. l.], v. 10, n. 1, p. 59–81, 2017.

DE OLIVEIRA SILVA, R.; BARIONI, L. G.; MORAN, D. Fire, deforestation, and livestock: When the smoke clears. **Land Use Policy**, [s. l.], v. 100, n. July 2020, p. 104949, 2021. Disponível em: https://doi.org/10.1016/j.landusepol.2020.104949

ELDERING, A.; WENNBERG, P. O.; CRISP, D.; SCHIMEL, D. S.; GUNSON, M. R.; CHATTERJEE, A.; LIU, J.; SCHWANDNER, F. M.; SUN, Y.; O'DELL, C. W.; FRANKENBERG, C.; TAYLOR, T.; FISHER, B.; OSTERMAN, G. B.; WUNCH, D.; HAKKARAINEN, J.; TAMMINEN, J.; WEIR, B. The Orbiting Carbon Observatory-2 early science investigations of regional carbon dioxide fluxes. **Science**, [s. l.], v. 358, n. 6360, 2017.

ESTEVES, V. P. P.; ESTEVES, E. M. M.; BUNGENSTAB, D. J.; LOEBMANN, D. G. dos S. W.; DE CASTRO VICTORIA, D.; VICENTE, L. E.; DE QUEIROZ FERNANDES ARAÚJO, O.; DO ROSÁRIO VAZ MORGADO, C. Land use change (LUC) analysis and life cycle assessment (LCA) of Brazilian soybean biodiesel. **Clean Technologies and Environmental Policy**, [s. l.], v. 18, n. 6, p. 1655–1673, 2016.

FALAHATKAR, S.; MOUSAVI, S. M.; FARAJZADEH, M. Spatial and temporal distribution of carbon dioxide gas using GOSAT data over IRAN. **Environmental Monitoring and Assessment**, [s. l.], v. 189, n. 12, 2017.

FRANKENBERG, C.; O'DELL, C.; BERRY, J.; GUANTER, L.; JOINER, J.; KÖHLER, P.; POLLOCK, R.; TAYLOR, T. E. Prospects for chlorophyll fluorescence remote sensing from the Orbiting Carbon Observatory-2. **Remote Sensing of Environment**, [s. l.], v. 147, p. 1–12, 2014.

GOLKAR, F.; AL-WARDY, M.; SAFFARI, S. F.; AL-AUFI, K.; AL-RAWAS, G. Using OCO-2 satellite data for investigating the variability of atmospheric CO2 concentration in relationship with precipitation, relative humidity, and vegetation over Oman. **Water (Switzerland)**, [s. l.], v. 12, n. 1, 2020.

GUJARATI, D.N. and PORTER, D.C., 2011. *Econometria básica-5*. Amgh Editora

GUO, M.; LI, J.; HUANG, S.; WEN, L. Feasibility of using MODIS products to simulate sun-induced chlorophyll fluorescence (SIF) in boreal forests. **Remote Sensing**, [s. l.], v. 12, n. 4, 2020.

GUO, M.; LI, J.; XU, J.; WANG, X.; HE, H.; WU, L. CO2 emissions from the 2010 Russian wildfires using GOSAT data. **Environmental Pollution**, [s. l.], v. 226, p. 60–68, 2017.

GUO, M.; WANG, X.; LI, J.; YI, K.; ZHONG, G.; TANI, H. Assessment of global carbon dioxide concentration using MODIS and GOSAT data. **Sensors (Switzerland)**, [s. l.], v. 12, n. 12, p. 16368–16389, 2012.

HAKKARAINEN, J.; IALONGO, I.; TAMMINEN, J. Direct space-based observations of anthropogenic CO2 emission areas from OCO-2. **Geophysical Research Letters**, [s. l.], v. 43, n. 21, p. 11,400-11,406, 2016.

LABZOVSKII, L. D.; JEONG, S. J.; PARAZOO, N. C. Working towards confident spaceborne monitoring of carbon emissions from cities using Orbiting Carbon Observatory-2. **Remote Sensing of Environment**, [s. l.], v. 233, n. August 2018, 2019.

LEVINE, P. A.; RANDERSON, J. T.; CHEN, Y.; PRITCHARD, M. S.; XU, M.; HOFFMAN, F. M. Soil moisture variability intensifies and prolongs eastern Amazon temperature and carbon cycle response to El Niño-Southern Oscillation. **Journal of Climate**, [s. l.], v. 32, n. 4, p. 1273–1292, 2019.

LI, X.; XIAO, J.; HE, B. Chlorophyll fluorescence observed by OCO-2 is strongly related to gross primary productivity estimated from flux towers in temperate forests. **Remote Sensing of Environment**, [s. l.], v. 204, n. October 2017, p. 659–671, 2018.

LIU, J.; BOWMAN, K. W.; SCHIMEL, D. S.; PARAZOO, N. C.; JIANG, Z.; LEE, M.; BLOOM, A. A.; WUNCH, D.; FRANKENBERG, C.; SUN, Y.; O'DELL, C. W.; GURNEY, K. R.; MENEMENLIS, D.; GIERACH, M.; CRISP, D.; ELDERING, A. Contrasting carbon cycle responses of the tropical continents to the 2015–2016 El Niño. **Science**, [s. l.], v. 358, n. 6360, 2017.

LONGO, M.; SAATCHI, S.; KELLER, M.; BOWMAN, K.; FERRAZ, A.; MOORCROFT, P. R.; MORTON, D. C.; BONAL, D.; BRANDO, P.; BURBAN, B.; DERROIRE, G.; DOS-SANTOS, M. N.; MEYER, V.; SALESKA, S.; TRUMBORE, S.; VINCENT, G. Impacts of Degradation on Water, Energy, and Carbon Cycling of the Amazon Tropical Forests. **Journal of Geophysical Research: Biogeosciences**, [s. l.], v. 125, n. 8, p. 1–27, 2020.

MALHI, Y.; WOOD, D.; BAKER, T. R.; WRIGHT, J.; PHILLIPS, O. L.; COCHRANE, T.; MEIR, P.; CHAVE, J.; ALMEIDA, S.; ARROYO, L.; HIGUCHI, N.; KILLEEN, T. J.; LAURANCE, S. G.; LAURANCE, W. F.; LEWIS, S. L.; MONTEAGUDO, A.; NEILL, D. A.; VARGAS, P. N.; PITMAN, N. C. A.; QUESADA, C. A.; SALOMÃO, R.; SILVA, J. N. M.; LEZAMA, A. T.; TERBORGH, J.; MARTÍNEZ, R. V.; VINCETI, B. The regional variation of aboveground live biomass in old-growth Amazonian forests. **Global Change Biology**, [s. l.], v. 12, n. 7, p. 1107–1138, 2006.

MOUSAVI, S. M.; FALAHATKAR, S.; FARAJZADEH, M. Assessment of seasonal variations of carbon dioxide concentration in Iran using GOSAT data. **Natural Resources Forum**, [s. l.], v. 41, n. 2, p. 83–91, 2017.

PATRA, P. K.; CRISP, D.; KAISER, J. W.; WUNCH, D.; SAEKI, T.; ICHII, K.; SEKIYA, T.; WENNBERG, P. O.; FEIST, D. G.; POLLARD, D. F.; GRIFFITH, D. W. T.; VELAZCO, V. A.; DE MAZIERE, M.; SHA, M. K.; ROEHL, C.; CHATTERJEE, A.; ISHIJIMA, K. The Orbiting Carbon Observatory (OCO-2) tracks 2-3 peta-gram increase in carbon release to the atmosphere during the 2014-2016 El Niño. **Scientific Reports**, [s. l.], v. 7, n. 1, p. 1–12, 2017.

QIU, R.; HAN, G.; MA, X.; SHA, Z.; SHI, T.; XU, H.; ZHANG, M. CO2 concentration, a critical factor influencing the relationship between solar-induced chlorophyll fluorescence and gross primary productivity. **Remote Sensing**, [s. l.], v. 12, n. 9, 2020.

RESCHKE, G.A., ELOI, C. and SILVA, R., 2011. Caracterização climática da Amazônia maranhense. **Amazônia maranhense: diversidade e conservação**. Belém: MPEG, pp.47-67.

ROSSI, F. S.; SANTOS, G. A. de A. Fire dynamics in Mato Grosso State, Brazil: the relative roles of gross primary productivity. **Big Earth Data**, [s. l.], v. 4, n. 1, p. 23–44, 2020. Disponível em: https://doi.org/10.1080/20964471.2019.1706832

RUIZ-VÁSQUEZ, M.; ARIAS, P. A.; MARTÍNEZ, J. A.; ESPINOZA, J. C. Effects of Amazon basin deforestation on regional atmospheric circulation and water vapor transport towards tropical South America. **Climate Dynamics**, [s. l.], v. 54, n. 9–10, p. 4169–4189, 2020. Disponível em: https://doi.org/10.1007/s00382-020-05223-4

SANQUETTA, C.; PAULA, A.; CORTE, D.; SANQUETTA, M.; PELISSARI, A.; TOM, M. Greenhouse gas emissions due to land use change in Brazil from 1990 to 2015 : comparison of methodological approaches. [s. l.], v. 53, p. 25–37, 2020.

SANTOS DE LIMA, L.; MERRY, F.; SOARES-FILHO, B.; OLIVEIRA RODRIGUES, H.; DOS SANTOS DAMACENO, C.; BAUCH, M. A. Illegal logging as a disincentive to the establishment of a sustainable forest sector in the Amazon. **PLoS ONE**, [s. l.], v. 13, n. 12, p. 1–21, 2018.

STACKHOUSE, P.W., WESTBERG, D., HOELL, J.M., CHANDLER, W.S. AND ZHANG, T. Prediction of Worldwide Energy Resource (POWER)-Agroclimatology methodology-(1.0 latitude by 1.0 longitude spatial resolution). Hampton, NASA Langely Research Center. 2015

SCHIMEL, D.; STEPHENS, B. B.; FISHER, J. B. Effect of increasing CO2 on the terrestrial carbon cycle. **Proceedings of the National Academy of Sciences of the United States of America**, [s. l.], v. 112, n. 2, p. 436–441, 2015.

SCHWANDNER, F. M.; GUNSON, M. R.; MILLER, C. E.; CARN, S. A.; ELDERING, A.; KRINGS, T.; VERHULST, K. R.; SCHIMEL, D. S.; NGUYEN, H. M.; CRISP, D.; O'DELL, C. W.; OSTERMAN, G. B.; IRACI, L. T.; PODOLSKE, J. R. Spaceborne detection of localized carbon dioxide sources. **Science**, [s. l.], v. 358, n. 6360, 2017.

SILVA JUNIOR, C. H. L.; CELENTANO, D.; ROUSSEAU, G. X.; DE MOURA, E. G.; VARGA, I. van D.; MARTINEZ, C.; MARTINS, M. B. Amazon forest on the edge of collapse in the Maranhão State, Brazil. **Land Use Policy**, [s. l.], v. 97, n. May, 2020.

SOUZA, C. M.; KIRCHHOFF, F. T.; OLIVEIRA, B. C.; RIBEIRO, J. G.; SALES, M. H. Long-term annual surface water change in the Brazilian Amazon Biome: Potential links with deforestation, infrastructure development and climate change. **Water (Switzerland)**, [s. l.], v. 11, n. 3, 2019.

STRAND, J.; SOARES-FILHO, B.; COSTA, M. H.; OLIVEIRA, U.; RIBEIRO, S. C.; PIRES, G. F.; OLIVEIRA, A.; RAJÃO, R.; MAY, P.; VAN DER HOFF, R.; SIIKAMÄKI, J.; DA MOTTA, R. S.; TOMAN, M. Spatially explicit valuation of the Brazilian Amazon Forest's Ecosystem Services. **Nature Sustainability**, [s. l.], v. 1, n. 11, p. 657–664, 2018. Disponível em: http://dx.doi.org/10.1038/s41893-018-0175-0

VEDOVATO, L. B.; FONSECA, M. G.; ARAI, E.; ANDERSON, L. O.; ARAGÃO, L. E. O. C. The extent of 2014 forest fragmentation in the Brazilian Amazon. **Regional Environmental Change**, [s. l.], v. 16, n. 8, p. 2485–2490, 2016.

VILLALOBOS, Y.; RAYNER, P.; THOMAS, S. Was Australia a sink or source of CO 2 in 2015 ? Data assimilation using OCO-2 satellite data Australian Carbon Budget Why we should care about about it ? [s. l.], n. May, p. 1–15, 2020.

WALKER, W. S.; GORELIK, S. R.; BACCINI, A.; ARAGON-OSEJO, J. L.; JOSSE, C.; MEYER, C.; MACEDO, M. N.; AUGUSTO, C.; RIOS, S.; KATAN, T.; DE SOUZA, A. A.; CUELLAR, S.; LLANOS, A.; ZAGER, I.; MIRABAL, G. D.; SOLVIK, K. K.; FARINA, M. K.; MOUTINHO, P.; SCHWARTZMAN, S. The role of forest conversion, degradation, and disturbance in the carbon dynamics of Amazon indigenous territories and protected areas. **Proceedings of the National Academy of Sciences of the United States of America**, [s. l.], v. 117, n. 6, p. 3015–3025, 2020.

WANG, J.; ZENG, N.; WANG, M. Interannual variability of the atmospheric CO2 growth rate: Roles of precipitation and temperature. **Biogeosciences**, [s. l.], v. 13, n. 8, p. 2339–2352, 2016.

WANG, S.; ZHANG, Y.; HAKKARAINEN, J.; JU, W.; LIU, Y.; JIANG, F.; HE, W. Distinguishing Anthropogenic CO2 Emissions From Different Energy Intensive Industrial Sources Using OCO-2 Observations: A Case Study in Northern China.

Journal of Geophysical Research: Atmospheres, [s. l.], v. 123, n. 17, p. 9462–9473, 2018.

WEI, J.; TANG, X.; GU, Q.; WANG, M.; MA, M.; HAN, X. Using solar-induced chlorophyll fluorescence observed by OCO-2 to predict autumn crop production in China. **Remote Sensing**, [s. l.], v. 11, n. 14, p. 1–14, 2019.

WERTH, D. The local and global effects of Amazon deforestation. **Journal of Geophysical Research**, [s. l.], v. 107, n. D20, 2002.

YOKOTA, T.; YOSHIDA, Y.; EGUCHI, N.; OTA, Y.; TANAKA, T.; WATANABE, H.; MAKSYUTOV, S. Global concentrations of CO2 and CH4 retrieved from GOSAT: First preliminary results. **Scientific Online Letters on the Atmosphere**, [s. l.], v. 5, n. 1, p. 160–163, 2009.

CHAPTER 5 – Final remarks

The increase in the planet's average temperature in recent decades is tied to the increase in greenhouse gas concentration (GHG) resulting from anthropogenic activities. Therefore, the evidence of the effects of human activities on climate is clear. Given this worrying scenario, the development of research that points to mitigating and adapting to climate change is essential for the survival of the planet.

In this sense, with the emergence of the era of earth observation in high resolution, remote sensing data exponential growth has been occurring in recent years. Given this, remote sensing data is part of the big data era. Thanks to this, monitoring the environment on a large scale has become possible since research has been developed with remote sensing data with different time scales, spatial and sensor types. Many of these studies monitor environmental and atmospheric CO_2 concentrations on a global and regional scale.

In this study, several sources of data were used to obtain carbon feedback. Thus, it was observed that both in biomes and forest areas in the state of Mato Grosso do Sul, the temporal variation of atmospheric CO_2 concentration is mainly governed by photosynthesis (Solar induced chlorophyll fluorescence-SIF, NDVI, and EVI) and that photosynthesis is positively related to evapotranspiration and air temperature. In Mato Grosso and eastern Amazonia, SIF is also an important variable in explaining the temporal variability of X_{CO2}. However, in these regions, this relationship is also observed spatially. In general, the time variations of X_{CO2} in the north-central region of Brazil vary between the dry and rainy periods, this was clear in all studies. As for the spatial variation of X_{CO2}, it varies according to the type of land use and the time of year.

Knowing this dynamic of temporal variation of atmospheric CO_2 in time and space is a powerful tool in decision-making in public policies focused on climate change. Spatial interpolation techniques and the verification of "hot spots" and "hot moments" can contribute to the construction of strategies aimed at mitigating CO_2 emissions in specific locations and periods.

Given the results presented in this work, it is clear that big data and remote sensing are valuable tools in understanding the carbon cycle since the relationships

observed in the intersection of these data generate results that are clearly explained by the physical and biological processes around the soil-plant-atmosphere system.

In this respect, it is essential to emphasize that understanding these relationships is essential in searching for carbon sources and sinks in the biosphere. The search for the balance between carbon emission and absorption in the ecosystem varies according to environmental factors that affect both photosynthesis (carbon uptake) and carbon source.

It is worth stressing that climate change and changes induced by the disturbance of ecosystems can affect photosynthesis processes and breathing differently and, therefore, resulting in the change in the balance of carbon exchanges in ecosystems. An unwanted reduction in carbon capture intensity by ecosystems and forests will bring positive feedback to the carbon cycle, resulting in the increased greenhouse effect and worsening climate change.

Finally, In the next years, new space missions with greenhouse gas monitoring will be launched, such as MicroCarb from the French Government Space Agency and the continuation of the GOSAT mission with the launch of GOSAT-3, both scheduled to launch in 2021. In 2023, the launch of the Geostationary Carbon Cycle Observatory (GeoCARB), his principal goal, will measure the carbon cycle. All of these missions will complement those that already exist, such as OCO-2 / OCO-3, GOSAT-GOSTA-2, SENTINEL-5, MODIS, Soil Moisture Active Passive (SMAP). For this reason, I encourage my colleagues to make massive use of this data so that science can protect society from the effects of climate change through technical strategies.

APPENDICES

APPENDIX A**.** Descriptive statistics for X_{CO2} (ppm) and SIF (W m^{-2} sr^{-1} μm^{-1}) in the rainy and dry periods for the state of Mato Grosso, Brazil (CHAPTER 3).

Variable	N	Mean	Median	Minimum	Maximum	SD	SE	Kurtosis
2015 - Wet								
X_{CO2}	441	393.96	393.81	389.97	399.97	2.08	0.10	-0.05
SIF	421	0.71	0.71	0.01	1.45	0.30	0.01	-0.31
2015 - Dry								
X_{CO2}	611	395.20	395.16	390.14	399.91	1.40	0.06	1.18
SIF	585	0.47	0.46	0.02	1.30	0.19	0.01	0.22
2016 - Wet								
X_{CO2}	506	394.85	394.67	390.18	399.97	1.92	0.09	-0.08
SIF	490	0.71	0.72	<0.01	1.45	0.30	0.01	-0.32
2016 - Dry								
X_{CO2}	656	395.76	395.77	390.26	399.99	1.41	0.06	1.69
SIF	622	0.47	0.46	0.01	1.43	0.22	0.01	0.92
2017 - Wet								
X_{CO2}	398	394.03	393.94	389.99	399.56	2.03	0.10	-0.23
SIF	370	0.74	0.75	0.01	1.43	0.30	0.02	-0.27
2017 - Dry								
X_{CO2}	581	394.78	394.73	389.99	400.01	1.42	0.06	1.66
SIF	547	0.49	0.49	0.03	1.34	0.22	0.01	1.18
2018 - Wet								
X_{CO2}	422	394.13	394.14	390.01	399.85	2.02	0.10	-0.29
SIF	392	0.77	0.79	<0.01	1.42	0.31	0.02	-0.44
2018 - Dry								
X_{CO2}	564	395.14	395.17	390.16	399.91	1.36	0.06	1.84
SIF	540	0.50	0.49	<0.01	1.37	0.22	0.01	0.62

N= number of points; SD= standard deviation; SE= standard error of the mean.

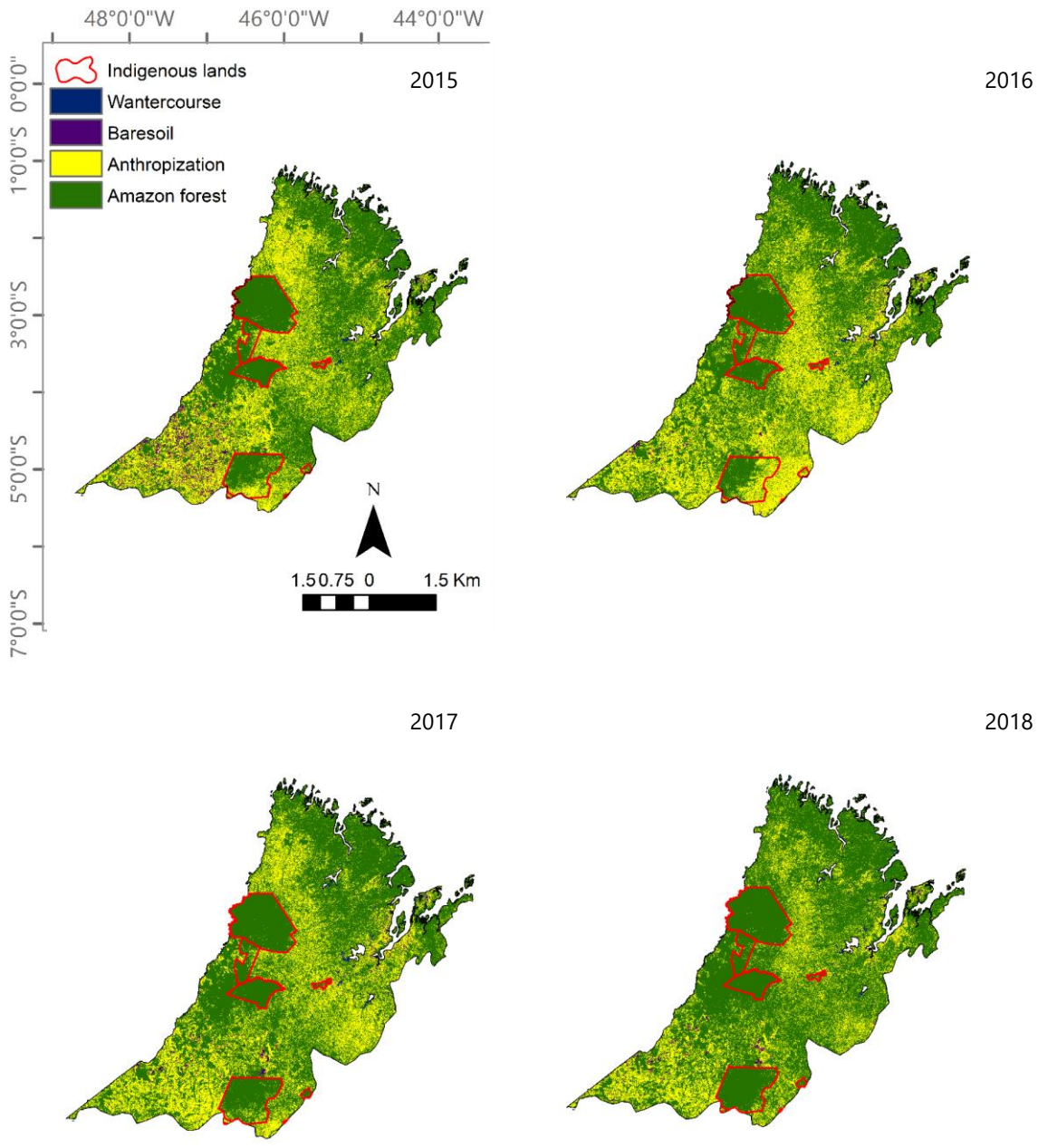

APPENDIX B**.** Land use cover to Amazonia rainforest of Maranhão, Brazil.